AMERICAN MUSEUM NOVITATES

Number 4033, 66 pp. March 11, 2025

Two New Specimens of *Conchoraptor gracilis* (Theropoda: Oviraptorosauria) from the Late Cretaceous of Mongolia

WILLIAM FOSTER,[1] MARK A. NORELL,[2] AND AMY M. BALANOFF[1, 2]

ABSTRACT

Despite a relatively abundant fossil record, the enigmatic and morphologically bizarre oviraptorosaurs suffer from a sparse and often taxonomically convoluted descriptive body of literature. Loss of important holotype material and continued reference to elusive papers often limits access for researchers interested in oviraptorosaur anatomy and systematics. In this work, we provide comprehensive, bone-by-bone descriptions of two extremely well-preserved specimens of *Conchoraptor gracilis*, an oviraptorid from the Late Cretaceous of Mongolia. This marks the most comprehensive anatomical description of this taxon—previous literature providing only short descriptions of fragmentary material or as a part of wider phylogenetic analyses. We present an updated diagnosis for the genus, including a novel cranial autapomorphy, that aims to increase the resolution by which small-bodied, crestless oviraptorids can be differentiated in the future. We particularly target the *Conchoraptor/Heyuannia* species complex, as these taxa tend to be conflated. A phylogenetic analysis of the described specimens, including character scoring for previously unknown regions of the skeleton, produces a topology consilient with the majority of recent oviraptorosaur phylogenies.

INTRODUCTION

Central Asia has been key to expanding the known Late-Cretaceous dinosaur fauna, including a morphologically bizarre group of nonavian theropods belonging to Oviraptoridae.

[1] Center for Functional Anatomy and Evolution, Johns Hopkins University School of Medicine, Baltimore.
[2] Division of Paleontology, American Museum of Natural History.

Copyright © American Museum of Natural History 2025 ISSN 0003-0082

Alongside numerous well-preserved fossil specimens, oviraptorids have yielded some of the most important fossil data for the interpretation of dinosaur paleobiology, such as nesting behavior (Norell et al., 2018; Tanaka et al., 2018; Yang et al., 2018; Yang and Sander, 2022), population ecology (Funston et al., 2018), and embryonic development (Bi et al., 2021; Xing et al., 2022). Oviraptorid research has also been crucial in understanding the evolutionary origins of modern avian reproductive biology (Varricchio et al., 2008; Varricchio and Jackson., 2016), neuroanatomy (Kundrát, 2007; Balanoff et al., 2013; 2014; 2018), and integument (Ji et al., 1998; Norell et al., 2002; Kundrát and Janáček., 2007; Persons et al., 2015).

The Late Cretaceous sediments of the Nemegt Basin, southern Mongolia, have been a focal point for the discovery of exceptionally well-preserved oviraptorid fossils. The status of one such taxon, *Conchoraptor gracilis* (hereafter simply "*Conchoraptor*"), is paradoxical in that reported specimens are numerous, and yet few are figured and described in the literature. The current situation is problematic, yet represents a rare opportunity for population-level character sampling if more specimens of *Conchoraptor* can be carefully described. The taxon was originally erected by Barsbold (1986), who refers to a nearly complete holotype skull and scattered postcranial material (IGM-D 100/20). Unfortunately, this text is difficult to source with an English translation and the specimen is poorly figured. Osmólska et al. (2004) list a partial skeleton with a skull, four partial skulls, and fragments of both cranial and postcranial material but does not include specimen numbers. A schematic drawing of a skull is also included, but there is no reference to the material on which it is based (Osmólska et al., 2004: fig. 8.1G). Another plate features line drawings of appendicular material from the holotype that is based on the sketches of Barsbold (1986). Funston (2018) provides the most recent description of the holotype cranial material accompanied by high-quality figures, but notes that it is poorly preserved, having been subjected to a preservative lacquer that has caused irreparable damage to delicate surface features. An incomplete cranial specimen, Zpal Mg-D 1/95, is briefly described, but those analyses were focused on endocranial and sinus morphology (Kundrát, 2007; Kundrát and Janáček, 2007, respectively). One of the specimens described in this paper, IGM 100/3006, is included in recent endocast studies (Balanoff et al., 2013, 2014, 2018), and tangentially in a comparative work (Norell et al., 2018), but those analyses did not necessitate a comprehensive description of all skeletal material.

The primary objective of this work is to provide detailed comparative descriptions of two exceptionally preserved specimens of *Conchoraptor*, IGM 100/3006 (MPC-D 100/3006) and IGM 100/1203 (MPC-D 100/1203) that were collected on the 1997 joint expedition of the American Museum of Natural History and the Mongolian Academy of Science (figs. 1–6). Similar to previous classic oviraptorosaur descriptions (e.g., Clark et al., 2002; Balanoff et al., 2009; Balanoff and Norell, 2012), this work includes extensive photographs of cranial and postcranial material as well as CT visualizations of internal skull anatomy. It is our aim to help compensate for the historically poor documentation of *Conchoraptor* fossils, and we hope that it will be of use in future works as a repository of high-resolution phylogenetic data.

A second objective is to address the unfortunate case of deep-set taxonomic conflation that exists between *Conchoraptor* and *Heyuannia yanshini* (originally *Ingenia yanshini*) (Barsbold,

1983). Both are small-bodied oviraptorids that suffer from poor descriptive coverage; however, the true source of confusion lies in the pervasive reference to a "chimera" mount that mixes the holotype cranium of *Conchoraptor* with multiple postcranial specimens of *H. yanshini*. These scattered finds include the *H. yanshini* holotype (IGM-D 100/30) and two other individuals (IGM-D 100/31 and IGM-D 100/32), all recovered by Barsbold (1983). Understandably, continued reference to this mount (e.g., Osmólska et al., 2004) has caused a misunderstanding in the research community as to exactly what material exists for each taxon and what features, if any, differentiate them. We also take the opportunity to present observations that aid in the differentiation of *Conchoraptor* and *Khaan mckennai* (Clark et al., 2001; Balanoff and Norell, 2012), another small bodied, crestless oviraptorid from the Nemegt Basin.

MATERIALS AND METHODS

Geologic Setting: IGM (Geological Institute of Mongolia, Ulaan Baatar) 100/3006 and IGM 100/1203 were collected adjacent to one another from the Baruungoyot Formation at the Khulsan locality, Gobi Desert, Mongolia (see Fanti et al., 2018), between 24 and 26 July 1997. The lithology of this locality is Late Cretaceous in age and is comprised of a well-sorted red sandstone. The environment at the time of deposition has been interpreted as aeolian dunes with interdune deposits (Gradziński and Jerzykiewicz, 1974a, 1974b). The specimens were likely killed together in a dune collapse as is typical of other fossils that have been recovered from similar Mongolian localities.

Materials: IGM 100/3006 consists of an isolated braincase, partial rostrum, and a nearly complete, disarticulated postcranial skeleton. This specimen, however, lacks the forelimb and parts of the vertebral column. IGM 100/1203 is a nearly complete, articulated postcranial skeleton. The skull of IGM 100/1203 is not preserved.

CT Scanning: The braincase of IGM 100/3006 was scanned in 2006 on the GE eXplorer Locus *in vivo* Small Animal MicroCT Scanner at the MicroCT Facility at Ohio University. IGM 100/3006 was scanned along the coronal axis for a total of 550 slices at an image size of 1024 × 1024 pixels. The voxels are cubic with a length of 0.092 mm. Although the contrast between matrix and bone in the original scan images is poor, sutural contacts and the morphology of internal spaces are visible.

All slice data and additional animations of the specimen are available on Morphosource (https://www.morphosource.org/concern/media/000589149?locale=en). Institutional and anatomical abbreviations are listed in the appendix.

Comparisons and Phylogenetic Analysis: Comparisons of anatomical variation between relevant taxa are established based on published descriptions and on the personal observation of specimens housed in museum collections (table 1). Citations for anatomical observations sourced from published works will follow the initial mentioning of a taxon unless otherwise noted.

The specimens described here were scored according to the recent and comprehensive oviraptorosaur character matrix of Atkins-Weltman et al. (2024) (based on the original matrix

TABLE 1. Citations for anatomical comparisons of oviraptorosaur taxa.

Species	References
Citipati osmolskae	Clark et al., 2002; Norell et al., 2018
Khaan mckennai	Clark et al., 2001; Balanoff and Norell, 2012
Incisivosaurus gauthieri	Xu et al., 2002, Balanoff et al., 2009
Gigantoraptor erlianensis	Xu et al., 2007
Caudipteryx zoui	Ji et al., 1998; Zhou and Wang, 2000
Chirostenotes pergracilis	Currie and Russel 1988; Funston and Currie, 2021
Epichirostenotes currei	Sues, 1997
Heyuannia huangi	Lü, 2002; Lü, 2005
Nemegtomaia barsboldi	Lü et al., 2004; Fanti et al., 2012
Microvenator celer	Makovicky and Sues, 1998
Banji long	Xu and Han, 2010
Avimimus portentosus	Kurzanov, 1981, 1985
Similicaudipteryx yixianensis	He et al., 2008
Heyuannia yanshini	personal observation by A.M.B. IGM-D 100/30, Funston et al., 2018
Conchoraptor gracilis	personal observation IGM 100/20; Barsbold, 1986; Kundrát, 2007; Kundrát and Janáček, 2007; Funston et al., 2018
Nomingia gobiensis	Barsbold, et al., 2000
Caenagnathus	Currie et al., 1993
Nankangia jiangxiensis	Lü et al., 2013b
Yulong mini	Lü et al., 2013b; Wei et al., 2022
Wulatelong gobiensis	Xu et al., 2013
Rinchenia mongoliensis	personal obs. IGM 100/32; Barsbold, 1997, Funston et al., 2018
Tongtianlong limosus	Lü et al., 2016
Ganzhousaurus nankangensis	Wang et al., 2013
Corythoraptor jacobsi	Lü et al., 2017
Oksoko avarsan	Funston et al., 2020a; Funston, 2024

of Funston et al., 2020a. We performed two analyses. The first included IGM 100/3006 and 100/1203 as a separate taxon "*Conchoraptor_New*," scoring only characters that could be ascertained from those fossils. In the second analysis, characters that could not be scored in our new fossils were filled in by those available in the original scoring of *Conchoraptor*, which was subsequently pruned prior to analysis. Our scoring of *Conchoraptor* modified the states of three previously published characters: 51 (1 to 2), 58 (- to 1), and 59 (1 to 0). We were able to score 14 characters that were previously unscored for *Conchoraptor*: 45 (0 to 1), 53 (? to 1), 112 (? to 1), 172 (? to 0), 173 (? to 0), 187 (? to 0), 207 (? to 0), 208 (? to 1), 209 (? to 1), 211 (? to 0), 212 (? to 0), 238 (? to 1), 239 (? to 1), and 240 (? to 0). Both analyses were run with the fol-

lowing parameters: All characters were treated as unordered and of equal weight. The matrix includes 42 taxa (43 in analysis 1) and 246 characters. To construct our consensus trees, we performed a maximum parsimony analysis in TNT v1.6 (Goloboff and Morales, 2023). First, a traditional search was conducted with random seed set to 1 and with 10,000 replications. Our most parsimonious trees were then subjected to a second round of TBR branch swapping. Strict consensus trees were generated using the in-built functions of TNT 1.6. Bremer support values were generated from existing suboptimal trees using the in-built functions of TNT 1.6 and with 'Retain trees suboptimal by' set to 15 steps.

CRANIAL DESCRIPTION

Only IGM 100/3006 has associated cranial material, consisting of a braincase, partial rostrum, and partial mandible (figs. 1, 2, 4–12). The braincase includes the paired postorbital, laterosphenoid, prootic, squamosal, quadrate, exoccipital, pterygoid, quadratojugal, jugal, and epipterygoid, as well as the midline basioccipital and supraoccipital (figs. 1, 2, 5). The frontal and parietal are in articulation with the chondrocranial portion of the braincase. Many of these elements have been slightly displaced from their original position because of mediolateral compression, but they lack any type of plastic distortion. Their unfused nature may be an indication that this specimen is skeletally immature, although it also allows a detailed description of each individual element.

The braincase of IGM 100/3006 has a flat calvarium with no obvious crest or ornamentation on the dorsal surface, similar to other crestless oviraptorids such as *Khaan*, *H. yanshini*, *Heyuannia huangi* (Lü, 2002, 2005), *Yulong mini* (Lü et al., 2013a; Wei et al., 2022), *and Tongtianlong limosus* (Lü et al., 2016). The flat skull roof most closely approaches the morphology apparent in *H. yanshini* (IGM-D 100/30 Barsbold, 1983; Funston, 2018) and differs considerably from the rounded, dome-shaped roof of *Khaan* (Balanoff and Norell, 2012: fig. 5) and *Tongtianlong*. As in all known crestless oviraptorosaur taxa, only a weakly developed sagittal crest extends along the midline of the dorsal surface of the parietal. The supratemporal fenestra is anterodorsally elongate (fig. 2A). The transverse nuchal crest is well developed and rises above the skull table. This morphology produces a 90° angle between the dorsal and occipital surfaces of the braincase. This is potentially an autapomorphic character for *Conchoraptor*, as this occipital-dorsal transition is made at an obtuse angle in most oviraptorids (see Discussion).

The occipital surface of IGM 100/3006 faces somewhat posterodorsally but diverts little from the vertical plane (figs. 1D, 5). This condition is present in most oviraptorosaurs (Osmólska et al., 2004) but contrasts with the more oblique angle apparent in *Citipati osmolskae* (IGM 100/978; Clark et al., 2002; see also Norell et al., 2018) and the completely vertical orientation in the caenagnathid *Epichirostenotes currei* (ROM 43250; Sues, 1997: fig. 3B). A weakly developed, longitudinal nuchal crest spans the length of the supraoccipital from the transverse nuchal crest to the foramen magnum. The shape of the foramen magnum cannot be determined in IGM 100/3006 because the exoccipitals, which form its lateral edges, are displaced. The occipital condyle is oval and transversely elongate (figs. 1D, 5). It is made up almost exclu-

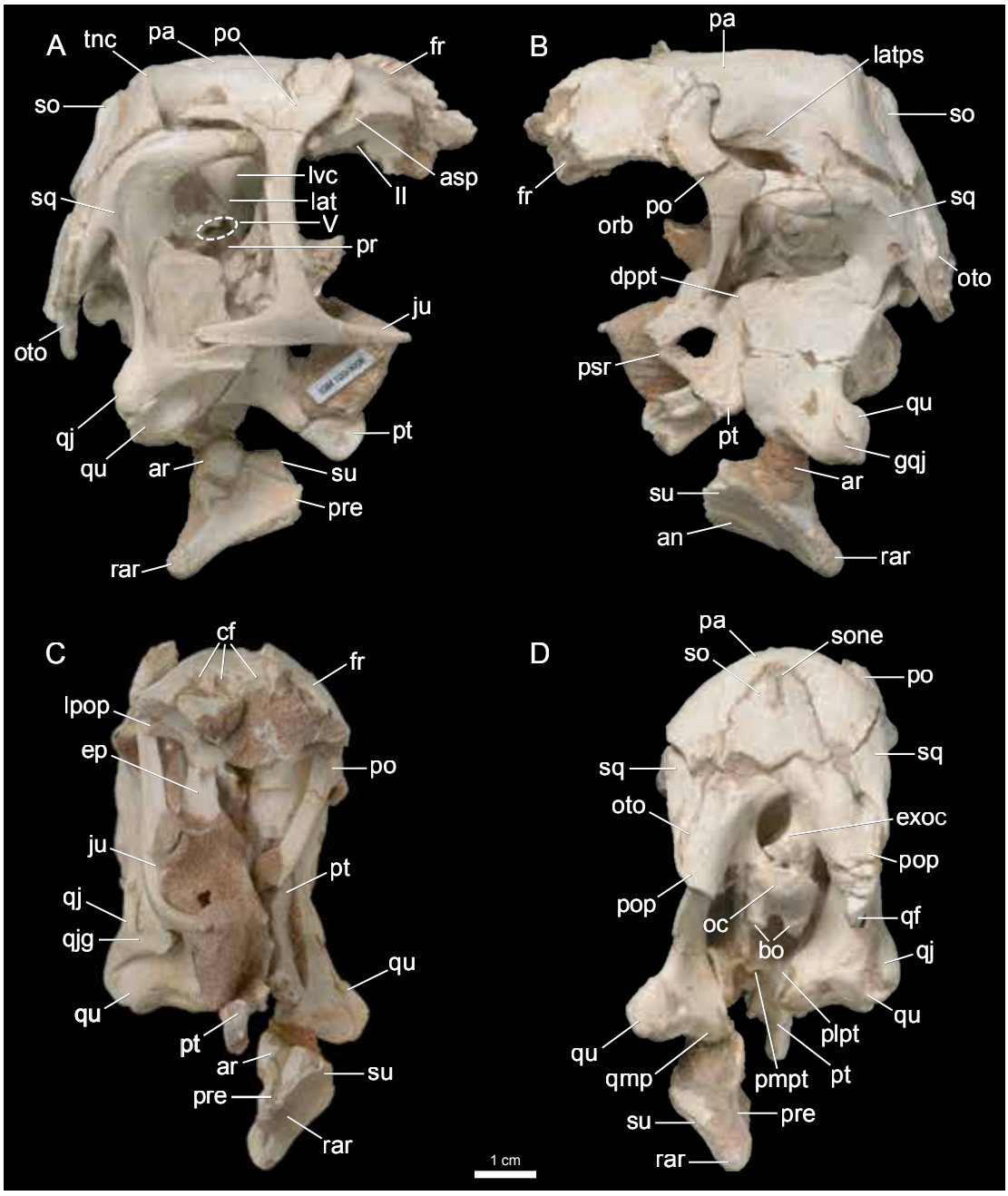

FIGURE 1. Cranium of IGM 100/3006 in **A,** right lateral, **B,** left lateral, **C,** anterior, and **D,** posterior view. See appendix for anatomical abbreviations.

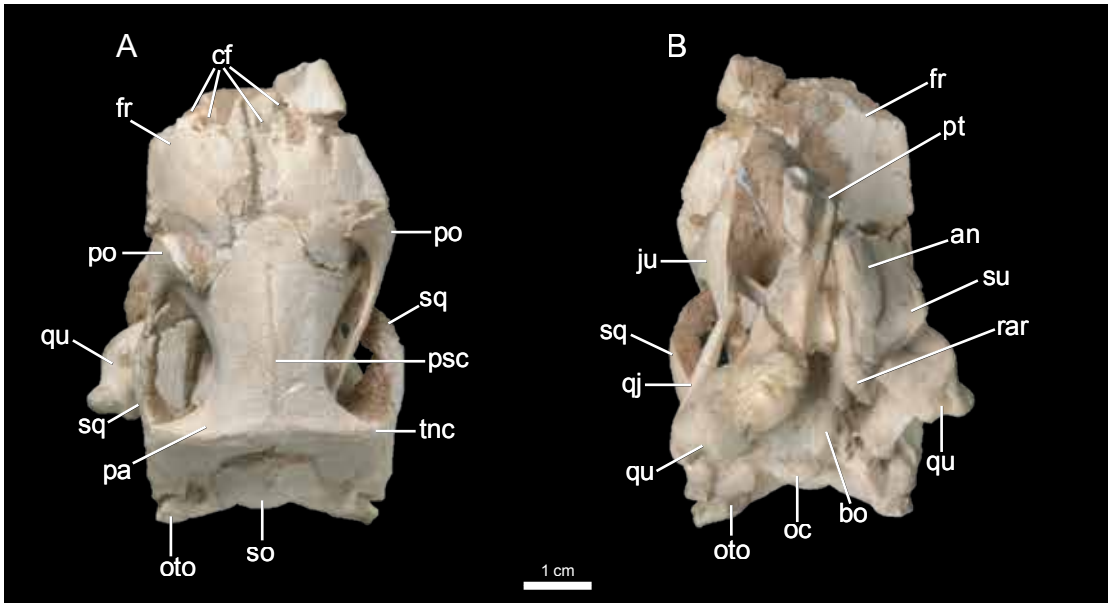

FIGURE 2. Cranium of IGM 100/3006 in **A,** dorsal and **B,** ventral view. See appendix for anatomical abbreviations.

sively of the basioccipital with a small dorsolateral contribution from the paired exoccipital. The neck of the condyle lacks constriction, as in most oviraptorosaurs (Osmólska et al., 2004). *Avimimus portentosus* (Kurzanov, 1981; 1985; Vickers-Rich et al., 2002) and *Epichirostenotes*, however, have a ventral constriction. The neck of the condyle is rostrocaudally short, unlike in *Citipati*, which has an autapomorphic condition wherein the neck extends markedly past the occipital surface of the skull (Clark et al., 2002: fig. 3). The articular surface of the condyle of IGM 100/3006 also lacks the distinct central depression present in *Citipati*. The squamosal, opisthotic and exoccipital form the ventrally curving, pendant-shaped paraoccipital process (see exoccipital description for more detail).

The lateral surface of the braincase is best preserved on the right side (fig. 1A). The lateral temporal fenestra is rectangular, being taller than it is wide. The fenestra has rounded edges, the most exaggerated of which is the posterodorsal corner formed entirely by the squamosal. A similar shape is present in most oviraptorosaurs, including *Incisivosaurus* (Xu et al., 2002; Balanoff et al., 2009), *Khaan*, *Rinchenia mongoliensis* (Barsbold, 1997; Funston et al., 2018), *Nemegtomaia* (Lü et al., 2004; Fanti et al., 2012), and *Oksoko avarsan* (Funston et al., 2020a; Funston, 2024) however, the angle of the posteroventral corner of the lateral temporal fenestra in *Conchoraptor* and all the aforementioned taxa is wider (~90°) than in *Citipati* (~60°). A large wing comprised of the otic process of the quadrate and the pterygoid forms the medial wall of the lateral temporal fenestra, as it does in all known oviraptorosaurs (Osmólska et al., 2004; Balanoff et al., 2009; Balanoff and Norell, 2012). The epipterygoid, as in *Citipati* (Clark et al., 2002: fig. 2), makes a substantial contribution to the anterior margin of this structure. This wing extends anteriorly to the jugal process of the postorbital, therefore covering the majority of the lateral surface of the brain-

TABLE 2. Cranial measurements of IGM 100/3006 (in mm).

Premaxilla height (below naris)	20.9
Frontal length	16.7
Parietal length	31.2
Infratemporal fenestra width	22
Infratemporal fenestra height	22
Supratemporal fenestra width	8.1
Supratemporal fenestra length	18.6
Braincase Length	59.1
Skull width at temporal fossa	16.1
Supratemporal fenestra width	7.1
Supratemporal fenestra length	19.3
Braincase width at postorbital process	33.3
Braincase width at nuchal crest	33.3
Lateral temporal fossa height	28.7
Lateral temporal fossa width	21.6
Braincase height from quadrate to nuchal crest	55.8
Foramen magnum height (dorsoventral)	10

case and obscuring almost all morphology posterior to the trigeminal foramen. The posterior margin of the wing is overlapped laterally by the ventral extension of the squamosal.

The ventral surface of the braincase of IGM 100/3006 is largely covered by the extensive, winglike pterygoid, leaving the basioccipital as the only visible element (fig. 1E).

Premaxilla

Figures 3, 4

The left premaxilla is disarticulated from the braincase of IGM 100/3006 and is present in the jacket of IGM 100/1203 (figs. 3, 4). Because the right element is not exposed, it is impossible to tell whether the paired elements were fused as in the oviraptorids *Citipati*, *Tongtianlong*, and the Zamyn Khondt oviraptorid (IGM 100/79) (Funston, 2019; fig. 4.13) or unfused as in the more basally diverging oviraptorosaurs *Caudipteryx* and *Incisivosaurus*. Although only the anteroventral margin of the external naris is visible, it was likely elliptical as defined by the nasal process of the premaxilla.

The nasal process of the premaxilla sweeps posterodorsally and likely would have contacted the premaxillary process of the nasal, which is missing in IGM 100/3006 (fig. 4). The angle of ascent of the nasal process is shallow and most closely approximates that of *Khaan* and *Gobiraptor minutus* (Lee et al., 2019) as opposed to the almost vertical orientation of the process in

FIGURE 3. IGM 100/1203 in dorsal view.

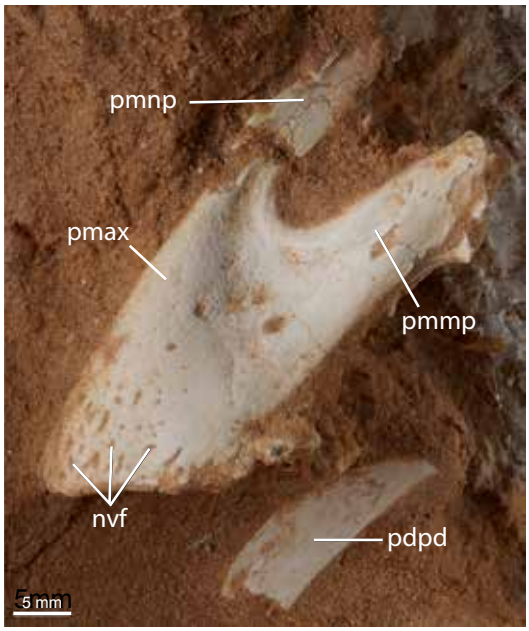

FIGURE 4. Disarticulated distal rostrum of IGM 100/3006. See appendix for anatomical abbreviations.

Citipati, *Oksoko*, *Rinchenia*, and the Zamyn Khondt oviraptorid. The maxillary process of the premaxilla extends posterodorsally at a lower angle (30°) and would have contacted the descending process of the nasal, thus delimiting both the posteroventral margin of the external naris and the anterodorsal margin of the antorbital fossa—effectively excluding the maxilla from participating in the margin of the external naris, as in most oviraptorids. A slight depression marks the lateral surface of this process as was described by Kundrát and Janáček (2007). The lateral surface of the premaxilla overall is pneumatized with several neurovascular foramina that occur dorsal to the lingual margin, as in most oviraptorids (e.g., *Citipati*, *Khaan*, and *Corythoraptor jacobsi* (Lü et al., 2017). These foramina would likely have transported sensory nerve fibers (CN V) and arterial branches to a keratinous beak in life. The occlusal margin of the "beak" is edentulous and, based on the exposed surface, likely would have been U-shaped in ventral view as in most oviraptorosaurs. The triturating surface is rugose due to taphonomic wear.

Frontal

Figures 1, 2, 7–9

The frontal is most completely preserved on the right side of IGM 100/3006 (fig. 1A). In dorsal view the element is roughly rectangular and tapers slightly anteriorly (fig. 2A). The abbreviated length of the frontals in *Conchoraptor* and *Khaan* (~1/4 the length of the parietal; table 2) differs from that seen in other oviraptorosaurs such as *Incisivosaurus*, *Caudipteryx*, and the oviraptorid *Citipati*, in which the frontals are at least half the length of the parietal. The midline contact between the opposing frontals is weakly fused, however, the left frontal is displaced slightly dorsally, revealing a minor degree of interdigitation. The parietal overlaps the frontal dorsally (fig. 7D) and forms a sinuous, saddle-shaped contact with the anteriormost margin of the suture at the midline (fig. 2A). This distinct suture shape is similar to that of *Khaan* but differs from that of *Citipati*, which has a straight, posterolaterally angled (starting at the midline) contact with the parietals (see Clark et al., 2002: fig. 5). The postorbital in IGM 100/3006 overlaps the dorsolateral surface of the frontal posterolaterally, and a small, circular articular surface for the postorbital is visible at the frontoparietal contact in line with the supraorbital margin (fig. 1A). The ventral edge of the frontal is excluded from the supratem-

poral fenestra by the anterior process of the postorbital (fig. 2A), as in *Khaan. Incisivosaurus*, *Citipati*, and *Oksoko* all have a frontal contribution to the anterior border of the supratemporal fenestra. Maniraptorans outside of Oviraptorosauria also typically possess a frontal contribution to the supratemporal fenestra (Clark et al., 1994; Norell et al., 2006, 2009).

The anteriormost region of the dorsal surface of the frontal in IGM 100/3006 is rugose and possesses the small, circular "fenestrae" (figs. 1C, 2A) described by Osmólska et al. (2004) as present in most oviraptorosaurs (although they are lacking in the basally diverging oviraptorosaur *Incisivosaurus*). These openings connect to the pneumatic frontal sinus described below, as indicated by CT data (fig. 7D). The same connections are visible in *Khaan* (IGM 100/973; IGM 100/1127), *Citipati* (IGM 100/978), and previously described specimens of *Conchoraptor* (ZPAL MgD-I/95; Kundrát and Janáček, 2007).

In lateral view the frontal is rectangular and dorsoventrally deep at the frontal-parietal suture, tapers slightly anteriorly, and expands again at its anterior edge (fig. 1A, B). The dorsoventral depth of the frontal does not reach the extent observed in *Corythoraptor*, *Rinchenia*, and *Oksoko*, wherein the element is integrated into a pronounced cranial crest. The dorsolateral edge of the frontal forms the majority of the supraorbital margin, and the dorsal and medial walls of the orbit are formed by the ventral extension of the frontal. The small, laterally abbreviated postorbital process is comprised of the posterolateralmost part of the frontal, the postorbital, and the laterosphenoid.

CT data are able to reveal some pertinent features of the internal morphology of the frontal of IGM 100/3006. A pneumatic frontal sinus runs anteroposteriorly along the midline of the element, similar to that observed in *Citipati* (IGM 100/978; Clark et al., 2002), *Khaan* (IGM 100/973; Balanoff and Norell, 2012), and a previously described specimen of *Conchoraptor* (ZPAL MgD-I/95, Kundrát and Janáček, 2007) (fig. 7D). *Incisivosaurus*, however, lacks this enlarged sinus. A medial septum divides the frontal sinus as it does ZPAL MgD-I/95 (Kundrát and Janáček, 2007) and *Khaan*. Although a septum was previously reported by Clark et al. (2002) as absent in *Citipati*, more recent CT data also show its presence (Balanoff, 2011). While the anterior extent of this paired pneumatic cavity cannot be determined in IGM 100/3006, it fails to penetrate the parietals. In ZPAL MgD-I/95 the cavity extends anteriorly into the nasals, also failing to enter the parietals (Kundrát and Janáček, 2007: fig. 3).

Parietal

Figures 1, 2, 7–11

The paired parietals are fused at the midline into a single, anteroposteriorly elongate element. In dorsal view the element has an hourglass shape, expanding posterolaterally, tapering anteriorly to form the medial and posterior portion of the supratemporal fossa, and expanding again anterolaterally at the frontoparietal contact to contribute to the small postorbital process (fig. 2A). This morphology is present in both *Incisivosaurus* and *Khaan*. It diverges from the condition of *Yulong*, *Citipati*, and *Rinchenia*, which lack a postorbital expansion and exhibit a strongly tapered anterior process that contacts the posterior margin of the frontals. The pos-

terolateral expansion of the parietal in is the lateralmost extent of the element, as in *Citipati*, *Incisivosaurus*, and *Khaan*.

No ornamentation is present on the dorsal surface of the parietal in IGM 100/3006 as there is in *Rinchenia* and possibly *Oviraptor* (Osborn, 1924; Barsbold, 1986; Clark et al., 2002). A weakly formed sagittal crest runs along the midline, expanding transversely at the posteriormost edge to form the transverse nuchal crest which, although weakly developed compared to other coelurosaurs, is well developed in comparison to other oviraptorosaurs such as *Incisivosaurus*, *Khaan*, and *Citipati* (fig. 2A).

The lateral surface of the parietal is obscured by the overlapping squamosal and laterosphenoid (fig. 1A, B). Nonetheless, it forms the majority of the medial surface of the supratemporal fossa, with a very minor contribution from the posterior margin of the laterosphenoid. Posterolaterally the parietal abuts the squamosal in a straight, posteroventrally oriented contact that extends onto the occipital surface. This condition is also present in *Citipati*, *Incisivosaurus*, and *Khaan*. The left laterosphenoid in IGM 100/3006 is displaced, so that its articular surface on the parietal—a large, roughened, anteroposteriorly elongate surface—is visible (fig. 1B). The ventral part of the parietal abuts the dorsal edge of the prootic, preserved on the left side of IGM 100/3006 (fig. 1B). This region of the parietal lacks the depression for the dorsal tympanic recess that is present in *Incisivosaurus*, *Citipati*, *Khaan*, as well as several maniraptorans outside of Oviraptorosauria (see Currie and Zhao, 1993; Xu et al., 2002; Norell et al., 2006). The frontal process of the postorbital overlies a small portion of the anterolateral margin of the parietal (fig. 1A, B). This condition is divergent from that of *Citipati*, *Incisivosaurus*, and *Khaan*, wherein there is no overlap.

The flat occipital surface of the parietal is featureless and surrounds the lateral margins of the supraoccipital (fig. 1D). Similar to other archosaurs, the junction of the parietal, supraoccipital, exoccipital, and squamosal forms the opening for the external occipital vein to exit the cranium. This foramen is large and the sulcus for the path of the vein can be observed on the internal surface of the parietal in the CT data (figs. 7A, 8B, C).

Jugal

Figures 1, 2, 9–12

The jugal is preserved only on the right side of IGM 100/3006 (fig. 1A). The anterior (maxillary) process tapers anteriorly and forms the ventral margin of the orbit. The general morphology of the jugal falls between the dorsoventrally expanded, "straplike" condition of *Incisivosaurus* and *Oksoko* and the slender, more gracile condition observed in *Citipati*, *Khaan*, and *Yulong*. The ascending (postorbital) process contacts the postorbital and, similar to most other oviraptorids, both elements extend almost the entire dorsoventral height of the lateral temporal fenestra (Norell et al., 2006; Turner et al., 2012; fig. 1A). This is unlike the morphology of *Incisivosaurus*, *Yulong*, *Banji long* (Xu and Han, 2010), *and Tongtianlong*, however, wherein the jugal and postorbital contribute equally, each extending about one-half the height of the fenestra. The ascending process of the jugal in IGM 100/3006 is oriented almost verti-

cally (making the anteroventral angle of the lateral temporal fenestra slightly less than 90°), as it is in most oviraptorosaurs. This angle differs from the plesiomorphic condition for Maniraptora in which the postorbital process of the jugal slants further posteriorly to form a more acute angle (see Currie, 1995; Burnham et al., 2000). The posterior (quadratojugal) process of the jugal sits in a shallow groove on the dorsal surface of the quadratojugal that, because of a slight medial displacement of the jugal, is visible in IGM 100/3006 (fig. 1A). These elements form the ventral margin of the lateral temporal fenestra. The posterior process of the jugal forms the anterior two-thirds of the fenestra and tapers posteriorly as in *Khaan*, but unlike Incisivosaurus, *Citipati*, *Banji*, *Yulong*, *Tongtianlong*, and *Oksoko* wherein this process extends only halfway along the margin. The mediolaterally compressed, tapering morphology of the posterior process differs from the more rodlike morphology in other oviraptorids such as *Citipati*, *Rinchenia*, and *Khaan* as well as the basal oviraptorosaur *A. portentosus*. CT imagery shows that the jugal is hollow, with a slender canal running the length of each process (fig. 9D); however, there is no pneumatic foramen in the jugal as in more basal coelurosaurs (see Brochu, 2003).

Postorbital

Figures 1, 2, 5, 8–12

The triradiate postorbital is preserved on both sides of IGM 100/3006 (fig. 1A, B). The frontal (anterior) process of the postorbital is strongly dorsomedially curved, and overlaps the frontal, parietal, and laterosphenoid. Although this morphology is present in most oviraptorosaurian taxa including *Banji*, *Yulong*, *Citipati*, *Khaan* (Holtz, 1998), and *Oksoko*. The process in the basal oviraptorosaur *Incisivosaurus* differs substantially by following the contour of the orbit not curving dorsally. The other extreme can be seen in *Rinchenia* and *Oksoko* in which the frontal process forms a 90° angle with the squamosal process (Barsbold, 1986; Osmólska et al., 2004; Funston et al., 2020a; Funston, 2024).

As in all oviraptorosaurs, the ventral two-thirds of the ventral (jugal) process is grooved posteriorly for the reception of the jugal, and together these elements form the complete postorbital bar, which is present only on the right side of IGM 100/3006 (fig. 1A). Based on the articulation surface on the dorsal process of the jugal, the ventral process of the postorbital would have formed almost the entire posterior margin of the orbit. This condition has been proposed as a *Conchoraptor* autapomorphy (Funston et al., 2018) (see Discussion).

The posterior (squamosal) process of the postorbital is straight and overlies the squamosal, forming the lateral margin of the anteroposteriorly elongate supratemporal fossa (fig. 2A) and the dorsal margin of the lateral temporal fenestra (fig. 1A). This overlap is dorsal in *Conchoraptor* (IGM 100/3006 and IGM 100/20), *Incisivosaurus*, and *Citipati* (Barsbold, 1986), but in *Rinchenia* the squamosal process is positioned more laterally (Osmólska et al., 2004: fig. 8.1E). The postorbital extends almost the entire anteroposterior length of the supratemporal fossa as it does in most other oviraptorosaurs. The crested oviraptorids *Citipati*, *Corythoraptor*, *Rinchenia*, and *Oksoko*, however, possess a squamosal process that extends only half the length of the fenestra (Barsbold, 1986).

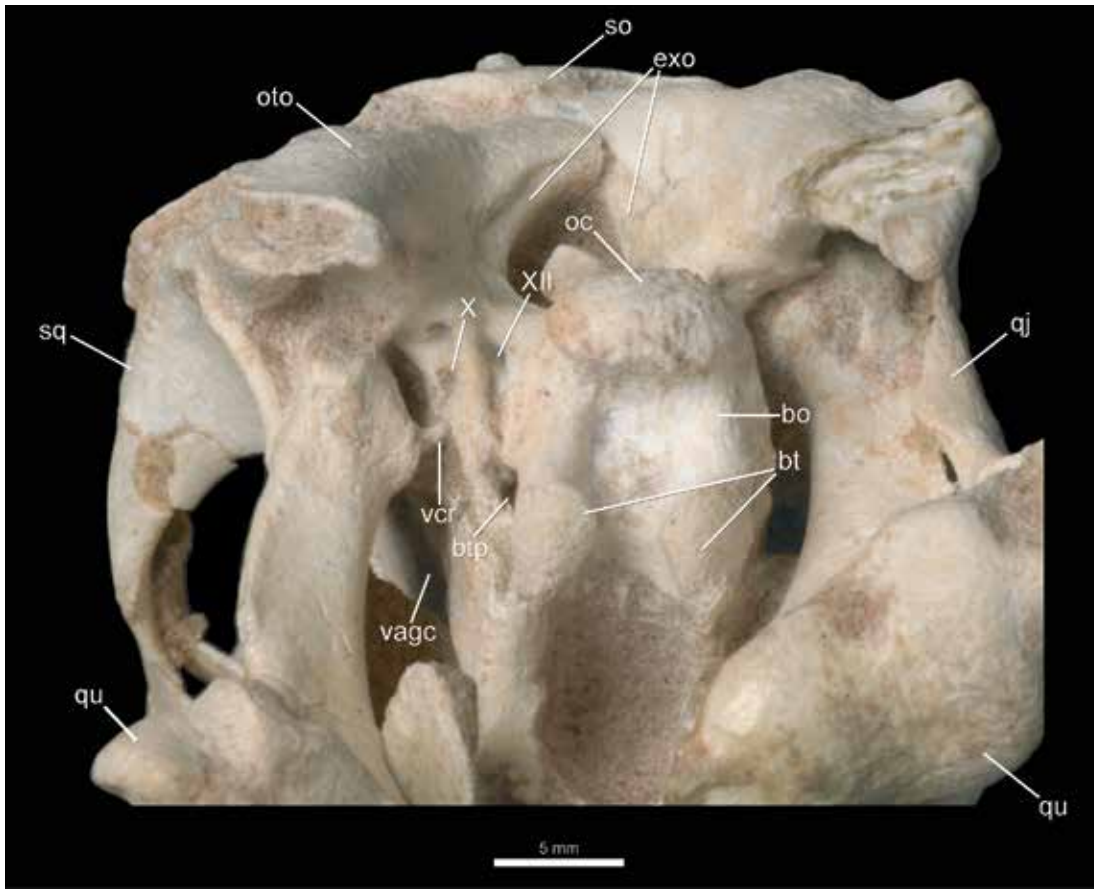

FIGURE 5. Occipital region of IGM 100/3006 in oblique ventral view. See appendix for anatomical abbreviations.

Squamosal

Figures 1, 2, 5, 9–12

The squamosal of IGM 100/3006 is well preserved. It is a large, roughly triradiate element with an anterior and posterior process and an elongate, sheetlike descending process (figs. 1A, B). In dorsal view the anterior process of the squamosal contacts the postorbital to form approximately half the length of the lateral margin of the supratemporal fossa (fig. 2A). It is grooved laterally for the reception of the overlying postorbital. In lateral view, the anterior process extends the entire length of the lateral temporal fenestra, forming its dorsal margin (fig. 1A). This process is ventrally concave in lateral view and contacts the postorbital in a roughly horizontal orientation, similar to *Citipati*, *Khaan*, and *Oksoko*, but unlike *Incisivosaurus*, which exhibits a straight, anterodorsally oriented process.

The descending process of the squamosal is best seen in lateral view (fig. 1A, B). It is anteroposteriorly broad and divided into anterior and posterior rami. A connecting web of

FIGURE 6. Disarticulated mandible of IGM 100/3006 inside the jacket of IGM 100/1203 in left lateral view. See appendix for anatomical abbreviations.

bone extends between the anterior and posterior rami and overlaps a large region of the quadrate, likely yielding the articulation between these elements akinetic. The quadratojugal contact with the squamosal lies along the posterior surface of the descending process, and these elements make up the posterior margin of the lateral temporal fenestra. The squamosal contribution extends about two-thirds of the height of the fenestra, as in *Citipati* and *Khaan*, but unlike *Banji* wherein the squamosal contribution is restricted by a long dorsal process of the quadratojugal. This condition is also unlike that of *Yulong*, wherein the descending process contributes to only one-third the structure's length. The anterior ramus overlies the lateral surface of the prootic just posterior to the trigeminal foramen (fig. 1A). This extension is not present in coelurosaurs outside of Oviraptorosauria nor in more basally diverging members like *Incisivosaurus*. In occipital view, the contact of the squamosal with the parietal begins approximately midway along the length of the squamosal and curves posteroventrally onto the paraoccipital process (fig. 1D). CT data indicate that the entire squamosal is highly pneumatized, but it is unclear if this pneumatization is via the dorsal tympanic recess as it is in living birds (Kundrát and Janáček, 2007; fig. 11B).

Supraoccipital

Figures 1, 2, 5, 7, 8, 11

The roughly triangular supraoccipital forms the majority of the occipital surface of the skull (figs. 1D, 2A, 5). It is surrounded by the parietals laterally and the exoccipitals ventrally. These are the only contacts visible on the occipital surface, but CT data reveal that the endocranial surface of the supraoccipital also contacts the opisthotic at its ventrolateral margin (fig. 7A).

Based on the position of the left exoccipital, the ventral margin of the supraoccipital would have been excluded from the foramen magnum—the same configuration seen in *Citipati*. In *Incisivosaurus*, *Epichirostenotes*, *Banji*, *Oksoko*, the Zamyn Khondt oviraptorid, and likely *Khaan* the supraoccipital does contribute to this border. This relationship cannot be assessed

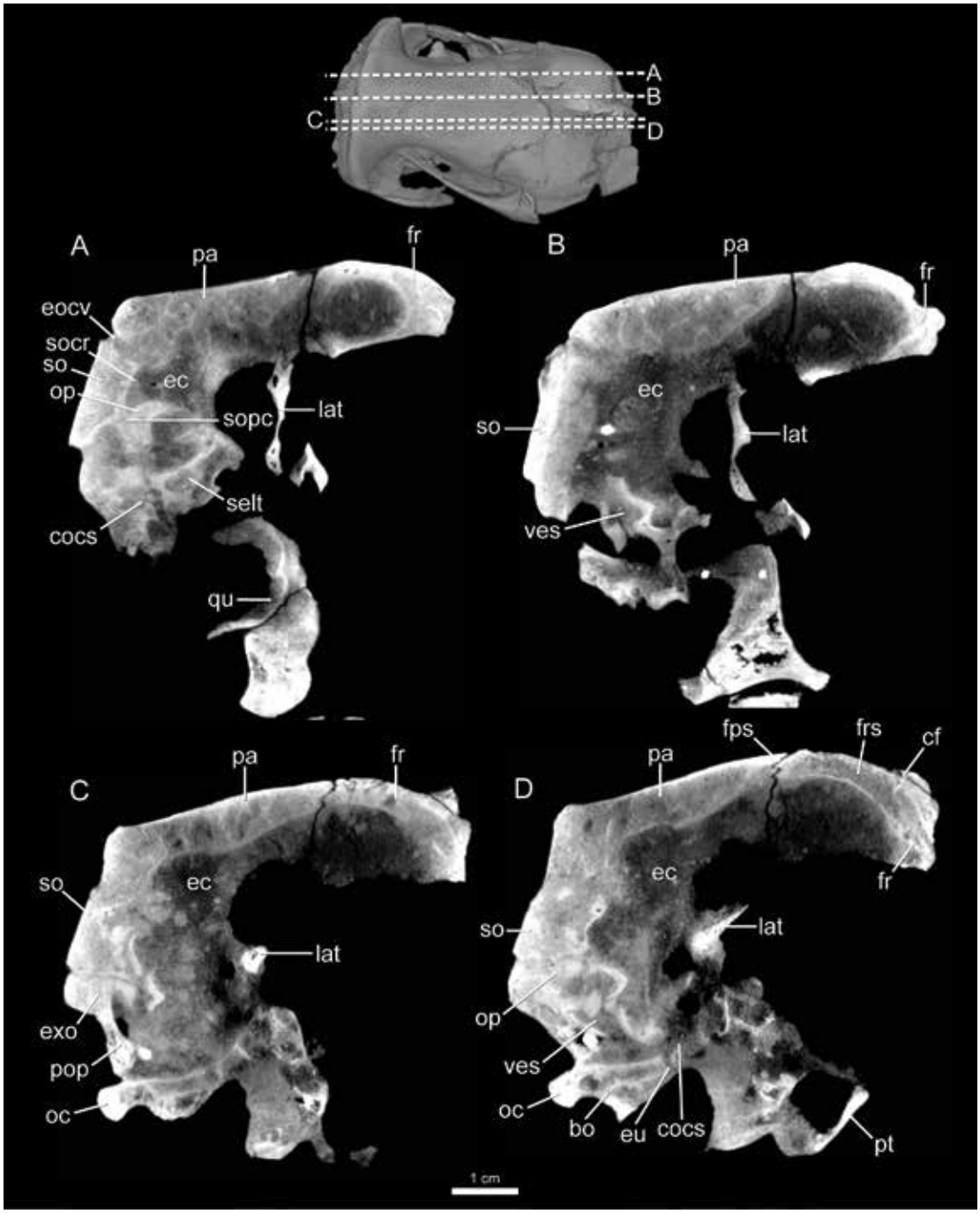

FIGURE 7. Sagittal CT slices through the cranium of IGM 100/3006. Volume rendering of specimen shows the location of slice plains. See appendix for anatomical abbreviations.

in ZPAL MgD-I/95 as the supraoccipital is not preserved in this specimen (see Osmólska, 1976, and Kundrát, 2007).

The external surface of the supraoccipital is slightly convex with a small, longitudinal nuchal eminence running along the midline (fig. 1D). This prominence extends from the dorsalmost edge of the supraoccipital to about the midheight of the element. A longitudinal nuchal eminence is also present in *Citipati* and *Khaan*—although in the latter, the eminence terminates at the dorsal margin of the magnum foramen. The endocranial surface, which is visible in the CT imagery, is deeply recessed to receive the posterodorsal extent of the cerebellum (fig. 7A). This fossa is a relatively shallow, V-shaped indention dorsally that widens ventrally.

Exoccipital

Figures 1, 5

The exoccipital makes up a large portion of the occipital surface of the skull (figs. 1D, 5). The right element is slightly displaced, but the left one remains in place. In occipital view (fig. 1D) the dorsomedial edge of the exoccipital fits into the curved ventral edge of the supraoccipital (see supraoccipital description). The lateral part of the element curves ventrolaterally to form the majority of the paraoccipital process, as in *Incisivosaursus*, *Citipati*, *Khaan*, and *Oksoko*. The paraoccipital process as a whole is oriented ventrolaterally and is roughly pendant shape, a character distributed throughout Oviraptorosauria (e.g., Sues, 1997; Clark et al., 2002; Xu et al., 2003; Norell et al., 2006; Balanoff et al., 2009; Balanoff and Norell, 2012) and other maniraptoran taxa (Norell et al., 2006; Turner et al., 2012). The paraoccipital process of *Conchoraptor*, similar to that of *Khaan* and *Incisivosaurus*, is slender and lacks the dorsoventral expansion seen in *Citipati* and *Epichirostenotes*. The process is extensively pneumatized by the caudal tympanic recess as in most coelurosaurs. The opening to this recess cannot be observed externally but is visible in the CT data (fig. 12A). The medial edge of the exoccipital makes up the lateral and dorsal margins of the foramen magnum to the exclusion of the supraoccipital (figs. 1A, 5). Displacement of the exoccipitals makes estimation of the size of this structure difficult, but it is undoubtedly larger than the occipital condyle—the lateral edge of the foramen extending laterally past the lateral edge of the condyle (fig. 1D). The displacement of the right exoccipital medially complicates reconstruction of this opening. Its dorsoventral depth, however, is at least as tall as it is wide, implying that it was probably not a mediolaterally wide ovoid as in *Khaan* and likely appeared more circular as in *Citipati*. The exoccipital contributes to the neck of the occipital condyle but is largely excluded from the condyle itself—an arrangement that also presents in *Citipati* and *Khaan*. In taxa outside of Oviraptoridae, such as *Incisivosaurus*, *A. portentotus*, and *Epichirostenotes*, the exoccipitals contribute a large portion to the occipital condyle (Kurzanov, 1981; 1985).

A shallow fossa on the occipital surface of the exoccipital lateral to the occipital condyle houses several openings, including two small foramina for the transmission of the hypoglossal nerve (CN XII) (fig. 5). These foramina are separated from a larger vagal foramen by a narrow crista. CT imagery shows the vagal canal leading into the adult remnant of the metotic fissure

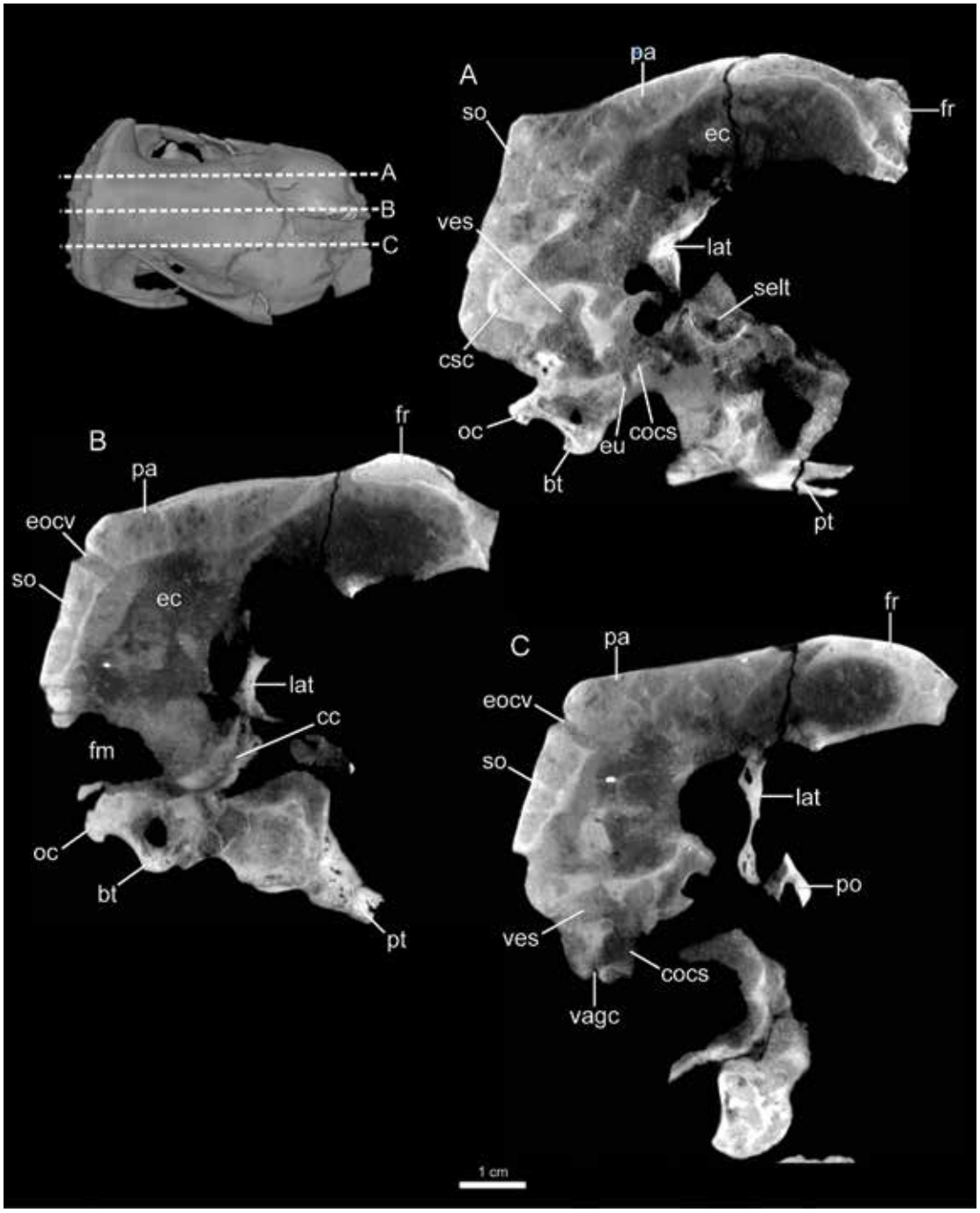

FIGURE 8. Additional sagittal CT slices through the cranium of IGM 100/3006. Volume rendering of specimen shows the location of slice plains. See appendix for anatomical abbreviations.

(fig. 8C). This canal likely transmitted the glossopharyngeal, vagus, and accessory cranial nerves (CN IX–XI) as well as the jugular vein, similar to the configuration in other coelurosaurs (Bever et al., 2013). The recessus scala tymapanae extends anteriorly and opens onto the lateral surface of the braincase as the fenestra pseudocochlearis (fig. 11D).

Opisthotic

Figure 7

The opisthotic is visible only in the CT slices (fig. 7A, D). These data show that it is fused to the exoccpital, forming an otoccipital, and shares contacts with the prootic anteriorly, epiotic anterodorsally, and exoccipital and supraoccipital posteriorly. The posterior and part of the horizontal semicircular canals run through the opisthotic.

Basioccipital

Figures 1, 2, 5, 7, 11

The basioccipital comprises the majority of the occipital condyle, with a small lateral contribution from the exoccipitals (fig. 2B). The straight contact between these elements runs along the dorsolateral surface of the basioccipital, remaining unfused in IGM 100/3006 (fig. 11D) The occipital condyle is oval, and wider than tall as it is in all observed oviraptorosaurs (Osmólska et al., 2004).

On the ventral surface of the basioccipital, the basal tubera, separated by a large depression, are short but distinct and oriented ventrally similar to the condition in *Khaan* (figs. 5, 8B, 9A, B, 11C). In contrast, the basal tubera of *Incisivosaurus*, *Epichirostenotes*, *Citipati*, and *Oksoko* are short but directed more ventrolaterally (Xu et al., 2003). In IGM 100/3006 the basal tubera are formed entirely by the basioccipital with no contribution from the basisphenoid. The pterygoids overlap the lateral surface of the basal tubera, a contact that is not apparent in any other oviraptorosaurs and thus is likely a result of taphonomic displacement of the pterygoids (fig. 1D). The lateral surface of the basal tubera is flat (not concave as in *Citipati*) and possesses a large pneumatic vacuity, communicating with the subotic recess (fig. 11C) (Kundrát and Janáček, 2007). These bilateral openings suggest that those in this same region of *Citipati* might not be due to breakage as first interpreted by Clark et al. (2002). The anterior extent of the basioccipital along the ventral surface of the braincase cannot be determined superficially because the overlying pterygoids obscure the ventral surface. CT imagery, however, shows that the basioccipital abuts the basisphenoid just anterior to the basal tubera in a flat contact (fig. 11C). Unlike *Citipati*, this contact is not fused, although this may be due to the skeletal immaturity of IGM 100/3006. The fusion of this contact in other oviraptorosaurs is difficult to determine due to poor preservation.

Parabasisphenoid

Figures 1, 7, 9–12

The fused parasphenoid and basisphenoid in IGM 100/3006 is not visible externally because of the anterodorsal slant of the braincase floor and the extensive palatal coverage of the pterygoid—two features present in all oviraptorosaurs (Barsbold, 1981; 1986; Elzanowski, 1999; Clark et al., 2002; Osmólska et al., 2004; Balanoff et al., 2009; Balanoff and Norell, 2012). Structures of the parabasisphenoid therefore are described using only CT imagery. The element is mediolaterally compressed and dorsoventrally tall. The suture between the basisphenoid and parasphenoid is not distinguishable. The parasphenoid rostrum is visible in lateral and anterior view (fig. 1A, C) and as in *Khaan* lacks the pneumaticity present in troodontids (Norell et al., 2009).

The basipterygoid processes are not easily identified in the CT images because, as in all oviraptorosaurs, they are extremely abbreviated a relative to other maniraptorans (Osmólska et al., 2004). The contact between the parabasisphenoid and the pterygoids accordingly lies nearly at the main body of the former element (fig. 11E).

The dorsolateral contact of the parabasisphenoid with the prootic lies at the level of the basisphenoid-basioccipital suture. The sella turcica sits at the anterior margin of the dorsal surface of the parabasisphenoid (figs. 7A, 8A, 9D, 12A, B). As previously mentioned, this region of the braincase is not well ossified, and the anterior wall of the fossa remains open as it does in other observed oviraptorosaurs including *Incisivosaurus*, *Citipati*, and *Khaan* (Franzosa, 2004; Balanoff and Norell, 2012). At the posterior margin of the sella turcica the cranial carotid canals open into the dorsum sellae (figs. 8B, 12A). Their path through the parabasisphenoid can be traced through the CT images beginning just posterior to the base of the parasphenoid rostrum on the ventral surface of the braincase and traveling dorsomedially. These canals do not anastomose within the parabasisphenoid as they do in some birds (Baumel and Witmer, 1993). An anastomosis is present in almost all coelurosaurs (Holtz, 1998) but is taxonomically variable (Baumel and Gerchman, 1968). The parabasisphenoid is highly pneumatized by the basisphenoid recess (fig. 9D) as in *Citipati*, *Oksoko*, and other maniraptorans (Witmer, 1997; Kundrát and Janáček, 2007; Bever and Norell, 2009; Bever et al., 2011, 2013).

Quadratojugal

Figures 1, 2, 5, 9–11

Only the right quadratojugal is preserved in IGM 100/3006. It is a roughly L-shaped element (fig. 1A) with a long ascending process, relatively short posteroventral (quadrate) process, and a mediolaterally thin jugal process that is approximately twice the length of the posteroventral process. This is a similar shape to all observed oviraptorids (e.g., Barsbold, 1986; Clark et al., 2002; Osmólska et al., 2004; Balanoff and Norell, 2012). The rounded quadrate process lies within the aforementioned groove on the lateral surface of the mandibular process of the quadrate. The length of the quadrate process varies considerably among oviraptorosaurs with *Citipati*, *Rinchenia*, *Nemegtomaia*, *Oksoko*, *and Banji* having a long, pronounced process (Bars-

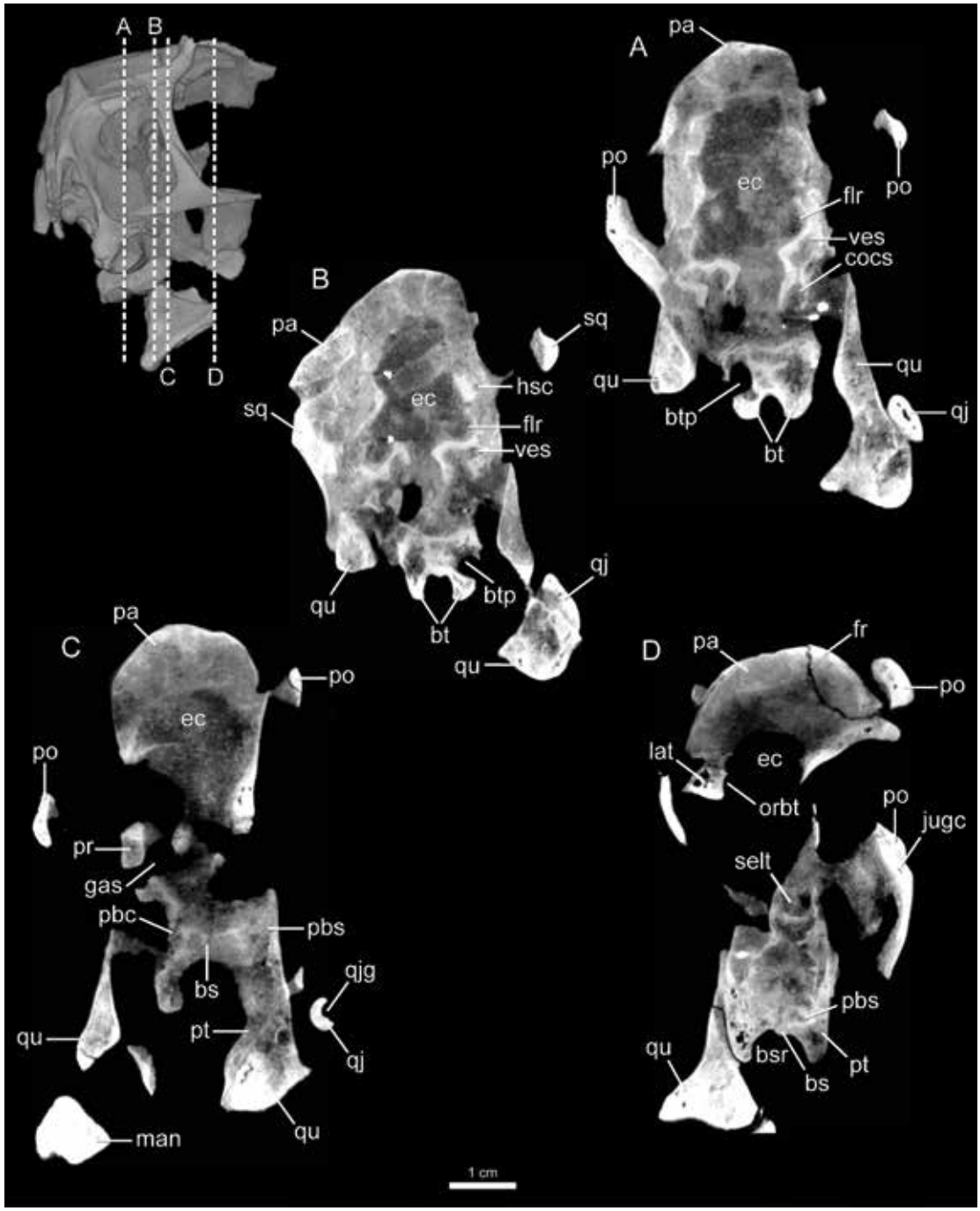

FIGURE 9. Coronal CT slices through the cranium of IGM 100/3006. Volume rendering of specimen shows the location of slice plains. See appendix for anatomical abbreviations.

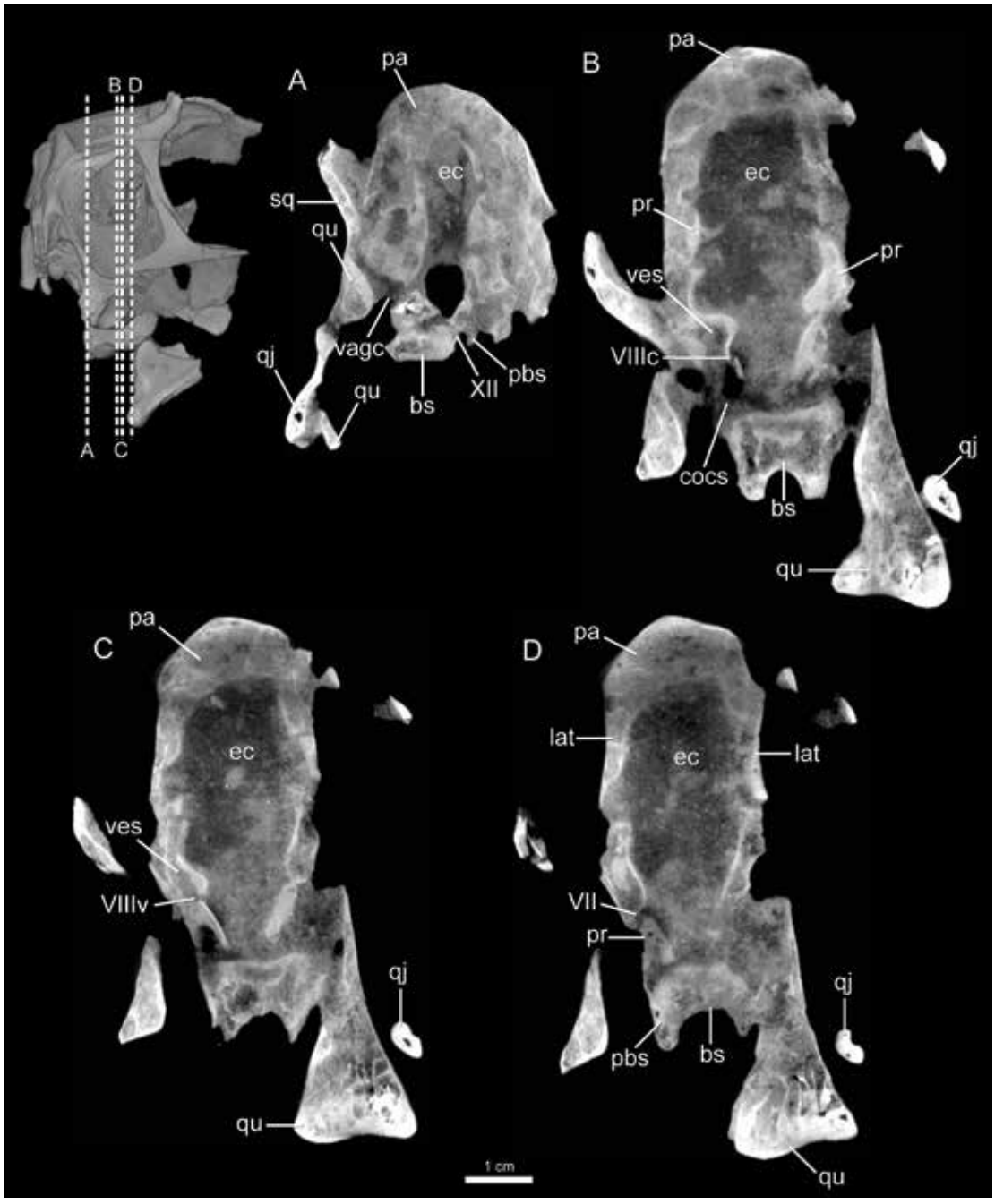

FIGURE 10. Additional coronal CT slices through the cranium of IGM 100/3006. Volume rendering of specimen shows the location of slice plains. See appendix for anatomical abbreviations.

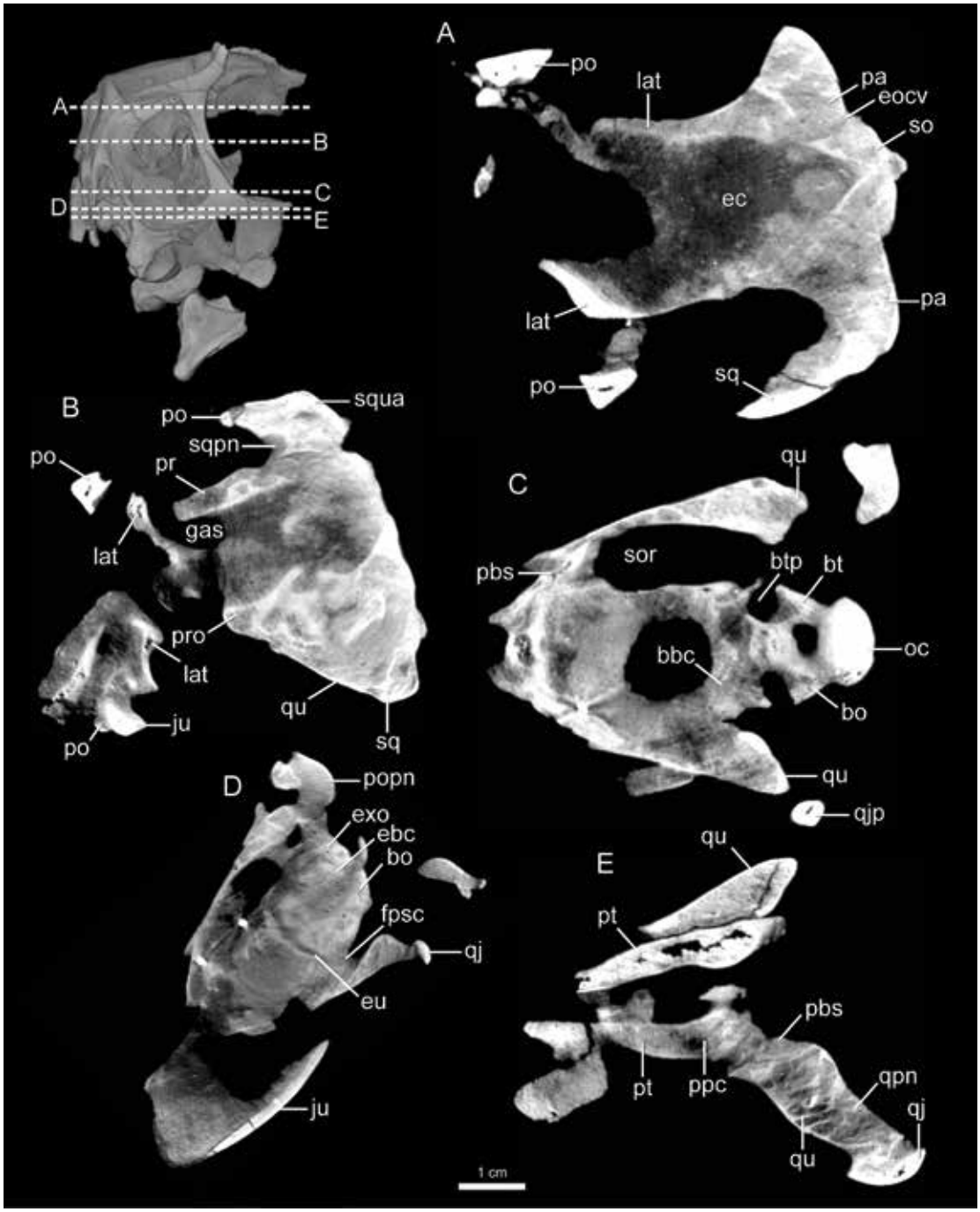

FIGURE 11. Horizontal CT slices through the cranium of IGM 100/3006. Volume rendering of specimen shows the location of slice plains. See appendix for anatomical abbreviations.

bold, 1986; Osmólska et al., 2004). In IGM 100/3006 this process is shorter than that of the aforementioned taxa, not extending beyond the posterior margin of the mandibular process of the quadrate, but still longer and slenderer than that of *Khaan* (Balanoff and Norell, 2012: fig. 5A). In more basally diverging taxa such as *A. portentosus* and *Incisivosaurus* the quadratojugal and jugal are fused, thus obscuring the morphology of the quadrate process. *Caudipteryx*, however, has a relatively short process that closely resembles the size and shape of *Khaan*.

The combination of the ascending process of the quadratojugal and descending process of the squamosal make up the posterior border of the lateral temporal fenestra, as in all oviraptorids. Although somewhat displaced from its original position, the ascending ramus of the quadratojugal extends approximately two-thirds the length of the lateral temporal fenestra (fig. 1A). In posterior view, the quadrate and quadratojugal form the quadrate foramen (fig. 1D). Along with the posterior process of the jugal, the jugal process of the quadratojugal makes up the ventral margin of the lateral temporal fenestra with the jugal and extends almost its entire length (fig. 1A). It bears a dorsolateral groove for the reception of the jugal. This process is straplike relative to the gracile, rodlike condition observed in *Incisivosaurus*, *Citipati*, and *Khaan*. In this way it is more similar to the condition in *Oksoko* and in the aforementioned taxa. The articular region of the anterior process is dorsoventrally deep and facilitates the equally tall posterior process of the jugal.

Quadrate

Figures 1, 2, 5, 7, 9–12

The quadrate resembles the general morphology of other oviraptorosaurs, possessing distinct otic, orbital (pterygoid), and mandibular processes, similar to the condition in living birds (fig. 1A, B). The orientation of the otic process is vertical, with an otic head that is in line with the mandibular process as it is in the oviraptorids *Citipati*, *Khaan*, and previously illustrated specimens of *Conchoraptor* (IGM 100/20; Barsbold, 1986: fig. 3; Osmólska et al., 2004). The vertical orientation is opposed to the somewhat more posteriorly oriented head of *Incisivosaurus*. The otic process is concave posteriorly with some medial flexure, which also is apparent in oviraptorid quadrates identified as either *H. yanshini* or *Conchoraptor* by Maryanska and Osmólska (1997). The articulation surface on the otic process is undivided but articulates with the prootic medially and the squamosal laterally as it does in all known oviraptorosaurs (Maryanska and Osmólska, 1997; Balanoff et al., 2009), alvarezsaurids (Chiappe et al., 1998), troodontids, and crown birds (Baumel and Witmer, 1993). The quadrate-squamosal contact is broad and probably lacked a large degree of movement (described above). The medial contact with the prootic is simple with the quadrate head sitting in a depression on the lateral surface of the prootic. The posterolateral edge of the otic process of the quadrate contacts the medial aspect of the dorsal process of the quadratojugal. These elements also contact each other ventrally (described below), forming a small, dorsoventrally elongate quadrate foramen between these two contacts (fig. 1D, 5). This foramen is smaller than that observed in dromaeosaurids (Norell et al., 2006); however, its presence contrasts with the basal oviraptorosaurs *A. portentosus* and *Incisivosaurus*.

The mandibular process of the quadrate is ventrally oriented and widely expanded in an anteromedial-posterolateral direction (fig. 1D) as it is in the oviraptorids *Citipati*, *Rinchenia*, *Khaan*, and *Nemegtomaia*. In more basally diverging oviraptorosaurs like *A. portentosus* and *Incisivosaurus*, this process is relatively narrower compared with the overall height of the quadrate. Maniraptoran taxa outside of Oviraptorosauria also tend to lack an expanded mandibular process (see Clark et al., 1994; Chiappe, 1998; Norell et al., 2006, 2009; Zanno, 2010). The mandibular process extends ventrally well beyond the level of the floor of the braincase (fig. 1D), a characteristic present in all oviraptorosaurs, though most pronounced in *Incisivosaurus* (Xu et al., 2003; Osmólska et al., 2004). The lateral surface of this process is grooved for the reception of the quadratojugal (fig. 1B). The anteromedial surface is flat and, with part of the confluent orbital process, overlies the quadrate process of the pterygoid (fig. 1D).

The orbital process of the quadrate is sheetlike, overlaps the lateral surface of the pterygoid, and lies medial to the descending process of the squamosal (fig. 1A, B). The orbital process of oviraptorosaurs contributes to the aforementioned lateral flange that obscures the lateral surface of the braincase and forms the lateral wall of the cranioquadrate space (Clark et al., 2002; Osmólska et al., 2004; Balanoff et al., 2009).

Prootic

Figures 1, 9–12

The prootic of IGM 100/3006 is only partially exposed on the lateral surface of the braincase; the majority of this element is obscured by the orbital wing of the quadrate and overlying squamosal (fig. 1A, B). The exposed anterior edge of the prootic abuts the posterior edge of the laterosphenoid in a straight contact that lacks suturing, forming a single large oval opening for the exit of the trigeminal nerve (CN V), as in *Khaan* and *Oksoko* (fig. 1A). The trigeminal foramen is not completely divided as it is in crown birds (Baumel and Witmer, 1993) but rather is pinched in the middle similar to the morphology present in *Incisivosaurus* and *Epichirostenotes* (Xu et al., 2002). All other observed oviraptorids (Clark et al., 2002; Balanoff and Norell, 2012), deinonychosaurs (Currie and Zhao, 1993; Norell et al., 2006; Norell et al., 2009), and *Archaeopteryx* (Wellnhofer, 1974, 1993; Rauhut, 2014) retain a single large, circular trigeminal foramen. CT imagery shows that IGM 100/3006 houses a fossa within the prootic for the trigeminal ganglion (figs. 9C, 11B) similar to *Epichirostenotes*.

Although much of the remainder of the lateral wall of the braincase, including the external ear, is obscured, CT images reveal some of this obstructed morphology. These data show a relatively large facial foramen piercing (CN VII) the wall of the prootic exiting internally from the internal acoustic fossa (fig. 10D). The vestibular and cochlear branches of the vestibulocochlear nerve (CN VIII) also enter this fossa and exit into the vestibular and cochlear fossae, respectively (fig. 10B, C). The cochlear branch is located farthest posteriorly and is the smaller of the two branches.

The posterior surface of the prootic articulates with the opisthotic and the contact remains unfused. The inner ear is housed primarily within the prootic and opisthotic and is described in Balanoff et al. (2014). A large floccular recess invades the junction of the prootic with the

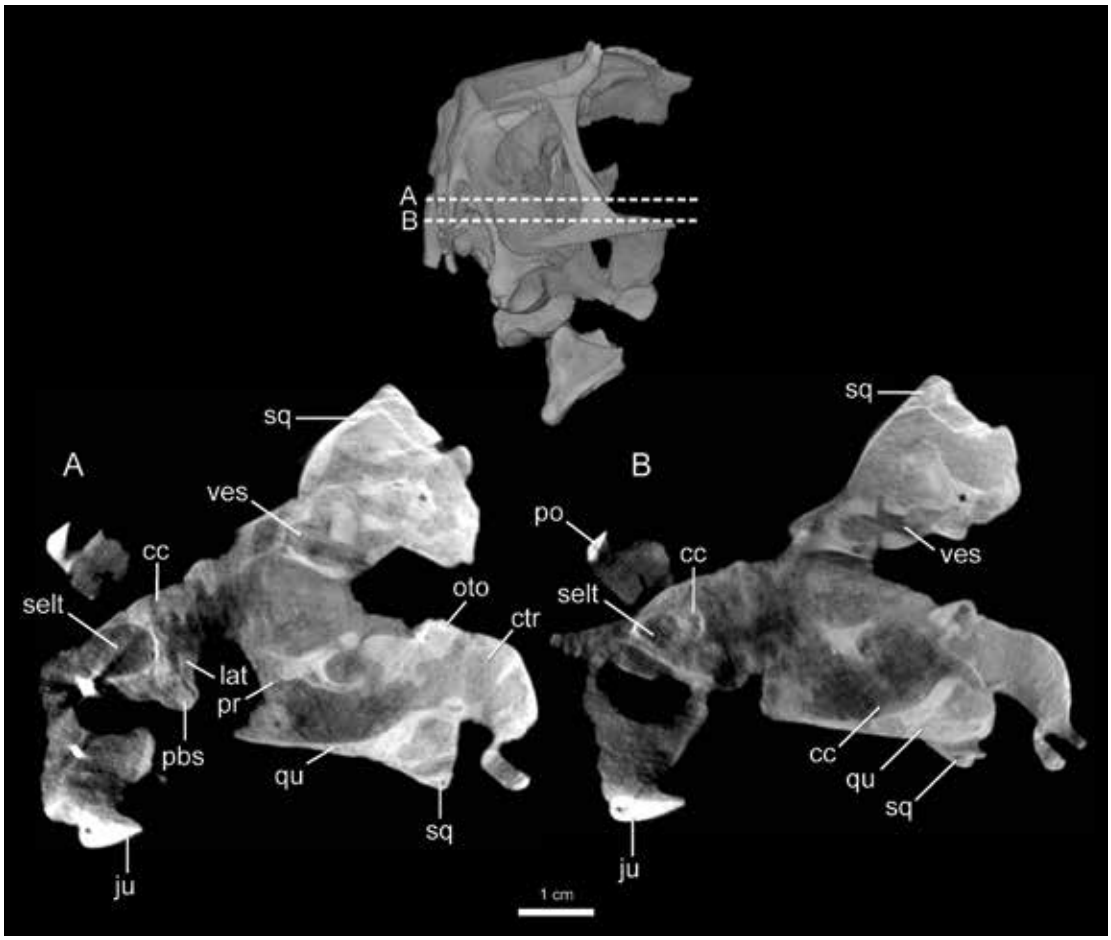

FIGURE 12. Additional horizontal CT slices through the cranium of IGM 100/3006. Volume rendering of specimen shows the location of slice plains. See appendix for anatomical abbreviations.

opisthotic and parietal (fig. 9A, B) but does not reach the exoccipital. The path of the anterior semicircular canal limits the anterior and posterior walls of the floccular recess. The horizontal semicircular canal lies at the lateral extent of the recess (Balanoff et al., 2014).

Laterosphenoid

Figure 1, 7, 8–12

Both left and right laterosphenoids are preserved in IGM 100/3006, but the left element is displaced medially from its original position (fig. 1B). The external surface possesses a vertically oriented crista that divides the anterior and lateral surfaces (fig. 1A). The anterior surface, which makes up the posterior wall of the orbit, is featureless except for a triangular articular facet at its ventromedial corner for the reception of the epipterygoid. This articulation is visible on the right side of IGM 100/3006 (fig. 1A). The ventro-

medial edge of the anterior surface is notched for the exit of the optic nerve (II) (fig. 1A). The optic foramen is a single opening formed by the midline contact of the paired laterosphenoids (Osmólska et al., 2004). It is possible that this single opening is the artifact of a missing or unossified orbitosphenoid, as is present in *Citipati* (IGM 100/978 and 100/42), *Rinchenia*, and *Nemegtomaia* (Barsbold, 1981; 1986). An orbitosphenoid is absent in all known specimens of *Conchoraptor* (Osmólska, 1976; Barsbold, 1986; Kundrát, 2007; Kundrát and Janáček, 2007) as well as *Khaan*. A long, slender postorbital process extends laterally from the dorsal margin of the element, marking the transition from the orbital to the lateral surface (fig. 1A). The postorbital process has a notable expansion at its distal end, making up the laterosphenoid contribution to the postorbital process as in most oviraptorosaurs. The contact with the frontal lies along the length of this postorbital process as well as along the dorsal edge of the orbital surface.

In lateral view, the posterior margin of the laterosphenoid abuts the prootic without any suturing, and these two elements form the foramen for the exit of the trigeminal nerve (CN V)—the majority of which is formed by the prootic (see Prootic description). Dorsal to the contact with the prootic, the laterosphenoid overlies much of the lateral surface of the parietal. The ventral contact with the parabasisphenoid is visible only in the CT slices and consists of a simple contact wherein the laterosphenoid sits on the dorsal surface the parabasisphenoid. The endocranial surface of the laterosphenoid, as viewed in CT data, forms part of the anterolateral wall of the braincase, which is concave to house the optic tectum (fig. 9D).

Pterygoid

Figures 1, 2, 7–9, 11

The anterior palatine wings of both the left and right pterygoid are missing, therefore only the posterior portions of this element are preserved in IGM 100/3006 (figs. 1, 2). The pterygoid contacts the epipterygoid dorsally, the parabasisphenoid medially, the quadrate laterally, and its opposite along the midline. Overall, the pterygoid is an elongate element as in most theropods, and as in most oviraptorosaurs, it obscures almost the entire ventral surface of the braincase outside of the basioccipital.

In IGM 100/3006 the dorsal (quadrate) process of the pterygoid is a thin, mediolaterally compressed wing that extends dorsally and lies deep to the otic process of the quadrate, contributing to the quadrate/pterygoid flange that is present in all oviraptorosaurs (see quadrate description). On the palatal surface, the posterior extremity of the pterygoid is forked. Laterally, a mediolaterally flattened posterolateral process contacts the medial surface of the mandibular process of the quadrate (fig. 1D). A posteromedial process expands dorsally and lies on the lateral surface of the parabasisphenoid (fig. 1D). Anterior to this contact, the opposing pterygoids converge along the midline as they do in *Citipati* (fig. 2B). This is unlike the condition in the basally diverging oviraptorosaur *Incisivosaurus* and the oviraptorids *Citipati*, *Jianxisaurus*, and *Oksoko*, wherein the pterygoids are separated by an interpterygoid vacuity that was likely bridged by soft tissue in life.

Epipterygoid

Figure 1

An ossified epipterygoid is found in most oviraptorids including another specimen of *Conchoraptor* (ZPAL MgD-I/95; Osmólska, 1976), *Citipati*, *Nemegtomaia*, *Khaan*, and *Oksoko*. The right epipterygoid in IGM 100/3006 is preserved as a small, triangular bone that is flattened anteroposteriorly (fig. 1C). Its dorsal extent overlaps the anterior surface of the laterosphenoid, and its ventral side contacts the quadrate wing of the pterygoid. The epipterygoid is relatively smaller than that of *Citipati*, and the dorsal tip does not twist dorsolaterally as it does in that taxon (Clark et al., 2002).

MANDIBLE DESCRIPTION

Only a small posterior portion of the mandible is preserved in articulation with the cranium of IGM 100/3006. This piece consists of the cranial articular surface of the articular, the retroarticular process of the surangular, the posteriormost portion of the angular, and the posteriormost extent of the prearticular (figs. 1, 2). The anteriormost extent of the mandible of IGM 100/3006 is found in the jacket of IGM 100/1203 and includes the dentary and distal extents of the angular and surangular (figs. 4, 6). Unfortunately, the most characteristic oviraptorosaurian features, e.g., the high coronoid eminence and enlarged mandibular fenestra, are not preserved. We can observe however, that the mandible is edentulous, possesses a downturned dentary symphysis as in *Oksoko* and *Jiangxisaurus*, and has a slender retroarticular process that extends to the posterior edge of the braincase, as in many most oviraptorosaurs (e.g., Clark et al., 2002; Balanoff and Norell, 2012; Lamanna et al., 2014). This condition differs from *Gobiraptor*, which lacks a prominent symphyseal process. The cranial articular surface is anteroposteriorly elongate and unbounded, indicating a sliding articulation as found in other oviraptorosaurs for which the mandible is known (Osmólska, 1976; Clark et al., 2002; Osmólska et al., 2004).

Dentary

Figures 3, 4, 6

The anteriormost portion of the left dentary is preserved in IGM 100/3006 (in the jacket of IGM 100/1203), including part of the symphyseal region and the posteroventral process (figs. 3, 6). The posterodorsal process is also present; however, it has broken away and is lying in the matrix adjacent to the premaxilla (fig. 3). Overall, the dentary is consistent with that of most other oviraptorid taxa in being edentulous, marked by numerous small nervous colliculi concentrated on the external surface of the anterior beak, and in having a downturned symphyseal region. The posteroventral process of the dentary is narrower than the basal oviraptorosaurs *Incisivosaurus* and *Caudipteryx* as well as the oviraptorids *H. huangi* (Lü, 2003), *Citipati*, *Rinchenia*, *Corythoraptor*, and *Khaan*. The width of this process in IGM 100/3006, however, compares closely with that of *Caenagnathus* Spp. (CMN 8776) (Currie et al., 1993).

Surangular

Figures 1, 2, 6

The surangular is represented by its anteroventral tip in the jacket of IGM 100/1203 (fig. 6) and by its posteriormost extent, which remains in articulation with the posterior mandible in IGM 100/3006 (figs, 1, 2B). It articulates with the angular ventrally, and with the angular posterodorsally, while extending posteroventrally to form the lateral surface of the retroarticular process as in other oviraptorids (e.g., Clark et al., 2002; Balanoff and Norell, 2012). The surangular does appear to have taken part in a surangular/articular/coronoid complex as in caenagnathids (Currie et al., 1993).

Angular

Figures 1, 2, 6

The angular is represented by an anterior fragment in the jacket of IGM 100/1203 (fig. 6) and by its posteriormost extent in articulation with the cranium of IGM 100/3006 (figs. 1, 2) The element's anterior contact with the posteroventral process of the dentary is not preserved, but its dorsal contact with the surangular remains. As in *Khaan*, *Rinchenia*, and *Oksoko*, the element tapers into a rounded termination that does not continue onto the retroarticular process as it does in *Citipati* and *Gigantoraptor erlianensis* (Xu et al., 2007).

Prearticular

Figure 1

The posterior end of the prearticular is the only portion of this element preserved (fig. 1A, D). It lies along the medial surface of the articular and extends posteroventrally onto the retroarticular process. It is in a similar position to other oviraptorids (see Clark et al., 2002: fig. 9B).

Articular

Figure 1

The articular is expanded anteroposteriorly and is the only mandibular element that makes contact with the quadrate, likely facilitating a sliding articulation (fig. 1A–C). In this way, the articular of *Conchoraptor* exhibits the classic oviraptorosaur morphology wherein the mandibular joint articulates via a cotyle that would not have permitted anterior-posterior movement. The retroarticular process of IGM 100/3006 is slender, as in all oviraptorids, and projects posteroventrally from the posterior extent of the articular surface (Holtz, 1998; fig. 1). The articular contacts the prearticular anteriorly along its ventral surface. Contact with the surangular is made laterally (only a thin splint of the posterior region of this element is preserved).

POSTCRANIAL DESCRIPTION

This description is based on both specimens of *Conchoraptor* (IGM 100/3006 and 100/1203). IGM 100/1203 is a nearly complete postcranial skeleton preserved primarily in dorsal view (fig. 3). Details of other surfaces come from IGM 100/3006, which although not preserved in its entirety, has representative elements from all regions of the skeleton except the forelimb. The postcranial skeleton generally resembles other small, "crestless" oviraptorids (Barsbold, 1981, 1986; Lü, 2003; Osmólska et al., 2004; Balanoff and Norell, 2012).

Axial Skeleton

Figures 3, 13–18

All vertebral counts are taken from IGM 100/1203 except for the sacral vertebrae, which are obscured by the overlying ilia and thus taken from IGM 100/3006. There are six preserved vertebrae in the cervical series of IGM 100/3006, including the atlas and axis (figs. 13–15). In IGM 100/1203, a total of nine articulated cervical vertebrae can be observed (fig. 3). Preservation of the cervical series in IGM 100/1203 deteriorates cranially, and so this count is unlikely to be reflective of the true number, which usually amounts to 12 or 13 in oviraptorosaurs (Osmólska et al., 2004). This number differs from most theropods, which typically possess no more than 10 cervical vertebrae.

The atlas is rarely preserved in oviraptorosaurs, and when present, is often obscured due to its close association with the occipital surface of the skull or with the cranial cervical series (e.g., Wei et al., 2013; Lü et al., 2015; Funston et al., 2018). The disarticulation of the atlas in IGM 100/3006 allows for a more comprehensive description of this element than in most other specimens. The atlas is anteroposteriorly compressed as in all theropods (Osmólska et al., 2004) and consists of an isolated, U-shaped intercentrum that is comparable in size to the axial intercentrum (fig. 13). The anterior surface of the atlantal intercentrum is concave for the reception of the occipital condyle (fig. 13E). The width of the atlantal intercentrum is approximately two times its height at the midline and has a V-shaped dorsal margin. Both left and right atlantal neurapophyses are present and ascend at a steep angle as mediolaterally thin plates (fig. 13A–D).

The axial vertebra is preserved, although the neural arch, centrum, and intercentrum are disarticulated (fig. 14). The odontoid process is present and fused with the centrum, a condition that is variable in oviraptorosaurs (Osmólska et al., 2004; fig. 14E, F). There is no evidence of pleurocoels in the lateral surfaces of the axial centrum contra the condition described for *Conchoraptor* by Osmólska et al. (2004), however, there is a pair of small foramina on the dorsal midline, suggesting that the element is pneumatized (fig. 14F). Pneumatization of the axial centrum typically is present in oviraptorosaurs (Osmólska et al., 2004) in which the second cervical vertebra is preserved (e.g., *Citipati* IGM 100/978; Clark et al., 2002) and in most theropods, excluding some basally diverging members (Benson et al., 2012). As in many of the vertebrae in IGM 100/3006, the centrum and neural arch of the axis are not yet fused. The

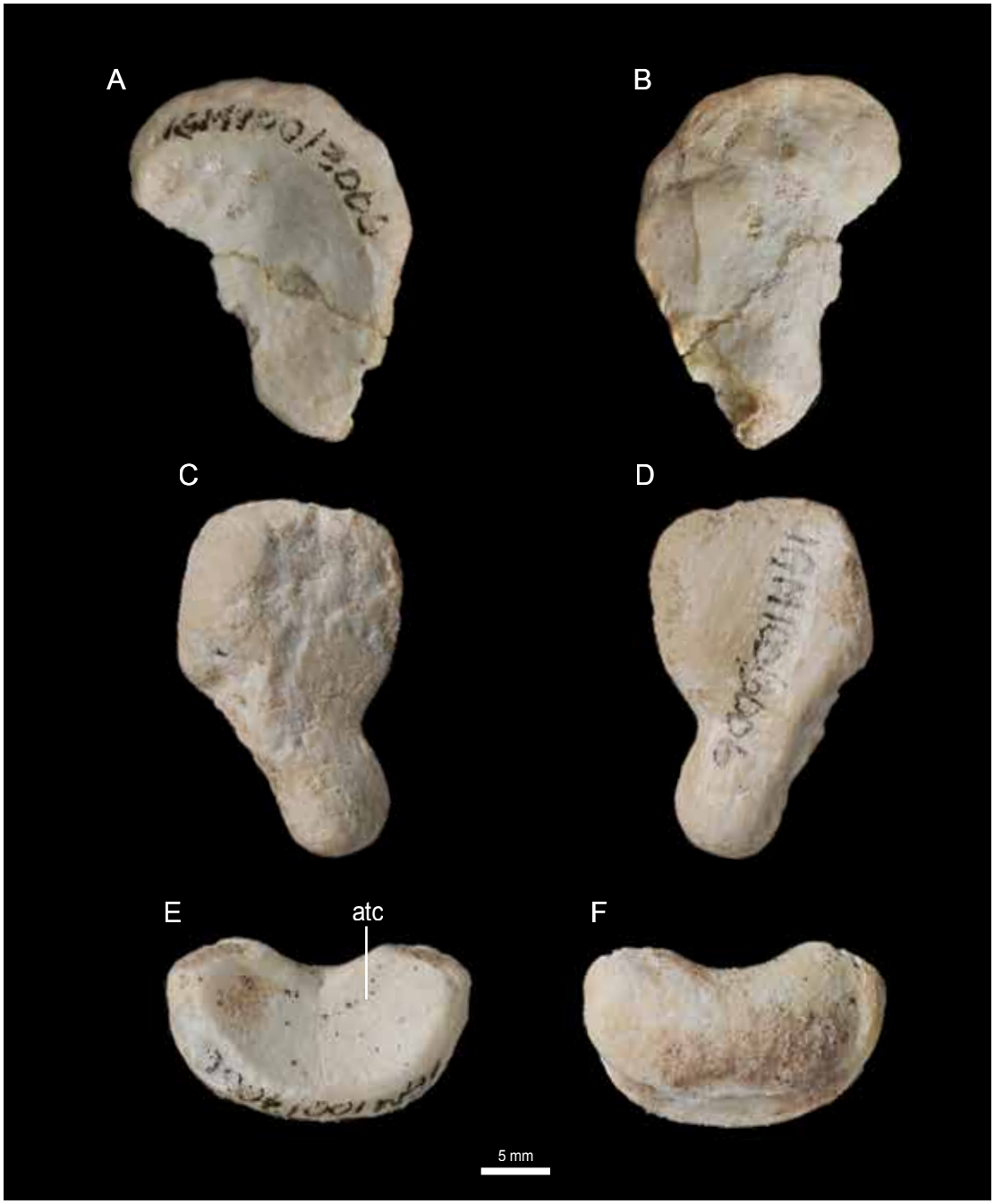

FIGURE 13. Atlantal complex of IGM 100/3006. Right neurapophysis in **A,** lateral and **B,** medial views. Left neurapophysis in **C,** lateral and **D,** medial view. Atlantal intercentrum in **E,** anterior and **F,** posterior view. See appendix for anatomical abbreviations.

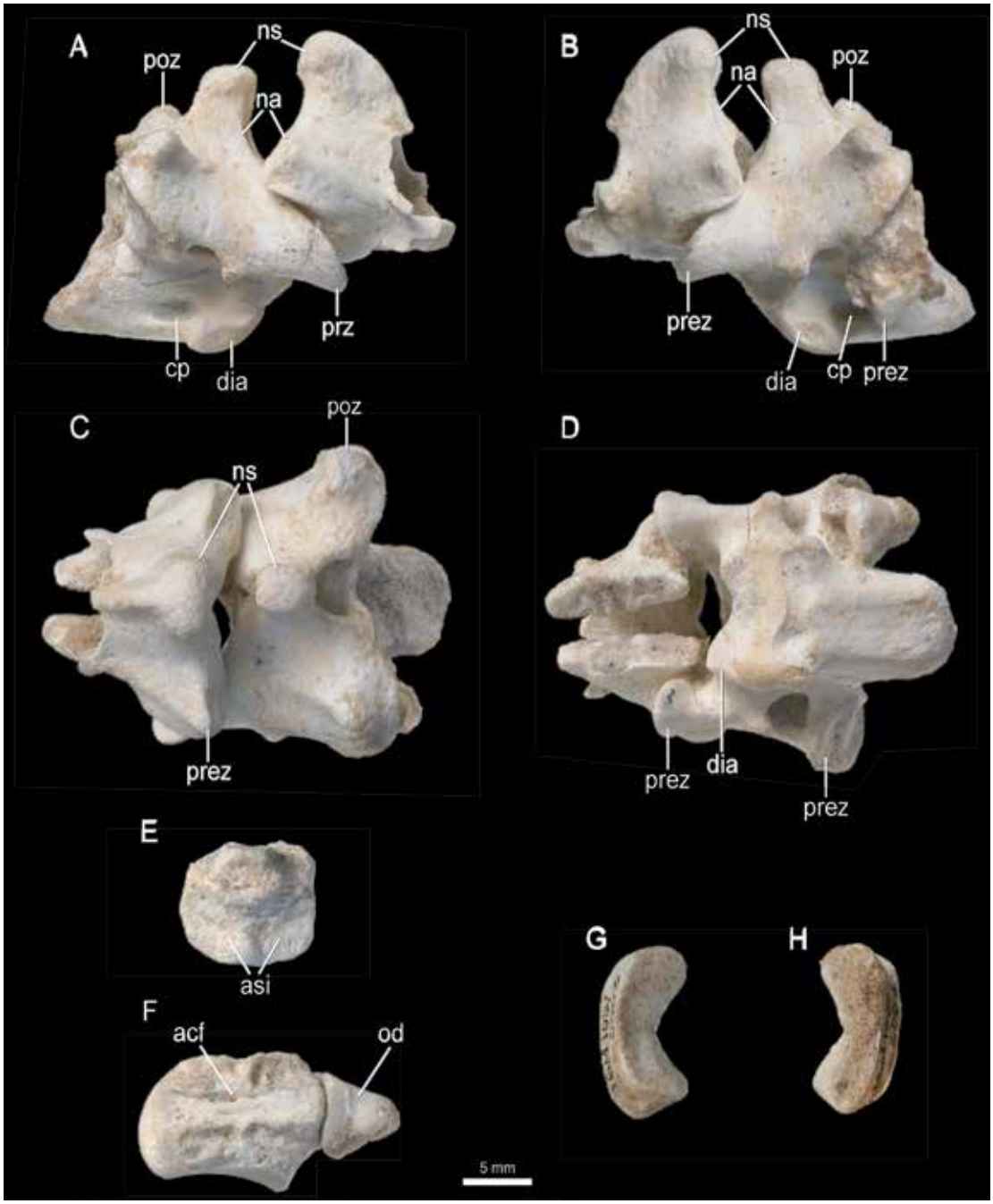

FIGURE 14. Axis and first post-axial cervical vertebrae of IGM 100/3006 in **A,** right lateral, **B,** left lateral, **C,** dorsal, and **D,** ventral view. Disarticulated axial centrum in **E,** anterior, and **F,** ventral views. Axial intercentrum in **G,** anterior and **H,** posterior view. See appendix for anatomical abbreviations.

anterior articular surface bears two ventral, parallel surfaces that received the axial intercentrum (fig. 14E). The neural arch of the axis is anteroposteriorly shorter than those in the remainder of the cervical series. In dorsal view the neural arch is triangular in shape, with the apex anteriorly positioned (fig. 14C). It bears a robust neural spine that is angled posteriorly in lateral view. The posterior surface of the neural spine base is excavated and contains two foramina that may be pneumatic (a pneumatized axial neural arch is not typically seen within Theropoda [Benson et al., 2012], but it is present in *Khaan*). Damage to the anterior portion of the axis prevents a description of the prezygapophyses. The postzygapophyses are strongly developed and comprise nearly half of the anteroposterior length of the neural arch. As in *Khaan*, there are weakly developed mammillary processes on the dorsal surface of the axial postzygapophyses. The presence of this feature in other oviraptorosaur taxa is unclear due to the susceptibility of this exposed region to erosion.

Description of the cervical centra is based exclusively on IGM 100/3006 because these surfaces are poorly exposed in the articulated specimen IGM 100/1203 (fig. 3). The anteriormost cervical centra have anterior articular faces that are at least twice as wide as the posterior faces as in other maniraptoriforms (Gauthier, 1986; Holtz, 1998; Maryanska et al., 2002; Zanno, 2010; Turner et al., 2012). Similar to the crown avian condition, the anterior face is saddle shaped (heterocoelous) (Baumel and Witmer, 1993), thus representing a convergently derived feature of the two groups (absent in all other maniraptorans; see Turner et al., 2012). In living birds, this morphology facilitates increased dexterity of the neck, and it likely served a similar function in oviraptorosaurs (Furet et al., 2022). The posterior articular face is square and amphiplatyan. The intercentral articulation of the postaxial cervical vertebrae is steeply inclined with the anterior surface facing anteroventrally and the posterior surface facing posterodorsally, a characteristic of all maniraptorans (Turner et al., 2012) that might be associated with sinusoidal neck curvature (Ostrom, 1969; Barsbold, 1983; Norell and Makovicky, 2004). As a result of this orientation, the posterior articular face of the cervical centra extends posteriorly beyond the margin of the neural arch of the succeeding vertebra. The dorsal surfaces of the centra are concave, forming the ventral wall of the neural canal. The ventral surfaces of the anterior cervical centra are flat and split anteriorly to form parapophyses for the unfused articulation of the cervical ribs. In all three complete postaxial cervical vertebrae, an anteroposteriorly elongate pleurocoel pierces the lateral surface of the centrum approximately midway along its length (fig. 14A, B).

Cervical neural arches are visible in both IGM 100/1203 and IGM 100/3006. Description of the lateral surfaces, however, is based on IGM 100/3006. The arches belonging to the anterior cervical vertebrae are roughly rectangular in dorsal view (fig. 15C), with the anterior end being slightly narrower than the posterior end. IGM 100/1203 shows that the dorsal surface becomes progressively more X-shaped posteriorly in the series (fig. 3). The neural spine is located centrally on the arch, similar to other oviraptorosaurs (Makovicky and Sues, 1998; Osmólska et al., 2004; Balanoff and Norell, 2012). The neural spines are rectangular in lateral view and are slightly longer anteroposteriorly as well as mediolaterally thinner proceeding from CV III–V (fig. 15A, B). Neural spines in the cervical series posterior to CV V are progressively reduced in height but remain centered on the neural arch (Makovicky and Sues, 1998; Osmólska et al.,

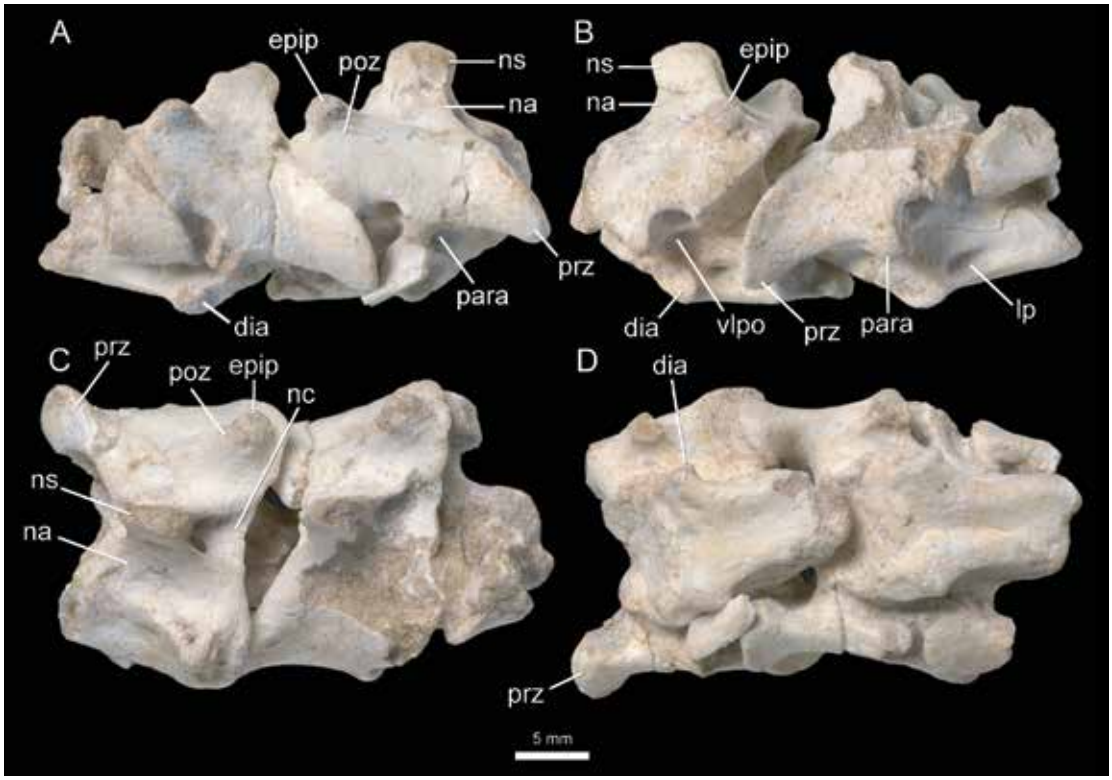

FIGURE 15. Second, third and fourth postaxial cervical vertebrae of IGM 100/3006 in **A,** right lateral, **B,** left lateral, **C,** dorsal, and **D,** ventral view.

2004). The pre- and postzygapophyses are robustly developed in all postaxial cervicals. The dorsal surface of the postzygapophysis is spherical and well defined, with moundlike epipophyses (fig. 15C). This condition is similar to that of *A. portentosus* and *Khaan*, but distinct from the linear morphology in *Microvenator celer* (Makovicky and Sues, 1998), *Similicaudipteryx yixianensis* (He et al., 2008), *Nomingia gobiensis* (Barsbold et al., 2000), and *Citipati*. As described previously for the axial vertebra, the neural arch is excavated anteriorly and posteriorly at the base of the neural spine. A small tubercle, or diapophysis, for the reception of the cervical rib is present at the anterior margin of the ventrolateral pneumatic opening, indicating that the cervical ribs in IGM 100/3006 are not fused, another indicator of skeletal immaturity. The cervical neural canal is wide, as dorsoventrally tall as the centra and as transversely wide, about the same size as the posterior articular face (fig. 15C).

No cervical ribs are preserved in IGM 100/3006 although two right elements can be seen articulating with the caudal cervical vertebrae in IGM 100/1203 (fig. 3). They do not deviate considerably from previously described oviraptorid taxa.

Three cervicodorsal vertebrae can be observed starting immediately caudal to the furcula in IGM 100/1203. As in *Khaan* and *Oksoko*, the neural arches are X-shaped in dorsal view, and associated ribs are proximodistally shorter than those of the dorsal series.

No dorsal vertebrae are preserved in IGM 100/3006; therefore, the description is taken exclusively from IGM 100/1203 (fig. 3). The posterior dorsal vertebrae are poorly preserved and tightly compressed, making it difficult to distinguish the position of the dorsosacral vertebra using morphology alone. Nonetheless, approximately 11 dorsal vertebrae are present, based on the number of elements that have associated ribs, a count that aligns with the usual range for oviraptorosaurs (Osmólska et al., 2004; Balanoff and Norell, 2012). Maniraptorans outside of Oviraptorosauria, however, range up to 12 dorsal vertebrae (Norell and Makovicky, 2004).

Similar to the cervicodorsal vertebrae, the anterior dorsal vertebrae have an X-shaped neural arch in dorsal view with a small neural spine centered on the arch. Proceeding posteriorly along the dorsal series the transverse processes trend toward a more purely lateral extension, become more rectangular, and anteroposteriorly longer. The presence or absence of pleurocoels on the dorsal centra cannot be confirmed as they are not exposed in IGM 100/1203 (fig. 3).

The dorsal ribs are preserved in articulation with their corresponding vertebrae, and several of the anteriormost elements on the right side are accompanied by ossified sternal ribs. The 3rd and 4th right and left dorsal ribs possess elongate uncinate processes that extend from the rib with which they originate posteriorly past the posterior margin of the succeeding rib. These have an expanded proximal articulation surface and narrow distally, with each successive element becoming smaller and more gracile. The processes are not fused to the ribs and overall bear a similar morphology to those in *Caudipteryx* (IVPP V 12430) and *Citipati* (IGM 100/979 and 100/1004; Clark et al., 1999: fig. 12; Norell et al., 2018). Due to the inaccessibility of the ventral extent of the dorsal ribs in IGM 100/1203, the "single ossified ventral rib segment," a character shared by dromaeosaurs and oviraptorids (Clark et al., 1999), cannot be ascertained. The left 7th and right 7th, 9th, 10th, and 11th dorsal ribs have associated sternal ribs. They are anteroventrally narrow and straplike, as in oviraptorosaurs generally (e.g., Lü, 2005; Funston and Currie, 2016; Balanoff and Norell, 2012).

The sacral vertebral count of IGM 100/3006 of six (fig. 16) is consistent with the number found in other oviraptorosaurs, which can vary between six and seven (Osmólska et al., 2004). In IGM 100/1203 the overlying ilium obscures the view of the sacral vertebrae (fig. 16). In IGM 100/3006, exposure is limited primarily to the ventral surface, but the centra, neural arches, and sacral ribs are visible and remain unfused at this stage of skeletal maturity (see Discussion). Fusion of these elements occurs in most oviraptorosaurs, including *Chirostenotes pergracilis* (TMP 79.20.1; Currie and Russell, 1988; Funston and Currie, 2021) and *Citipati* (IGM 100/978). The first vertebra in the sacral series of IGM 100/3006 is missing its anterior half. Overall, the anterior centra are wider and more dorsoventrally compressed than those in the posterior region, and all the sacral centra have anterior articular faces that are wider than the posterior articular faces. The width of the anteriormost centrum is approximately 3× its height; the posteriormost sacral vertebral centrum is about 2× as wide as tall. Lateral pleurocoels on the sacral centra are single and anteroposteriorly elongate, as in *H. huangi*, *Khaan*, *Oksoko*, and *Citipati*. In the anterior sacral vertebrae these are positioned midway along the length of the centrum. They become smaller and slightly more posteriorly positioned toward the caudal portion of the series. Pleurocoels are present within the sacral centra of caenagnathids (TMP 79.20.1; Currie

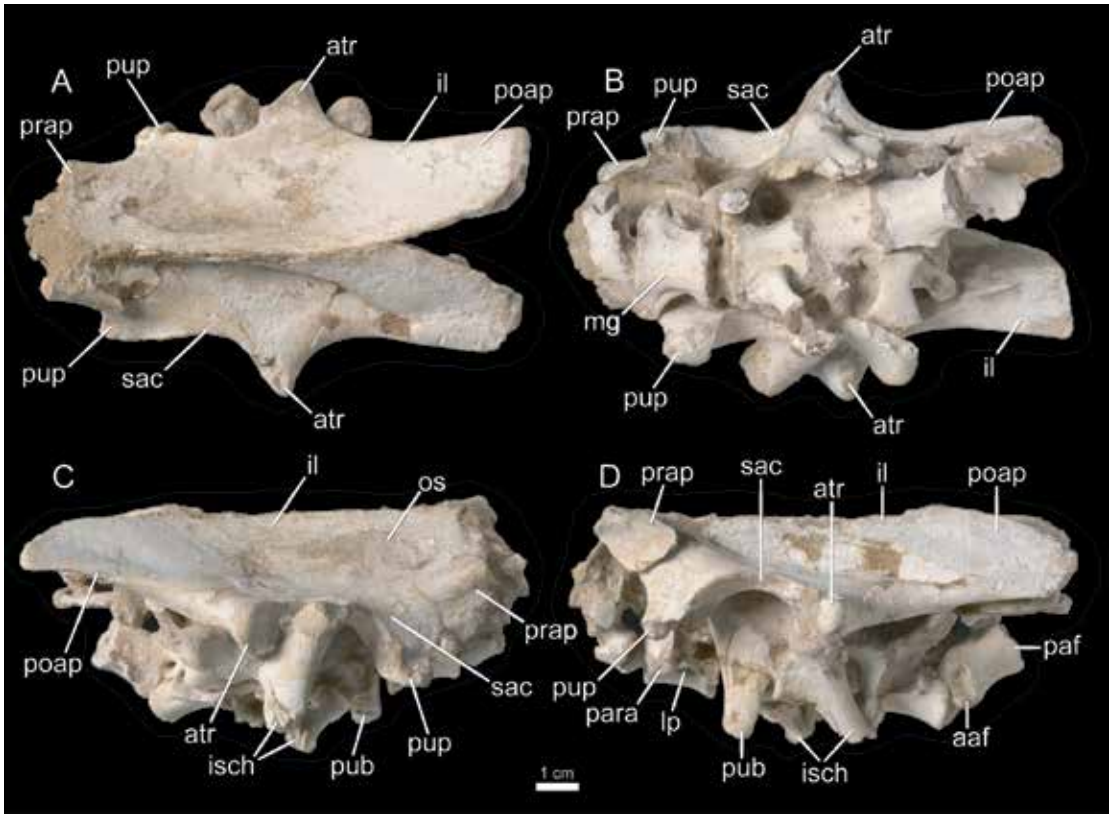

FIGURE 16. Pelvic girdle and sacral vertebrae of IGM 100/3006 in **A,** dorsal, **B,** ventral, **C,** right lateral, and **D,** left lateral view. See appendix for anatomical abbreviations.

and Russell, 1988), oviraptorids, and most other maniraptorans but absent in the more basally diverging oviraptorosaur *A. portentosus*. Large parapophyses for the sacral ribs are situated at the anterolateral edge of the centrum. The articular surfaces gradually lengthen, expanding their posterior margin in the more posterior part of the series. A shallow, rounded groove runs down the midline of the ventral surface of sacrals II–V (fig. 16B). The sulcus cannot be assessed on sacral I because of the broken surface. A midline groove also is present in *H. yanshini* (IGM 100/30), but absent in *Rinchenia* and *H. huangi*.

Three anterior caudal vertebrae are preserved in articulation in IGM 100/3006, and of these only the posteriormost vertebra in the series has an associated centrum (fig. 17). An additional disarticulated centrum and associated transverse process is also present in IGM 100/3006 (fig. 18). As observed in other regions of the vertebral column, the caudal vertebrae lack fusion between the centrum and neural arch. IGM 100/1203 preserves 13 caudal vertebrae but lacks the distalmost portion of the tail (fig. 3). A full caudal series in other oviraptorosaurs ranges from 22 in *Caudipteryx* to 32 in *Citipati* (IGM 100/978). Overall, the oviraptorosaur caudal series is reduced compared with other nonavian coelurosaurs, which can reach up to 43 vertebrae in taxa such as *Velociraptor* (Norell and Makovicky, 1999; Osmólska et al., 2004).

The caudal centra are not visible in IGM 100/1203; therefore, the description is based on the four vertebrae from IGM 100/3006 (figs. 17, 18). These vertebrae resemble the posterior sacral vertebrae in that the centrum is wider than tall and the anterior articular surface is wider than the posterior surface. The lateral surface bears an oval pleurocoel that is approximately the same size as those in the posterior sacral vertebrae, a character that is unknown outside of oviraptorids and caenagnathids (Maryanska et al., 2002; Benson et al., 2012) (figs. 17A, B, 18). It is located dorsally on the centrum, near the base of the neural arches. Caudal pleurocoels appear to be absent in *A. portentosus*, but may be present at least in the proximal portion of the tail in another basal oviraptorosaur, *Similicaudipteryx*.

The neural arches from the caudal series are described using both IGM 100/3006 and 100/1203. The neural arches of the anterior caudal vertebrae are more extensively pneumatized than other regions of the vertebral column. Both the dorsal and ventral surfaces of the transverse processes are pneumatized in IGM 100/3006, and the dorsal surface is pneumatized by anterior and posterior foramina (figs. 17C, 18A). Only an anterior foramen is present in IGM 100/1203 (fig. 3). The distribution of these pneumatic foramina is variable within Oviraptorosauria. *Citipati* (IGM 100/978), *Nomingia* and *A. portentosus* all lack pneumatization in their caudal neural arches, but like *Conchoraptor*, foramina are present on the dorsal surface of the transverse process in *H. huangi* (Lü, 2003) and *Khaan* and the ventral surface in *H. yanshini* (IGM 100/30). The transverse processes are elongate, thin, and extend laterally and slightly posteriorly. IGM 100/1203 does not exhibit a distinct transition point within the caudal vertebrae series as the transverse processes gradually shorten their lateral extent as they progress posteriorly (fig. 3).

The posteriorly positioned neural spines of the anterior caudal vertebrae from IGM 100/3006 are dorsoventrally taller and anteroposteriorly thinner in lateral view than those of the cervical or dorsal vertebrae (fig. 17A, B). That of the subsequent vertebrae is oriented dorsally and slightly more anteriorly. In IGM 100/1203, caudal vertebrae III–IX have a dorsally oriented neural spine that is triangular in lateral view. The subsequent vertebrae (X–XIII) possess a slightly posteriorly oriented spine. The anterior and posterior surfaces at the base of the neural spines are not excavated as they are in the cervical and dorsal vertebrae. The transverse processes of all the caudal vertebrae extend slightly posterolaterally and become gradually shorter toward the end of the tail. The prezygapophyses are small and narrow. They do not extend far beyond the margin of the centrum. The postzygapophyses, however, are larger and overlap the succeeding vertebral centrum, but not to the extent observed in deinonychosaurs.

Forelimb and Pectoral Girdle

Figures 3, 19

The forelimbs are preserved only in IGM 100/1203 (figs. 3, 19). The pectoral girdle preserves a partial furcula and both left and right scapulae. The coracoid is not visible in this specimen although its articulation surface on the scapula is visible. It therefore seems likely that the scapula and coracoid were not yet fused into a single element as they are in most oviraptorids. The left ramus of the furcula is largely complete (fig. 3). Although the right ramus

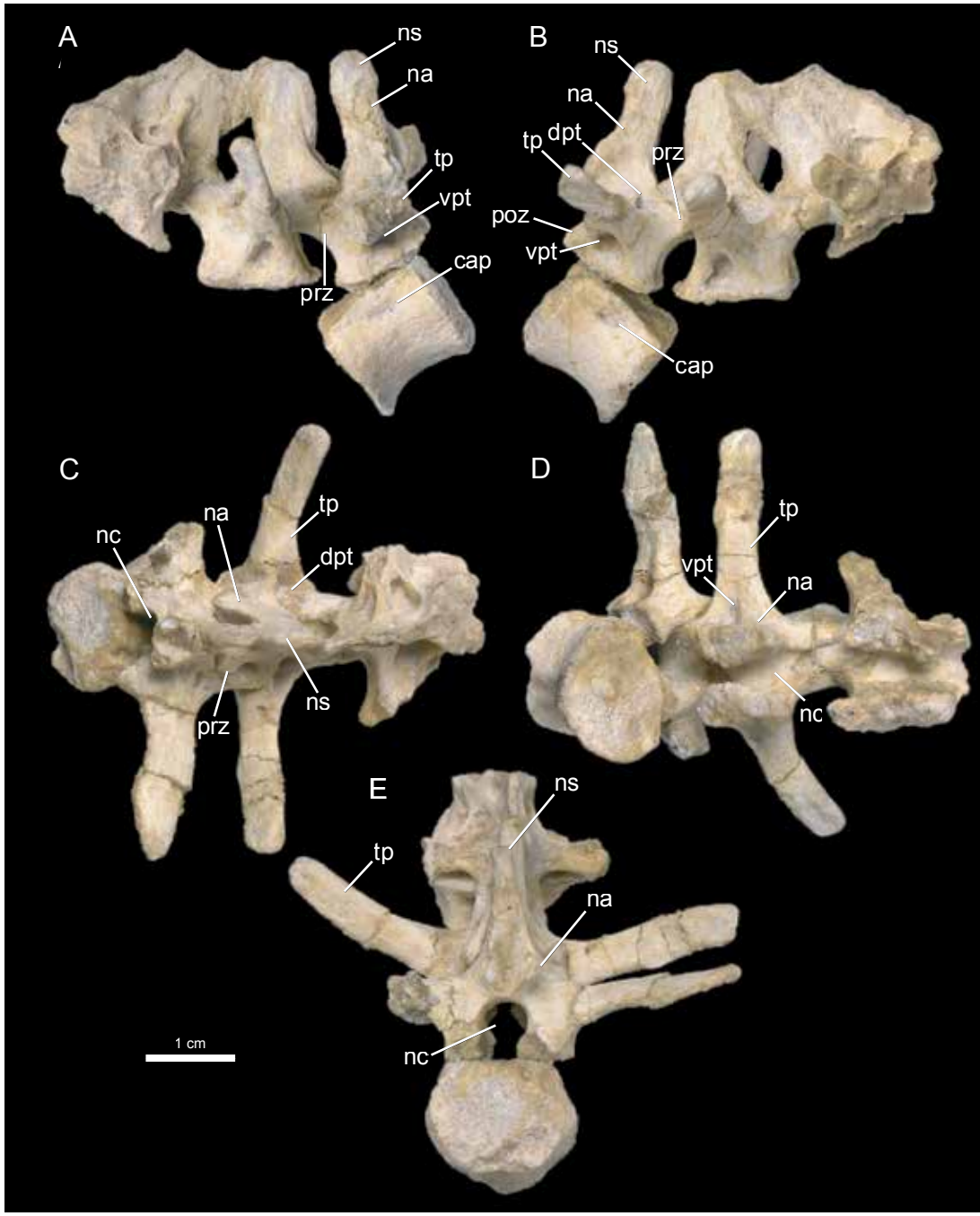

FIGURE 17. Anterior caudal vertebrae of IGM 100/3006 in **A,** left lateral, **B** right lateral, **C,** dorsal, **D,** anterior, and **E,** posterior views.

cannot be identified, a wide U-shape can be deduced, a character that is also present in *H. huangi*, *Khaan*, *Oksoko*, *H. yanshini*, *Yulong*, and *Tongtianlong*. This morphology is discordant with the acute V-shape of *Oviraptor* or *Citipati* (Nesbitt et al., 2009). The sternum is not visible in IGM 100/1203.

The left scapula of IGM 100/1203 is preserved in its entirety (figs. 3, 19), but the right element consists only of the midportion of the scapula blade. The scapula blade is approximately the same width along most of its length but expands slightly at its rounded distal extremity, similar to the condition present in other oviraptorosaurs (Osmólska et al., 2004; Balanoff and Norell, 2012; Funston, 2024). At the proximal end of the scapula, the acromion process is directed anteriorly and is relatively small, as in *Oksoko*. This contrasts with the large winglike acromion process in *H. yanshini* (IGM 100/1004) and the larger bodied oviraptorid *Citipati* (IGM 100/1004). The contribution of the scapula to the glenoid fossa is damaged, so it is difficult to determine in which direction the fossa was originally oriented.

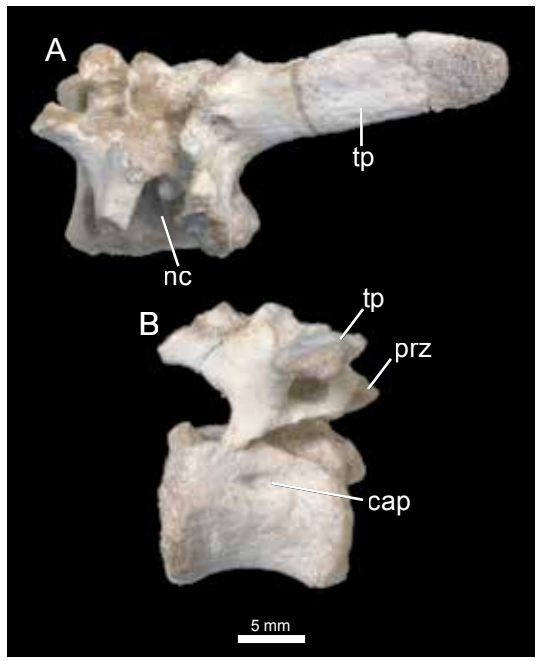

FIGURE 18 (column). Disarticulated caudal vertebra of IGM 100/3006 in **A,** left lateral, and **B,** dorsal views. See appendix for anatomical abbreviations.

The left humerus and right ulna and radius are preserved in IGM 100/1203 (fig. 3). Fragmentary pieces of the midshaft region of the left ulna and radius are recovered, but little morphology can be obtained. The humerus is broken into two pieces midway along the shaft. The humeral head and deltopectoral crest have also suffered damage, although its basic length and proportions can be reconstructed (table 3). The deltopectoral crest makes up approximately 40% of the length of the humerus as in *Nankangia*, *Tongtianlong H. yanshini*, and *H. huangi* but unlike *Citipati*, *Khaan*, and *Oksoko* wherein the crest stretches one third or less of its length. This region denies an assessment of the degree to which the crest is developed, however its apex is located at the distalmost end, as it is in other oviraptorids, differing from more basally diverging oviraptorosaurs *Microvenator* and *Gigantoraptor*, which have less pronounced, more rounded deltopectoral crests (Makovicky and Sues, 1998). The distal end of the humerus is not fully exposed although it can be ascertained that the medial condyle extends distinctly further distally than the lateral condyle.

Little can be determined about the partial right ulna present in IGM 100/1203 because it is broken into three pieces, although it was approximately 40% shorter than the humerus and circular in cross section. The olecranon process is weakly developed as it is in most maniraptorans.

TABLE 3. Postcranial measurements of IGM 100/3006 and IGM 100/1203 (in mm).

	IGM 100/3006	IGM 100/1203
Humerus length	–	65.23
Humerus width (at midlength)	–	6.39
Ulna length	–	36.92
Scapula length	–	99.75
Scapula width (at midlength)	–	8.44
Femur length	133.56	142.95
Femur width (at midlength)	14.58	15.63
Tibia length	197.25	174.91
Tibia width (at midlength)	19	14.34
Ilium length	109.73	164.61
Ilium depth (above acetabulum)	19.43	28.64
Fibular length	96.49	160.36
R metatarsal II length	77.4	53.18
R metatarsal III length	81.43	70.5
R metatarsal IV length	70.46	50.9

Hindlimb and Pelvic Girdle

Figures 3, 16, 20–27

The hindlimb and pelvic girdle of *Conchoraptor* as determined from IGM 100/1203 is "dolichoiliac," meaning that the pre- and postacetabular processes of the ilia are elongate and the pubes and ischia are gracile as in most theropods. This is in contrast with the condition in sauropodomorph saurischians, which exhibit rostrocaudally short ilia with squat, platelike pubes and ischia (Colbert, 1964). The left and right ilia were recovered for IGM 100/3006; however, the majority of the preacetabular process is missing from both sides (fig. 16). In this specimen, the left ilium is crushed inward, but the right element is undistorted. *Conchoraptor* resembles most other oviraptorosaurs, with the exception of *Rinchenia* and *Caudipteryx* (Osmólska et al., 2004), in that the dorsoventral depth of the postacetabular process is approximately the same as that of the preacetabular process, and the dorsal margin is straight (Osmólska et al., 2004). The iliac blades remain completely separated in IGM 100/1203 (fig. 3) but come together along the midline in IGM 100/3006 (fig. 16). The preacetabular process has a slightly expanded anteroventral margin that, if the dorsal margin is held horizontally, does not reach the level of the pubic peduncle. A similar morphology is found in most oviraptorosaurs, but the ventral margin of the process extends beyond this level in *Caudipteryx*. The postacetabular process of *Conchoraptor* tapers slightly posteriorly but ends in a blunt posterior margin as in *Khaan*, rather than being rounded as in *Nomingia* or tapered as in *H. huangi* and *Nan-*

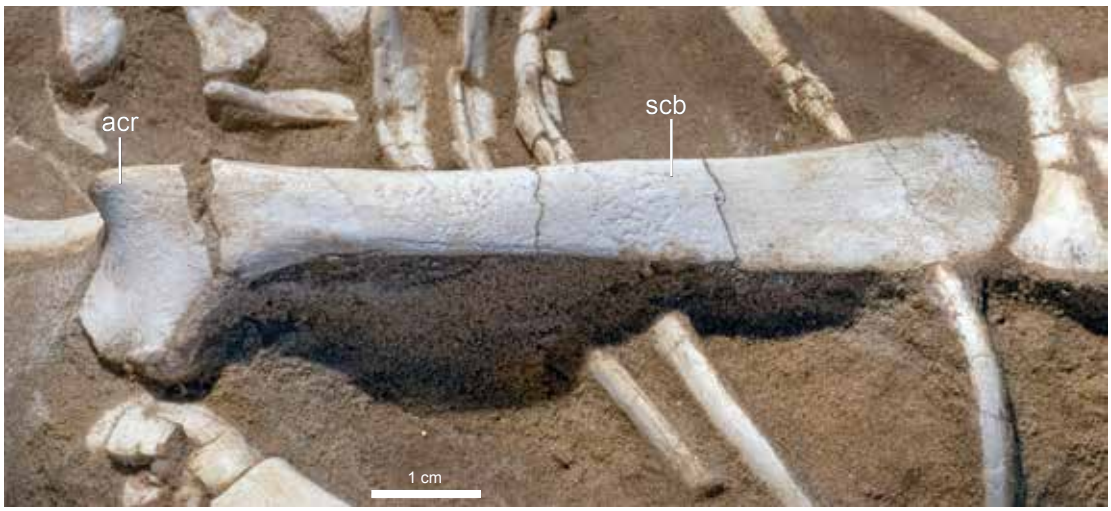

FIGURE 19. Left scapula of IGM 100/1203 in lateral view. See appendix for anatomical abbreviations.

kangia jiangxiensis (Lü et al., 2013b). The postacetabular blades diverge from one another and are not parallel as they are in most nonavian maniraptorans. An oval and anteroposteriorly elongate scar is present on the lateral surface of the ilium just anterodorsal to the acetabulum, which likely was for the attachment of the iliotibialis muscle (fig. 16C) (Shufeldt, 1909; Hutchinson, 2001). The remainder of the lateral surface of the element is featureless.

The supraacetabular crest in *Conchoraptor* is weakly developed with a prominent antitrochanter at its posterior margin (fig. 16). The pubic peduncle is not visible in IGM 100/1203; however, IGM 100/3006 exhibits one that, with the dorsal margin held horizontally, is slightly longer proximodistally and more medially directed than the ischiadic peduncle. The brevis fossa in IGM 100/3006 is present not as a deep fossa, but rather as a broad, ventral shelf similar to other oviraptorids and caenagnathids (Hutchinson, 2001; Osmólska et al., 2004. More basally diverging oviraptorosaurs such as *Caudipteryx* and *A. portentosus* preserve a well-formed brevis fossa.

The pubis is observable only in IGM 100/3006 and consists of a proximal shaft still attached to the ilium (fig. 16) and the corresponding pubic shaft, preserved as a separate piece (fig. 20). When articulated, these pieces form a ventrally projecting pubis. The preserved portion of the shaft is relatively straight, similar to *A. portentosus*, *Nomingia*, and *Citipati* (IGM 100/978). A more anteriorly concave pubis, however, is observed in *H. yanshini* (IGM 100/30), *Gigantoraptor*, *Khaan* (IGM 100/974), *Oksoko*, *Corythoraptor*, *Nankangia*, and *Wulatelong ganzhouensis* (Xu et al., 2013). The pubic shaft of *Conchoraptor* is compressed mediolaterally and joins its opposite at the distal extremity of the pubic boot. This narrow symphysis is extensively fused yet restricted to the posteromedial extent. IGM 100/3006 displays the plesiomorphic coelurosaur condition of a pubic boot that extends both anteriorly and posteriorly to the same degree, as in *Nomingia* but unlike *Khaan*, *Nankangia*, and *Corythoraptor* in which the anterior half of the boot is considerably more

developed than the posterior. The pubic apron extends medially starting approximately halfway along the length of the shaft to the broken end. It cannot be determined whether the pubic aprons come together as they do in *H. yanshini* (IGM 100/30) and *Citipati* (IGM 100/978).

In IGM 100/3006, the proximal end of the ischium is preserved in articulation with the ilium (fig. 16) and the distal section is preserved in isolation (fig. 21). The proximal shaft of the isolated piece is broken into two pieces on the right side, but the left side is relatively undistorted. Only the proximalmost part of the ischium can be seen in IGM 100/1203 because of the overlying ilium (fig. 3). Overall, this element in *Conchoraptor* is similar to that of other oviraptorosaurs in that it is short and triangular in shape due to an obturator process positioned approximately midway along the length of the shaft (fig. 21C) (Osmólska et al., 2004). The ventral margin of the ischium is straight with a slight dorsal curvature, tapering to a point as it extends posteriorly. The posterior margin, which can be variable in oviraptorosaurs, is relatively straight. The distal part of the ischium is platelike with a concave lateral surface, a derived feature of all known oviraptorosaurs (Norell et al., 2006). The paired ischia meet each other medially along the ventral margin. Although this may be a taphonomic feature, the same morphology has been reported for *Citipati* (Clark et al., 1999).

Femur

Figures 3, 22, 23

IGM 100/3006 and 100/1203 preserve both femora (figs. 22, 23), however, the distal half of the left side is missing in the former specimen. Only lateral and posterolateral views are observable in IGM 100/1203. The overall shape of the femur does not differ substantially from that of a typical theropod. The shaft is straight and roughly circular in cross section at its midlength. Only near the distal condyles does the shaft bow posteriorly and very slightly laterally. Proximally, the greater trochanter is prominent, and exhibits an excavated medial surface. The lesser trochanter extends as far dorsally as the greater trochanter, and is fingerlike, with only a shallow groove separating these structures as in most other oviraptorids. More basally diverging oviraptorosaurs, such as *Caudipteryx* and *Microvenator*, have a wider notch separating the femoral trochanters. Diverging from this pattern, *Citipati* (IGM 100/978) and *Gigantoraptor* share a continuous, arc-shaped trochanteric crest. As in *Oksoko*, there is no sign of a fourth trochanter, or a roughened surface as is present in troodontids (Makovicky and Norell, 2004) and *Khaan*. The femoral neck is not constricted, and the head is roughly hemispherical. At the distal end, the lateral condyle extends distally past the medial condyle as it does in all oviraptorosaurs (Osmólska et al., 2004). As in *Oksoko*, a deep popliteal fossa separates these two condyles, in contrast to the relatively shallow fossa apparent in *Khaan*. Similar to all oviraptorids, the circular crista tibiofibularis, which sits on the posteromedial surface of the lateral condyle, is large and extends well past the posterior margin of the femur (fig. 23B, C) (Osmólska et al., 2004). The size of this crista is closer to that of *Khaan* or *H. yanshini* than larger-bodied oviraptorosaurs such as *Citipati* or *Gigantoraptor*.

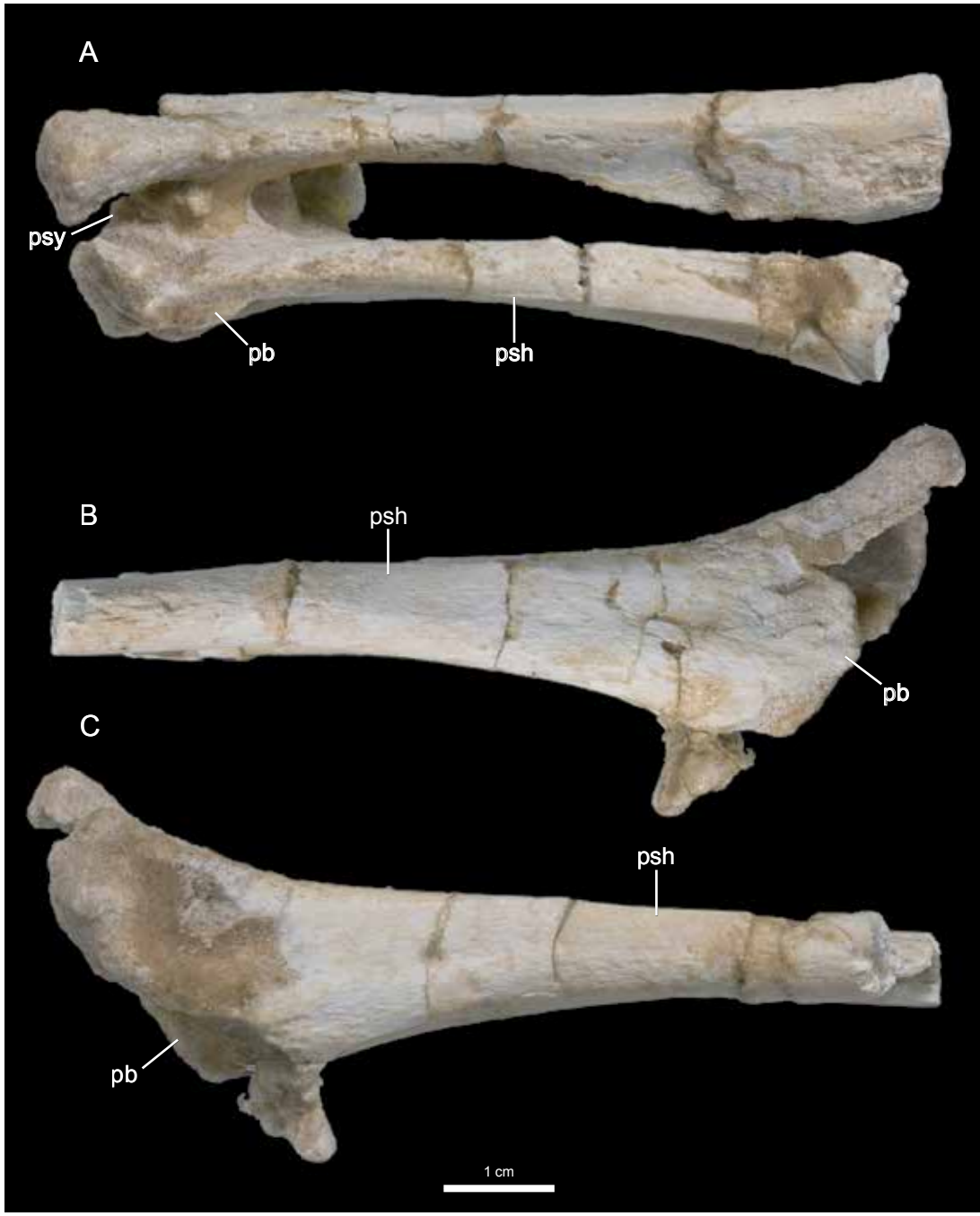

FIGURE 20. Pubes of IGM 100/3006 in **A,** anterior, **B,** right lateral, and **C,** left lateral views. See appendix for anatomical abbreviations.

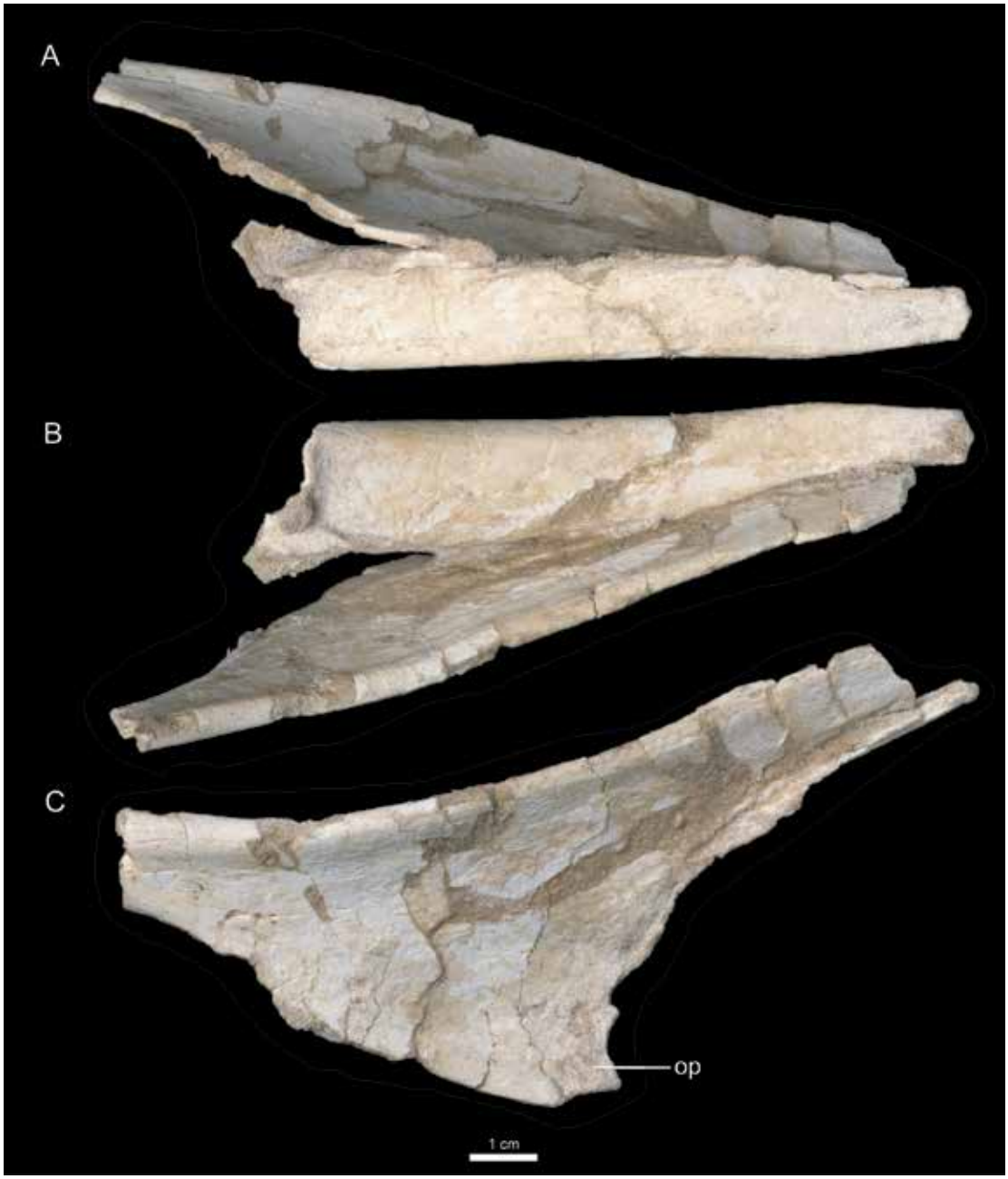

FIGURE 21. Ischium of IGM 100/3006 in **A,** dorsal, **B,** ventral, and **C,** right lateral views. See appendix for anatomical abbreviations.

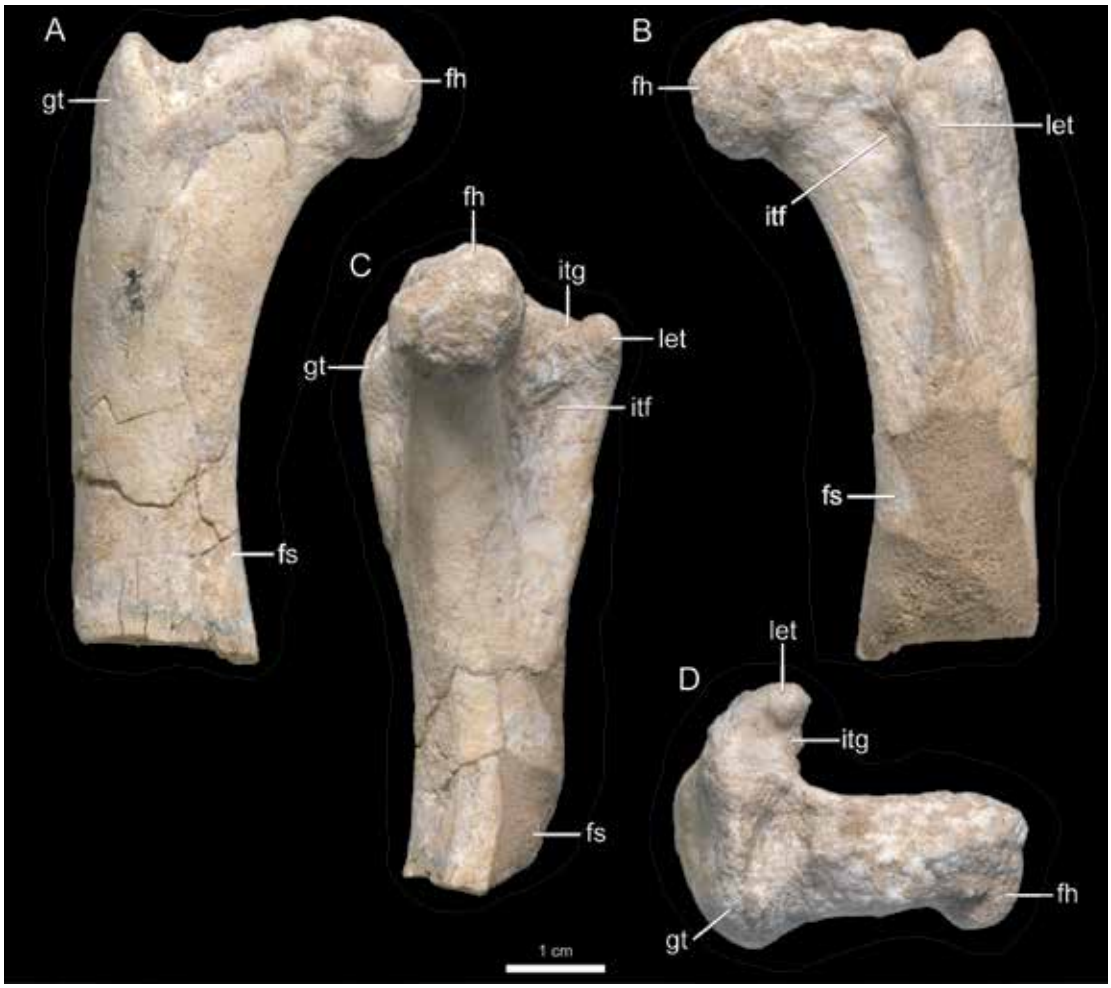

FIGURE 22. Left femur of IGM 100/3006 in **A,** anterior, **B,** posterior, **C,** medial, and **D,** proximal views. See appendix for anatomical abbreviations.

Tibia

Figures 3, 24

A complete right tibia is preserved in IGM 100/3006 (fig. 24), and both are preserved in 100/1203 (fig. 3). In IGM 100/1203, the left tibia is damaged at its proximal end, but the posterior surface of the right element is almost pristine. The tibia of *Conchoraptor* is approximately 25% longer than the femur and has a straight shaft (table 2) that is anteroposteriorly compressed. The proximal end possesses a weakly developed, anterolaterally directed cnemial crest, similar to the morphology found in *Khaan*, but contrasting with the more robust process present in *Citipati*, *Nomingia*, and *H. yanshini*. As in all observed oviraptorosaurs, the cnemial crest extends less than 1/5 of the length of the tibia (Balanoff and Norell, 2012). A fibular crista along the lateral surface extends about one-third of the length of the tibia in *Conchoraptor* (fig. 24A,

B). Immediately posterior to the distal end of the fibular crista of the right tibia of IGM 100/3006 is a large nutrient foramen (fig. 24B), also present in *Khaan* but lacking in other observed oviraptorids. The presence of this opening cannot be confirmed in other specimens of *Conchoraptor* and may be intraspecifically variable as it is in *Khaan*. This feature is relatively common among caenagnathids (Funston and Currie, 2018).

Fibula

Figures 3, 25

A partial right fibula that is missing its proximal end is preserved in IGM 100/3006 (fig. 25). IGM 100/1203 preserves both complete fibulae in articulation, and they can be seen tapering distally as they wrap slightly anteriorly around the tibiae (fig. 3). Generally, they resemble the morphology present in other oviraptorosaurs, being compressed mediolaterally and extending the entire length of the tibia to articulate with the calcaneum. The proximal head of the fibula is concave medially with a distinct posterior crista, where it articulates with the lateral articular face of the tibia (fig. 25A). A pronounced tuberculum is present laterally, just distal to the proximal head for the attachment of the iliofibularis muscle.

Astragalocalcaneum

Figures 3, 24

The astragalocalcaneum is preserved in both hindlimbs of IGM 100/1203 (fig. 3), although it is largely obscured by the articulated foot. The element is clearly visible in articulation with the distal surface of the right tibia of IGM 100/3006 (fig. 24). As in *Khaan*, *Oksoko*, and *Citipati*, the astragalus spans the entire width of the distal tibia. The ascending process similarly matches the width of the distal tibia at the level of the condyles, although it tapers proximally, so that its height is greater than the maximum width of the astragalus as in all oviraptorosaurs (Balanoff and Norell, 2012). The medial and lateral condyles of the astragalus are equally well developed, although the medial condyle does extend further anteriorly as in *Citipati*, *H. yanshini*, *Oksoko*, and *Gigantoraptor*. The intercondylar fossa is shallow as in *Khaan* and *H. yanshini*, contrasting the deep condition in *Citipati*. The lateral condyle is excavated laterally by a shallow depression that houses the calcaneum (fig. 24D). As in all oviraptorosaurs, the calcaneum is a small, kidney-shaped tab of bone and is otherwise unremarkable.

Distal Tarsals

Figures 3, 26

Fragments of distal tarsals are visible on the proximal surfaces of both left and right metatarsi in IGM 100/3006 (fig. 26) but are obscured posteriorly by the articulated astragalocalcaneum in IGM 100/1203 (fig. 3). These fragments in IGM 100/3006 are likely attributable to

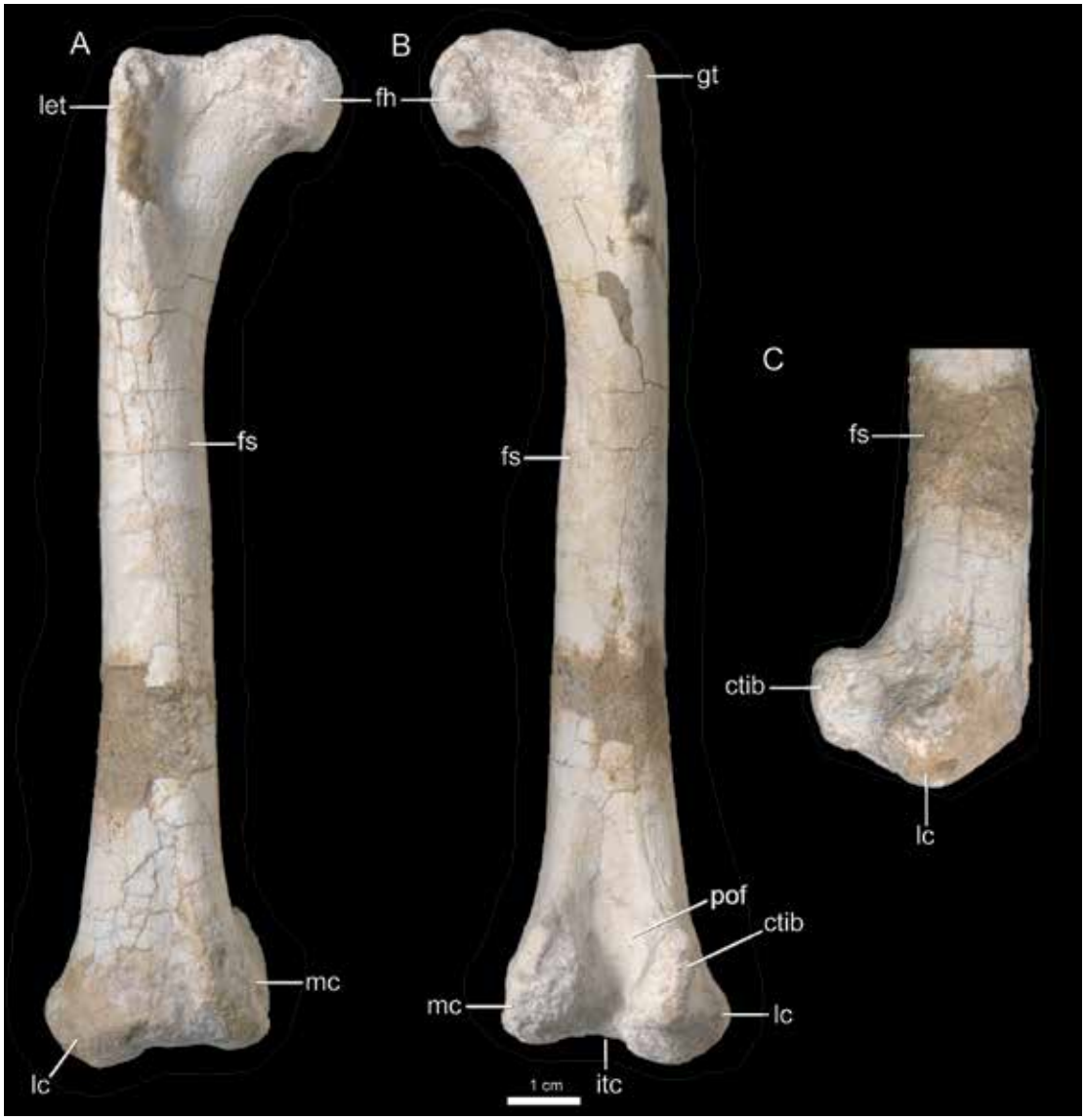

FIGURE 23. Right femur of IGM 100/3006 in **A,** anterior and **B,** posterior views. Photograph of the **C,** distal condyle of IGM 100/3006 in lateral view. See appendix for anatomical abbreviations.

distal tarsal III, being situated proximally to metatarsal II and slightly overlapping metatarsal III, as in *Tongianlong* and *Oksoko*. The fragments take the form of a roughly trapezoidal plate, but little more morphology can be ascertained. The loss of distal tarsal IV may indicate that these elements were not strongly fused to one another as in some skeletally mature oviraptorosaurs such as *Elmisaurus* (Currie et al., 2016; Funston et al., 2015) and *Avimimus nemegtensis* (Funston et al., 2018). There is no sign of advanced fusion between the distal tarsals and the proximal metatarsals as is present in *Oksoko*.

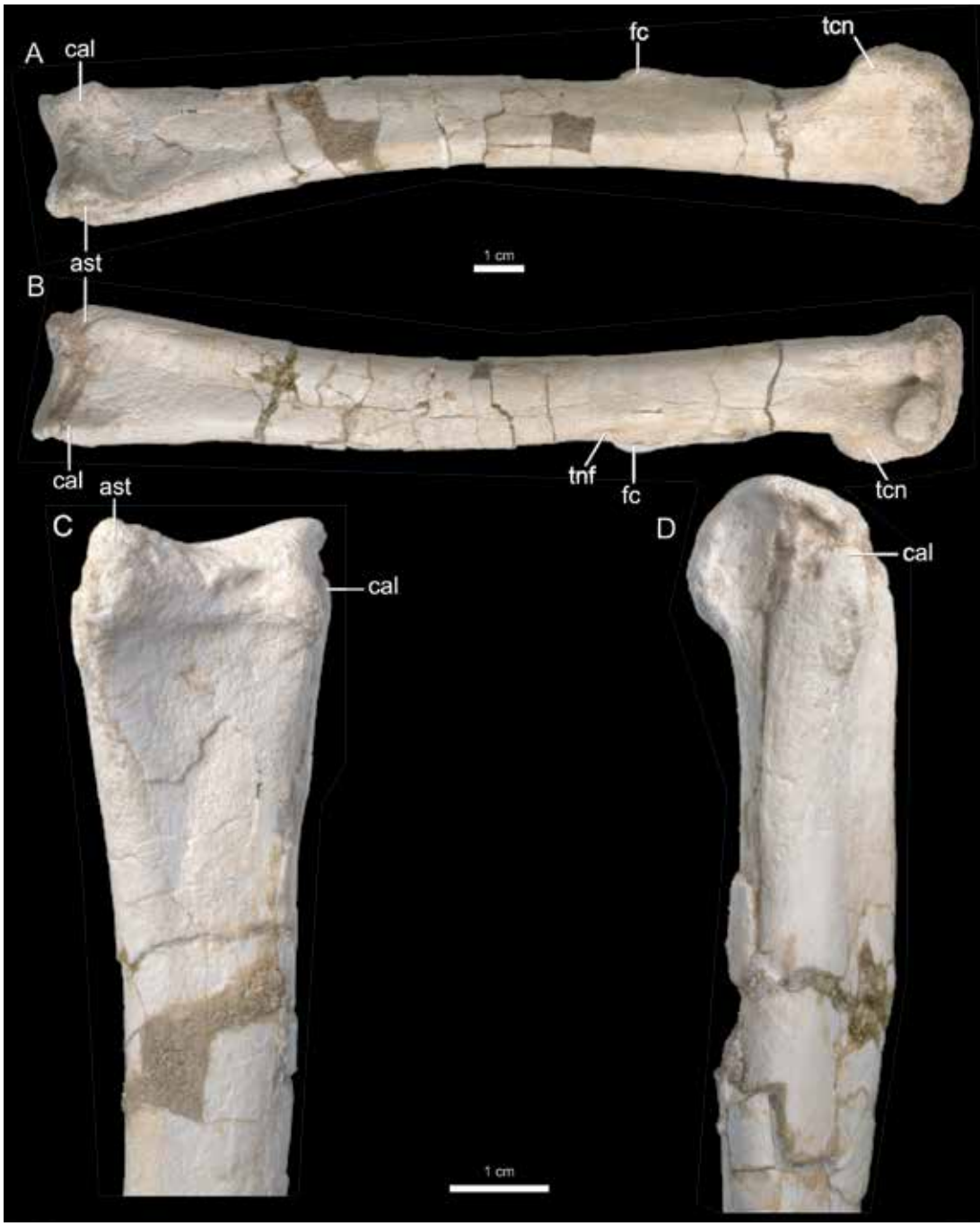

FIGURE 24. Right tibia of IGM 100/3006 in **A,** anterior and **B,** posterior views. Close-up photographs of the distal right tibia of IGM 100/3006 in **C,** anterior and **D,** lateral views. See appendix for anatomical abbreviations.

Pes

Figures 3, 26, 27

The feet are preserved in both specimens of *Conchoraptor* (figs. 3, 26, 27); although the right foot of IGM 100/3006 is the most completely preserved in articulation, missing only the 3rd ungual phalanx. The left foot is missing its 2nd and 4th ungual phalanges.

Metatarsals II–IV are preserved in both specimens. As is the case in all oviraptorids, *Conchoraptor* lacks a true arctometatarsalian condition (Osmólska et al., 2004), but MT III is slightly constricted at its proximal end (figs. 26A, 27D) similar to *Citipati* (IGM 100/978), *Corythoraptor*, *Ganzhousaurus nankangensis* (Wang et al., 2013), and *Wulatelong*. Other oviraptorid taxa such as *Khaan*, *Gigantoraptor*, *Oksoko*, and *Yulong* lack any constriction of MT III whereas more basal oviraptorosaurs such as *Caudipteryx* and *Similicaudipteryx* have a highly compressed metatarsal III (Ji et al., 1998). *A. portentosus* has an extreme condition in which the proximal end of metatarsal III is no longer present (Kurzanov, 1981, 1985). The metatarsals of *Conchoraptor* are not fused proximally as has been posited in other oviraptorid taxa (Osmólska et al., 2004; Lü, 2005), and this state in *Oviraptor* likely represents either taphonomic distortion or disease. Fusion of these elements is present in some caenagnathids such as *Elmisaurus* (Currie et al., 2016) and *Citipes* (Funston et al., 2016). In the foot of *Conchoraptor*, metatarsal III is longest, followed by IV and then II. The shafts of metatarsals III and IV are dorsoventrally (dorsopalmarly) compressed. On either side of the distal articular surfaces on the palmar surface is a flared process that likely served as an attachment point for extensor muscles in the foot. These processes are more pronounced in oviraptorids (especially *Citipati*) than other observed maniraptoran taxa (see Norell and Makovicky, 1999).

FIGURE 25. Right fibula of IGM 100/3006 in **A,** anterior and **B,** posterior views. appendix for anatomical abbreviations.

Although the first digit is not preserved in any of the specimens, the phalangeal formula is likely (2?)-3-4-5, preserving the plesiomorphic state of maniraptorans. Digit III is longest,

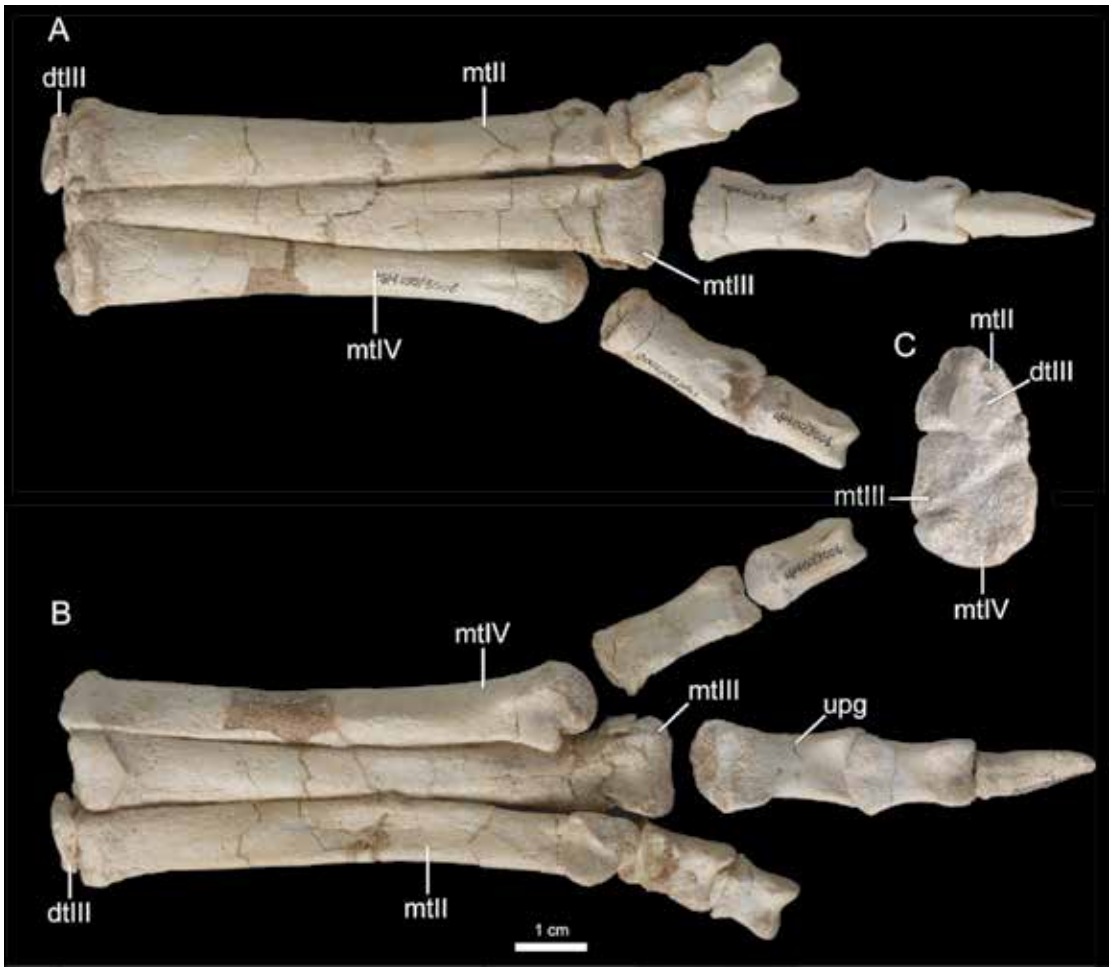

FIGURE 26. Right foot of IGM 100/3006 in **A,** anterior, **B,** posterior, and **C,** proximal views. See appendix for anatomical abbreviations.

followed by II and then IV. In digit III, the combined length of phalanges 1 and 2 is greater than that of phalanx 3, contra the derived condition for oviraptorids according to Osmólska et al. (2004). The ligamentary fossae on the lateral surfaces of the phalanges are deep and elongate similar to those observed in *Citipati* (IGM 100/978), not circular as in *Khaan*. The ungual phalanges are only weakly curved and are the longest phalangeal elements in the foot, with that of digit II the longest. All ungual phalanges possess a deep groove on the lateral surface extending from the distal edge approximately halfway along the length of the element.

PHYLOGENETIC ANALYSIS

Our first analysis (including both old and new scorings of *Conchoraptor*) resulted in 288 most parsimonious trees with a best score of 653. Our second analysis (including our compos-

ite scoring of *Conchoraptor*) resulted in 285 most parsimonious trees with a best score of 652. The strict consensus trees for both analyses were identical in terms of topology and Bremer support values, aside from the inclusion of our scoring of *Conchoraptor* in a polytomy with the previous scoring of *Conchoraptor* and the clade composed of *Nemegtomaia* and all other more deeply nested heyuannines (fig. 28). Oviraptorosauria is recovered, with *Incisivosaurus* as its most basally diverging taxon. The two most inclusive oviraptorosaurian clades, Caenagnathidae and Oviraptoridae, are well supported (Bremer values of 2 and 3 respectively). Heyuanninae is almost entirely resolved, although *Machairasaurus leptonychus* is sister to a polytomy consisting of *Nemegtomaia*, a monophyletic *Heyuannia*, and polytomy consisting of *Oksoko*, *Jiangxisaurus ganzhouensis*, and *Banji*. Citipatininae is recovered, but has a polytomy at its base. *Microvenator* is recovered as the basalmost diverging caenagnathid followed by *Gigantoraptor*. The remainder of Caenagnathidae forms a polytomy including a single clade formed by *Hagryphus giganteus* and *Chirostenotes*.

We interpret the polytomy containing both scorings of *Conchoraptor* and the clade formed by *Machairasaurus* and all other more deeply nested heyuannines to be a result of nonoverlapping scorings between the two entries of *Conchoraptor*. Our inability to score many characters in the anterior cranium of our specimen coupled with the lack of postcranial characters scored for the original entry is likely restricting the ability of the analysis to resolve a sister-group relationship. Indeed, our second analysis which supplemented our new scoring with those of the original entry places *Conchoraptor* in a position recovered in most other analyses as more deeply nested than *Khaan* but rootward of *Machairasaurus*.

DISCUSSION

Autapomorphic Characters of *Conchoraptor gracilis*

The only formalized autapomorphies for the genus *Conchoraptor* are presented by Funston et al. (2018) and are based on the holotype cranium (IGM 100/20). They include: maxilla with large accessory antorbital fenestra; nasals with three dorsal fenestrae per side; postorbital extending nearly to the bottom of the orbit. We cannot confirm or deny the presence of the former two characters in the cranial material of IGM 100/3006 as it does not preserve the relevant portions of the cranium. We do, however, observe the third condition. Although there is a minor disarticulation of the ventral (jugal) process of the postorbital with the dorsal process of the jugal (fig. 1), the articular surface on the latter element suggests that the postorbital would have extended to around the same level as it does in the holotype specimen of *Conchoraptor* (IGM 100/20) (Funston et al., 2018: fig. 6).

In this description of IGM 100/3006 we identify a potentially novel cranial autapomorphy of *Conchoraptor*: a well-developed transverse nuchal crest of the parietal that expands above the dorsal skull table and results in an almost 90° angle between the occipital and dorsal surfaces of the cranium (figs. 1A, 2A). This morphology is also present in the holotype specimen of *Conchoraptor* (Funston et al., 2018; fig. 6B). To our knowledge, this condition is in contrast to all other oviraptorids, wherein the transverse nuchal crest is low, or otherwise indistinguish-

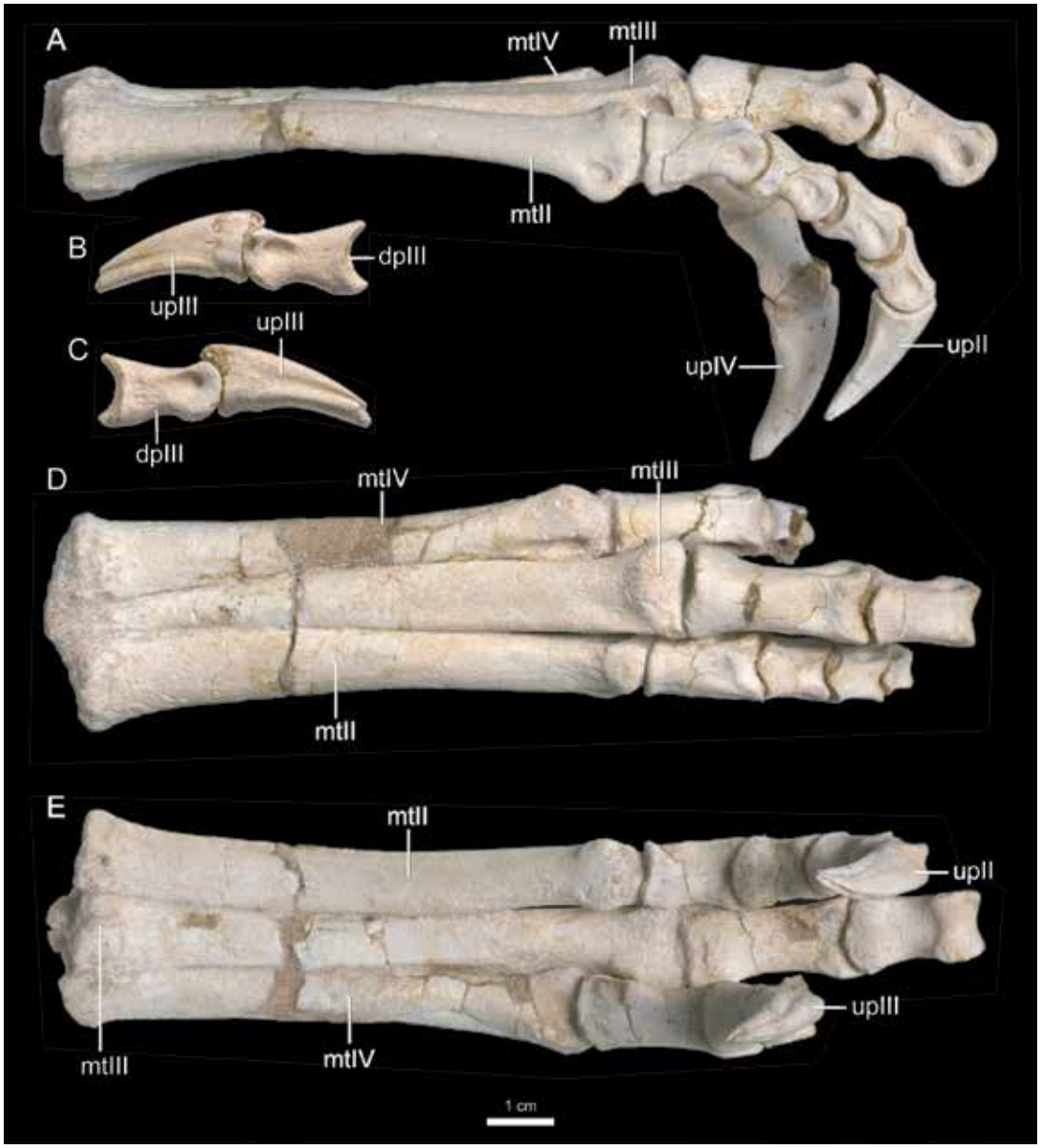

FIGURE 27. Left foot of IGM 100/3006 in **A,** medial, **B,** anterior, and **C,** posterior views. Photographs of the right third distal phalanx of IGM 100/3006 in **D,** lateral and **E,** medial views. See appendix for anatomical abbreviations.

able from the dorsal skull table, and the angle between said surfaces is significantly obtuse. This contrast is made obvious by comparison with the crestless oviraptorids *Khaan*, *Tongtianlong*, and *Banji* in which the occipital and dorsal surfaces of the skull are confluent and result in a smooth, "domed" transition between these regions. In oviraptorosaurs with extensive cranial ornamentation (e.g., *Corythoraptor*, *Rinchenia*, and *Oksoko*), the transverse nuchal crest is dis-

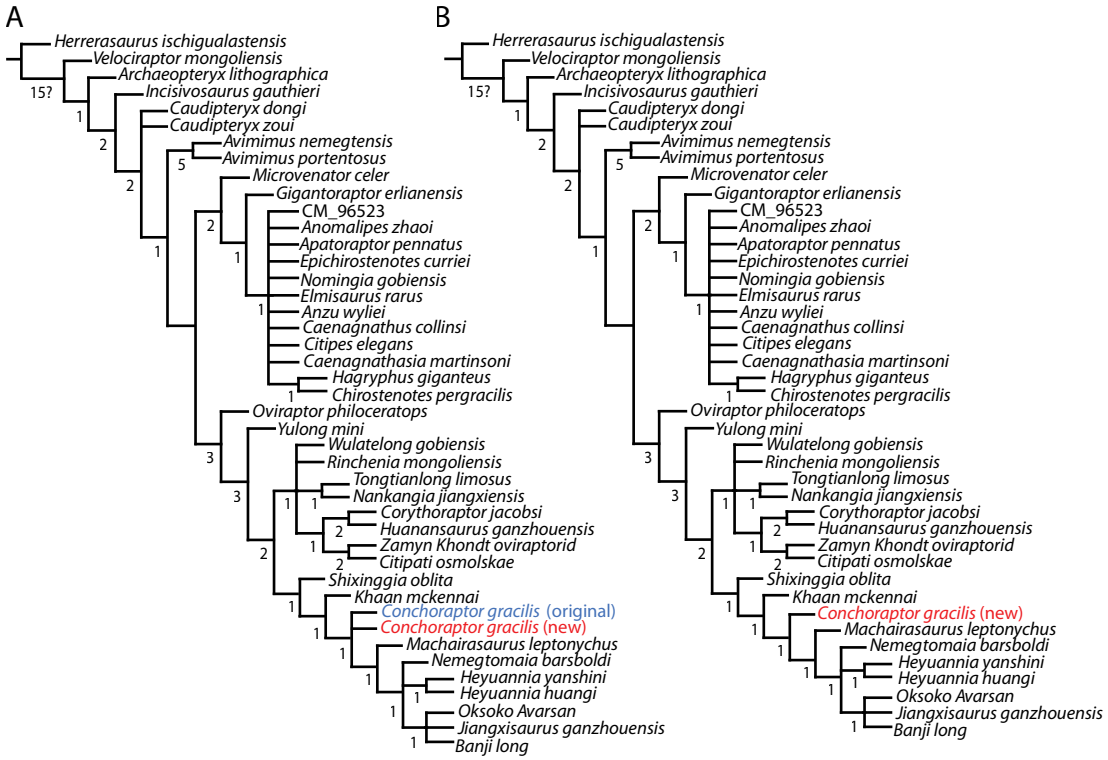

FIGURE 28. Strict consensus trees for both phylogenetic analyses: **A,** result of analysis including both our scoring of *Conchoraptor* (blue) based on IGM 100/3006 and IGM 100/1203 and the original scoring from the matrix of Atkins-Weltman et al., 2024 (red); **B,** result of analysis combining our scoring of IGM 100/3006 and IGM 100/1203 supplemented by character sampling from the previous scoring of Atkins-Weltman et al., 2024 (red).

rupted by the participation of the parietal in the exaggerated ornamentation itself. In *Oksoko*, for example, the crest is distinguishable in dorsal view (Funston, 2024; fig. 11), but does not present significantly above the skull table in lateral view or influence the angle between the stated surfaces. We do note that the skull of the Zamyn Khondt oviraptorid (IGM 100/79) (Funston, 2019: fig. 4.13) resembles the condition of *Conchoraptor* most closely, however the posterior region of the skull in that specimen is both heavily damaged and distorted, raising questions as to the reliability of its morphology.

We do not observe any autapomorphic characters in the postcranial skeleton of either IGM 100/3006 or IGM 100/1203, a testament to its largely generalized anatomy.

Additional Diagnostic Characters of *Conchoraptor gracilis*

A rudimentary diagnosis for *Conchoraptor gracilis*, based on specimen IGM-D 100/20, was provided by Barsbold (1986): "Small oviraptors, second and third non-reduced digits, the bones of which have narrow, straightened, claw-like phalanges." Barsbold (1986) also provides a brief comment on the comparative anatomy of the specimen: "The distinction of *Conchoraptor* from oviraptors proper consists, on account of the essentially smaller size, in the existence and straight-

ness of the claw phalanges and the third digits of the wrist," Funston et al. (2018) provides a more recent diagnosis based on the skull of the holotype (IGM-D 100/20) but notes that the use of a preservative lacquer prohibits the description of more delicate features. Osmólska et al. (2004) provides scattered reference to postcranial elements attributable to *Conchoraptor*, however, not all are figured, and the source of this material is unclear. Based on our description of the these more complete specimens, IGM 100/1203 and IGM 100/3006, we can contribute a more comprehensive diagnosis of *Conchoraptor* (characters taken from the diagnosis of Funston et al. [2018] are followed by a citation and autapomorphies are indicated with an asterisk):

Small oviraptorid oviraptorosaur diagnosed by the following features: cranium lacking a pronounced crest (Barsbold, 1986; Funston et al., 2018); premaxilla with vertical anterior margin (Funston et al., 2018); maxilla with large accessory antorbital fenestra* (Funston et al., 2018); nasals with three dorsal fenestrae per side* (Funston et al., 2018); postorbital extending nearly to the bottom of the orbit* (Funston et al., 2018); parietal with low sagittal crest (Funston et al., 2018); parietal with well-developed transverse nuchal crest that divides the occipital and dorsal surfaces of the skull at a roughly 90° angle*; enlarged first digit of manus (Funston et al., 2018); reduced acromion process of the scapula; weakly developed, anterolaterally directed cnemial crest of the tibia; metatarsals unfused proximally.

Differentiation of *Conchoraptor* from '*Ingenia*'

In this section we will review the taxonomic history of the originally erected "*Ingenia yanshini*" (referred to as *Heyuannia yanshini* in this text) in an effort to produce a resource for future workers that may be struggling with the contradictory descriptive literature surrounding this taxon. Drawing on our descriptions of *Conchoraptor* (IGM 100/3006 and IGM 100/1203), we provide a list of anatomical features that may be useful in distinguishing these taxa from one another, at least until more comprehensive material for *H. yanshini* is recovered and properly described. We will refer to the holotype specimen of *Conchoraptor* (IGM 100/20) and the two specimens of *H. yanshini* included within the Mongolian composite mount (IGM 100/30 and IGM 100/31). We refrain from including details derived from IGM 100/32 in our discussion due to existing doubts that it belongs to the genus *Heyuannia* (Funston et al., 2018), and that its morphology is not well documented in the literature.

The taxon "*Ingenia yanshini*" has been in a state of flux since its original description by Barsbold (1981), who named the taxon in honor of the Russian academic A.L. Yanshin. Taxonomic complications arose early, as the genus name was already preoccupied by a tripyloidid nematode, *Ingenia mirabilis* (Gerlach, 1957). In response, Paul (1988) employs *"Oviraptor yanshini*" as a possible synonym, however, this failed to gain traction in the research community (Easter, 2013; Yun, 2019). The issue was recognized and finally amended under the ICZN by Easter (2013), who erected the genus *Ajancingenia*. Unfortunately, it soon became apparent that this work was morally dubious and included plagiarized text and figures, resulting in a general reluctance by the research community to accept the new name. Funston et al. (2018) suggests synonymizing "*Ajancingenia yanshini*" with "*Heyuannia yanshini*," based on strong phylogenetic support for a sister relationship between "*Ingenia*" and *H. huangi*. Yun (2019)

recovers "Heyuanninae" as a monophyletic node-based clade composed of *Conchoraptor*, *Heyuannia huangi*, and "*Heyuannia yanshini*," effectively replacing the clade "Ingeniinae," defined by Osmólska et al. (2004) as composed of *Conchoraptor*, *Khaan*, and *H. huangi*.

The most prolific contribution to the description of "*Ingenia*" material in recent times has been that of Osmólska et al. (2004), who list a "partial skeleton with a skull" as the holotype. However, as pointed out by Funston et al. (2018), the mounted skeleton used for observations in this study (IGM-D 100/30) represents a composite of several specimens. The majority of the postcrania, including the radii, left metacarpus, pelvis, femora, right metatarsus, and pedal phalanges are from IGM-D 100/31 and the left manual digits are from IGM-D 100/32.

The pairing of a convoluted taxonomic history and an inconsistent descriptive literature has resulted in wide-scale misunderstanding as to exactly what characters differentiate *H. yanshini* from other small-bodied oviraptorids, especially those that are not well documented in the literature such as *Conchoraptor*. It should be noted that because all cranial material associated with the *H. yanshini* holotype has since been lost to science, we will compare only elements of the anatomy that reflect what can still be accessed by researchers. This limits us to postcranial bones (figures of the lost material can be found in Barsbold, 1983). The following features differ between *Conchoraptor* and *H. yanshini* (including the specimens in which they are present): (1) *Conchoraptor* (IGM 100/1203) possesses a reduced acromion process of the scapula relative to *H. yanshini* (IGM 100/30), wherein the process is winglike (fig. 29A, B). (2) The scapula blade in *Conchoraptor* (IGM 100/1203) widens distally, whereas in *H. yanshini* (IGM 100/30) it maintains the same width throughout (fig. 29A, B). (3) The pubic shaft in *Conchoraptor* (IGM 100/3006) tapers proximally to the "pubic boot," whereas in *H. yanshini* (IGM 100/31) it remains at a consistent width for its entire length (fig. 29E, F). (4) *Conchoraptor* (IGM 100/1203) exhibits a weakly developed, anterolaterally oriented cnemial crest on the tibia, unlike *H. yanshini* (IGM 100/30) wherein the crest is more robust (fig. 29C, D). (5) The transverse processes of the posterior caudal vertebrae in *Conchoraptor* (IGM 100/1203) are lobelike, whereas in *H. yanshini* (IGM 100/30) they are rectangular (fig. 29G, H).

As is so often an issue in the field of vertebrate paleontology, a lack of skeletal material critically reduces the resolution by which taxa can be differentiated from one another. The problem is compounded when specimens that are known to have existed in the past become lost. This issue is exemplified by the case of the *Conchoraptor–H. yanshini* complex, where we are limited to comparisons of only the postcranial characters of the skeleton due to the loss of the holotype cranium in the latter taxon. Despite this, we remain hopeful that more *H. yanshini* material will become available in the future, and that it will be a source of valuable data for unravelling the taxonomic relationships between these enigmatic dinosaurs.

Differentiation of *Conchoraptor* from *Khaan mckennai*

Understanding how closely related, and closely geographically associated oviraptorids differ from one another is critical to our ability to accurately reconstruct the Late Cretaceous ecosystems of the Nemegt Basin. As pointed out by Clark et al. (2001), *Khaan* shares many

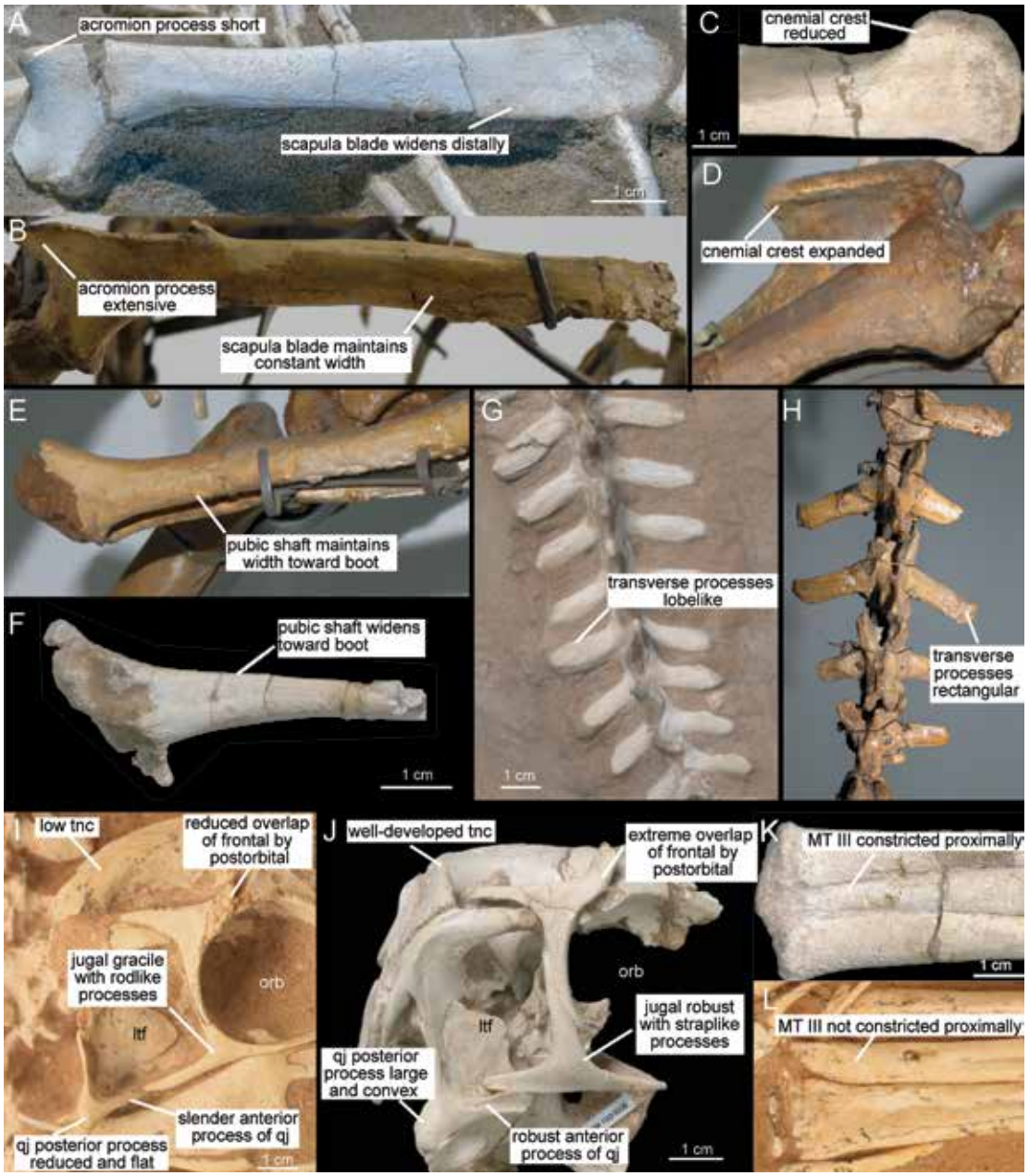

FIGURE 29. Anatomical comparisons between *Conchoraptor gracilis* and the other small bodied, crestless oviraptorids *Heyuannia yanshini* and *Khaan mckennai*: scapulae of **A,** *Conchoraptor* (IGM 100/1203) and **B,** *H. yanshini* (IGM 100/30); proximal tibiae of **C,** *Conchoraptor* (IGM 100/3006) and **D,** *H. yanshini* (IGM 100/30); pubes of **E,** *H. yanshini* (IGM 100/31) and **F,** *Conchoraptor* (IGM 100/3006); caudal vertebrae of **G,** *Conchoraptor* (IGM 100/1203) and **H,** *H. yanshini* (IGM 100/30); posterior crania of **I,** *Khaan* (IGM 100/1002) and **J,** *Conchoraptor* (IGM 100/3006); proximal metatarsals of **K,** *Conchoraptor* (IGM 100/3006) and **L,** *Khaan*. See appendix for anatomical abbreviations.

superficial similarities to *Conchoraptor*, including a small body size, a domed and crestless skull, and a generalized postcranial skeleton. We take this opportunity to clarify the divergent anatomical features between these taxa, integrating observations from IGM 100/1203 and IGM 100/3006. For previously established autapomorphies of *Khaan*, see Clark et al. (2001).

Clark et al. (2001) note that the cranium of *Khaan* differs from that of *Conchoraptor* in two ways: In *Khaan*, the long axis of the external naris is more horizontally oriented and the nasals are fused. Both newly described specimens of *Conchoraptor* lack these portions of the skull, so we cannot append detail here. In the remainder of the cranium, however, we report several differences (fig. 29I, J). The jugal and its comprising processes in *Conchoraptor* are more robust overall and anteroposteriorly shorter than in *Khaan*, which exhibits an extremely gracile jugal with delicate, rodlike processes. The ventral margin of the jugal in *Conchoraptor* is horizontal, unlike in *Khaan* where it ascends anterodorsally at a shallow angle. The posterior process of the quadratojugal in *Conchoraptor* is well developed and convex, whereas in *Khaan* it is poorly developed with a largely flat lateral surface. The anterior process of the quadratojugal in *Khaan* is slender, unlike in *Conchoraptor* where it is dorsoventrally deep. In *Conchoraptor*, the frontal process of the postorbital extensively overlaps the posterolateral surface of the frontal, whereas in *Khaan* this overlap is relatively minor. Finally, the transverse nuchal crest of the parietal is considerably more developed in *Conchoraptor* than in *Khaan*, resulting in a more abrupt transition from the occipital to dorsal surface of the skull in the former.

We also report a single difference in the postcranium: Metatarsal III in *Conchoraptor* is strongly constricted proximally, unlike in *Khaan* where it maintains its width for almost its entire length (fig. 29K, L).

Ontogenetic Interpretations

While we currently lack osteohistological data that have been hugely informative in reconstructing oviraptorosaur ontogeny (e.g., Funston and Currie, 2018; Funston et al., 2020; Cullen et al., 2021), we do have access to several external indicators of skeletal maturity that may give some indication of the relative growth stage in these specimens.

In IGM 100/3006, the frontals and parietals are fused along a tightly sutured midline contact and are not taphonomically dissociated, indicating that their fusion was largely complete (fig. 2A). Other oviraptorosaur descriptions paired with osteohistological data have demonstrated that fusion between contralateral dermatocranial and neurocranial elements occurred early in ontogeny, and thus these features are likely a poor landmark for posthatching ontogeny in these animals (Funston, 2024).

The cervical centra show obvious open neurocentral sutures with their respective neural arches (figs. 3, 14, 15), and some are broken clearly along the line of contact, indicating that they were not fused. Neurocentral fusion in the cervical series has been shown to be a relatively late-stage occurrence in oviraptorosaurs, with even adult individuals lacking fusion in some segments (Funston and Currie, 2016; Funston, 2024). In the anterior caudal series of IGM 100/3006, all neurocentral sutures are unfused. Again, this dynamic is restricted to later ontogeny in oviraptorosaurs with known osteohistological data. The most useful indicator of skeletal

maturity in IGM 100/3006 is the level of fusion in the sacral series. All sacral centra remain unfused to one another, preventing the identification of the primordial sacral vertebrae that have been observed to unify in at least one prehatching oviraptorosaur (Norell et al., 2001) (although see Wang et al., 2016, for an unfused embryonic sacral series). The size of this individual obviously prevents its identification as an embryo, although this observation does indicate that even the early fusion of these sacral vertebrae was weak. Fusion of sacral vertebrae is present in oviraptorosaur specimens for which osteohistological data assign an "early juvenile" status (Funston et al., 2020; Funston, 2024), suggesting that IGM 100/3006 may have been of an even earlier developmental stage.

Limited ventral exposure of the axial column in IGM 100/1203 restricts our ability to observe many of the above ontogenetic characters in this specimen, including fusion in the sacral series. A few cervical neurocentral sutures can be observed and are identical to the condition seen in those of IGM 100/3006, implying that the individual was not an adult. Given the similarity in the size of both specimens, it is likely that they represent individuals of approximately the same level of skeletal maturity.

Ultimately, the lack of fusion in any of the sacral vertebrae in IGM 100/3006 prevents us from assigning a level of maturity higher than or equal to other oviraptorosaur specimens designated as early juveniles by osteohistological data. We refrain from making further, more specific estimates and await the acquisition of histological data to better bracket the level of maturity in these specimens.

Phylogenetic Relationships of Oviraptorosaurians

Our phylogenetic analyses recover a topology that is broadly congruent with recent published phylogenies (e.g., Lü et al., 2015, 2016; Funston et al., 2020a) and is very similar to that of Atkins-Weltman et al. (2024) (fig. 28). The polytomy within Caenagnathidae is also recovered by Atkins-Weltman et al. (2024) and is only slightly better resolved than ours. As in the consensus tree of Atkins-Weltman et al. (2024), Bremer support values for both Oviraptoridae and Caenagnathidae are higher than in most previous oviraptorosaur phylogenies, suggesting that our ability to reliably resolve relationships at the base of these major clades is improving. Relationships among more deeply nested oviraptorosaur taxa will continue to benefit from detailed, character-rich descriptions such as this one, especially as an increasing number of specimens are subjected to study with computed tomography and can thus be sampled more thoroughly for phylogenetic characters. This contribution has allowed for a more comprehensive scoring of *Conchoraptor*, which will aid in future efforts to clarify relationships among these enigmatic and anatomically bizarre dinosaurs.

ACKNOWLEDGMENTS

We would like to thank both the Mongolian Academy of Sciences (MAS) for allowing the study of the fossils, and the curatorial staff at the American Museum of Natural History (AMNH) for facilitating our access to the material. Special thanks go to Mick Ellison (AMNH) who pro-

vided the numerous high-quality photographs of the specimens, to Carl Mehling who welcomed us into the AMNH collections, and to Marilyn Fox (Yale) who skillfully prepared both skeletons following their removal from the field. Fieldwork was supported by the Margaret and Will Hearst Paleontological Research Fund and the Frick Laboratory Endowment at the AMNH. We thank Larry Witmer who facilitated the CT imaging in his lab at Ohio State University. Gabriel Bever and all members of the Bever Lab (Johns Hopkins School of Medicine, Center for Functional Anatomy and Evolution) provided valuable discussion during the preparation of the manuscript and gave access to Amira 6.3.0 (FEIVSG Company) software for the utilization of CT data. We are grateful to Gregory Funston at the University of California, Davis, for his helpful review and for sharing with us several hard-to-find manuscripts early in the writing process.

REFERENCES

Atkins-Weltman, K.L., D.J. Simon, H.N. Woodward, G.F. Funston, and E. Snively. 2024. A new oviraptorosaur (Dinosauria: Theropoda) from the end-Maastrichtian Hell Creek Formation of North America. PLoS One 19: 1–27.

Balanoff, A.M. 2011. Oviraptorosauria: morphology, phylogeny, and endocranial evolution. Ph.D. dissertation, Department of Earth and Environmental Sciences, Columbia University, New York.

Balanoff, A.M., and M.A. Norell. 2012. Osteology of *Khaan mckennai* (Oviraptorosauria: Theropoda). Bulletin of the American Museum of Natural History 372: 1–77.

Balanoff, A.M., X. Xu, Y. Kobayashi, Y. Matsufune, and M.A. Norell. 2009. Cranial osteology of the theropod dinosaur *Incisivosaurus gauthieri* (Theropoda: Oviraptorosauria). American Museum Novitates 3651: 1–35.

Balanoff, A.M., G.S. Bever, T.B. Rowe, and M.A. Norell. 2013. Evolutionary origins of the avian brain. Nature 501: 93–96.

Balanoff, A.M., G.S. Bever, and M.A. Norell. 2014. Reconsidering the avian nature of the oviraptorosaur brain (Dinosauria: Theropoda). PLoS One 9: 1–15.

Balanoff, A.M., M.A. Norell, A.V. Hogan, and G.S. Bever. 2018. The endocranial cavity of oviraptorosaur dinosaurs and the increasingly complex, deep history of the avian brain. Brain, Behavior, and Evolution 91: 125–135.

Barsbold, R. 1981. Toothless carnivorous dinosaurs of Mongolia. Joint Soviet-Mongolian Paleontological Expedition Transactions 15: 28–39. [in Russian]

Barsbold, R. 1983. Carnivorous dinosaurs from the Cretaceous of Mongolia. Sovmestnaa Sovetsko-Mongol'skaa Palaeontologisceskaa Ekspedicia Trudy 19: 5–119.

Barsbold, R. 1986. Raubdinosaurier Oviraptoren. *In* E.I. Vorobyeva (editor), Herpetologische Untersuchungen in der Mongolischen Volksrepublik: 210–223. Akademia Nauk SSSR Institut Evolyucionnoi Morfologii I Ekologii Zhivotnikh. Moscow: A.M. Severtsova. [in Russian]

Barsbold, R. 1997. Oviraptorosauria. *In* P.J. Currie and K. Padian (editors), Encyclopedia of dinosaurs: 505–509. San Diego: Academic Press.

Barsbold, R., H. Osmólska, M. Watabe, P.J. Currie, and K. Tsogtbaatar. 2000. A new oviraptorosaur (Dinosauria, Theropoda) from Mongolia: the first dinosaur with a pygostyle. Acta Palaeontologica Polonica 45: 97–106.

Baumel, J.J., and L. Gerchman. 1968. The avian intercarotid anastomosis and its homologue in other vertebrates. American Journal of Anatomy 122: 1–18.

Baumel, J.J., and L. Witmer. 1993. Osteologia. *In* J.J. Baumel, A.S. King, J.E. Breazile, H.E. Evans, and J.C. Vanden Berge (editors), Handbook of avian anatomy: nomina anatomica avium, 2nd ed.: 45–132. Publications of the Nuttall Ornithological Club 23. Cambridge, MA: Nuttall Ornithological Club.

Benson, R.B., R.J. Butler, M.T. Carrano, and P.M. O'Connor. 2012. Air-filled postcranial bones in theropod dinosaurs: physiological implications and the 'reptile'-bird transition. Biological Reviews 87: 168–193.

Bever, G.S., and M.A. Norell. 2009. The perinate skull of *Byronosaurus* (Troodontidae) with observations on the cranial ontogeny of paravian theropods. American Museum Novitates 3657: 1–52.

Bever, G.S., S.L. Brusatte, A.M. Balanoff, and M.A. Norell. 2011. Variation, variability, and the origin of the avian endocranium: insights from the anatomy of *Alioramus altai* (Theropoda: Tyrannosauroidea). PLoS One 6: 1–10.

Bever, G.S., et al. 2013. The braincase anatomy of the late Cretaceous dinosaur *Alioramus* (Theropoda: Tyrannosauroidea). Bulletin of the American Museum of Natural History 376: 1–72.

Bi, S., et al. 2021. An oviraptorid preserved atop an embryo-bearing egg clutch sheds light on the reproductive biology of non-avialan theropod dinosaurs. Science Bulletin 66: 947–954.

Brochu, C.A. 2003. Osteology of *Tyrannosaurus rex*: insights from a nearly complete skeleton and high-resolution computed tomographic analysis of the skull. Journal of Vertebrate Paleontology 22: 1–138.

Burnham, D.A., et al. 2000. Remarkable new birdlike dinosaur (Theropoda: Maniraptora) from the Upper Cretaceous of Montana. University of Kansas Paleontological Contributions Paper 13: 1–14.

Chiappe, L.M., M.A. Norell, and J.M. Clark. 1998. The skull of a relative of the stem-group bird *Mononykus*. Nature 392: 275–278.

Clark, J.M., P. Altangerel, M.A. Norell, and Mongolyn Shinzhlėkh Ukhaany Akademi. 1994. The skull of *Erlicosaurus andrewsi*, a late Cretaceous "Segnosaur" (Theropoda, Therizinosauridae) from Mongolia. American Museum Novitates 3115: 1–39.

Clark, J.M., M.A. Norell, L.M. Chiappe, M.S.U. Akademi, and Mongolian-American Museum Paleontological Project. 1999. An oviraptorid skeleton from the late Cretaceous of Ukhaa Tolgod, Mongolia, preserved in an avianlike brooding position over an oviraptorid nest. American Museum Novitates 3265: 1–35.

Clark, J.M., M.A. Norell, and R. Barsbold. 2001. Two new oviraptorids (Theropoda: Oviraptorosauria), Upper Cretaceous Djadokhta Formation Ukhaa Tolgod, Mongolia. Journal of Vertebrate Paleontology 21: 209–213.

Clark, J.M., M.A. Norell, and T. Rowe. 2002. Cranial anatomy of *Citipati osmolskae* (Theropoda, Oviraptorosauria), and a reinterpretation of the holotype of *Oviraptor philoceratops*. American Museum Novitates 3364: 1–24.

Colbert, E.H. 1964. Relationships of the saurischian dinosaurs. American Museum Novitates 2181: 1–24.

Cullen, T.M., et al. 2020. Osteohistological analyses reveal diverse strategies of theropod dinosaur body-size evolution. Proceedings of the Royal Society of London B 287: 1–9.

Currie, P.J. 1995. New information on the anatomy and relationships of *Dromaeosaurus albertensis* (Dinosauria: Theropoda). Journal of vertebrate Paleontology 15: 576–591.

Currie, P.J., and D.A. Russell. 1988. Osteology and relationships of *Chirostenotes pergracilis* (Saurischia, Theropoda) from the Judith River (Oldman) Formation of Alberta, Canada. Canadian Journal of Earth Sciences 25: 972–986.

Currie, P.J., and X.J. Zhao. 1993. A new troodontid (Dinosauria, Theropoda) braincase from the dinosaur park formation (Campanian) of Alberta. Canadian Journal of Earth Sciences 30: 2231–2247.

Currie, P.J., S.J. Godfrey, and L. Nessov. 1993. New caenagnathid (Dinosauria: Theropoda) specimens from the Upper Cretaceous of north America and Asia. Canadian Journal of Earth Sciences 30: 2255–2272.

Currie, P.J., G.F. Funston, and H. Osmólska. 2016. New specimens of the crested theropod dinosaur *Elmisaurus rarus* from Mongolia. Acta Palaeontologica Polonica 61: 143–157.

Easter, J. 2013. A new name for the oviraptorid dinosaur "*Ingenia*" *yanshini* (Barsbold, 1981; preoccupied by Gerlach, 1957). Zootaxa 3737: 184–190.

Elzanowski, A. 1999. A comparison of the jaw skeleton in theropods and birds, with a description of the palate in the Oviraptoridae. Smithsonian Contributions to Paleobiology 89: 311–323.

Fanti, F., P.J. Currie, and D. Badamgarav. 2012. New specimens of *Nemegtomaia* from the Baruungoyot and Nemegt formations (Late Cretaceous) of Mongolia. PLoS One 7: 1–16.

Fanti, F., Cantelli, L. and Angelicola, L., 2018. High-resolution maps of Khulsan and Nemegt localities (Nemegt Basin, southern Mongolia): stratigraphic implications. Palaeogeography, Palaeoclimatology, Palaeoecology 494: 14–28.

Franzosa, J. W. 2004. Evolution of the brain in Theropoda (Dinosauria). Ph.D. dissertation, Austin: University of Texas at Austin.

Funston, G.F. 2019. Anatomy, systematics, and evolution of Oviraptorosauria (Dinosauria, Theropoda). Ph.D. dissertation, Department of Biological Sciences, University of Alberta, Alberta.

Funston, G.F. 2024. Osteology of the two-fingered oviraptorid *Oksoko avarsan* (Theropoda: Oviraptorosauria). Zoological Journal of the Linnean Society 2024: 1–47.

Funston, G.F., and P.J. Currie. 2016. A new caenagnathid (Dinosauria: Oviraptorosauria) from the Horseshoe Canyon Formation of Alberta, Canada, and a reevaluation of the relationships of Caenagnathidae. Journal of Vertebrate Paleontology 36: 1–19.

Funston, G.F., and P.J. Currie. 2018. A small caenagnathid tibia from the Horseshoe Canyon Formation (Maastrichtian): Implications for growth and lifestyle in oviraptorosaurs. Cretaceous Research 92: 220–230.

Funston, G.F., and P.J. Currie. 2021. New material of *Chirostenotes pergracilis* (Theropoda, Oviraptorosauria) from the Campanian Dinosaur Park Formation of Alberta, Canada. Historical Biology 33: 1671–1685.

Funston, G.F., P.J. Currie, and M.E. Burns. 2015. New elmisaurine specimens from North America and their relationship to the Mongolian *Elmisaurus rarus*. Acta Palaeontologica Polonica 61: 159–173.

Funston, G.F., S.E. Mendonca, P.J. Currie, and R. Barsbold. 2018. Oviraptorosaur anatomy, diversity and ecology in the Nemegt Basin. Palaeogeography, Palaeoclimatology, Palaeoecology 494: 101–120.

Funston, G.F., et al. 2020a. A new two-fingered dinosaur sheds light on the radiation of Oviraptorosauria. Royal Society Open Science 7: 1–15.

Funston, G.F., et al. 2020b. Histology of caenagnathid (Theropoda, Oviraptorosauria) dentaries and implications for development, ontogenetic edentulism, and taxonomy. Anatomical Record 303: 918–934.

Furet, M., et al. 2022. Estimating motion between avian vertebrae by contact modeling of joint surfaces. Computer Methods in Biomechanics and Biomedical Engineering 25: 123–131.

Gauthier, J. 1986. Saurischian monophyly and the origin of birds. Memoirs of the California Academy of Sciences 8: 1–55.

Gerlach, S.A. 1957. Die Nematodenfauna des Sandstrandes an der Küste von Mittelbrasilien (Brasilianische Meeres Nematoden IV). Mitteilungen aus dem Museum für Naturkunde in Berlin. Zoologisches Museum und Institut für Spezielle Zoologie (Berlin) 33: 411–459.

Goloboff, P.A., and M.E. Morales. 2023. TNT version 1.6, with a graphical interface for MacOS and Linux, including new routines in parallel. Cladistics 39: 144–153.

Gradziński, R., and T. Jerzykiewicz. 1974a. Dinosaur-and mammal-bearing aeolian and associated deposits of the Upper Cretaceous in the Gobi Desert (Mongolia). Sedimentary Geology 12: 249–278.

Gradziński, R., and T. Jerzykiewicz. 1974b. Sedimentation of the Barun Goyot formation. Palaeontologica Polonica 30: 111–146.

He, T., W. Xiao-Lin, and Z. Zhong-He. 2008. A new genus and species of caudipterid dinosaur from the Lower Cretaceous Jiufotang Formation of western Liaoning, China. Vertebrata PalAsiatica 46: 1–12.

Holtz, T.R. 1998. Theropod paleobiology, more than just bird origins. Gaia-Revista de Geociências 15: 1–3.

Hutchinson, J. R. 2001. The evolution of hindlimb anatomy and function in theropod dinosaurs. Ph.D. dissertation, University of California, Berkeley.

Ji, Q., P.J. Currie, M.A. Norell, and J. Shu-An. 1998. Two feathered dinosaurs from northeastern China. Nature 393: 753–761.

Kundrát, M. 2007. Avian-like attributes of a virtual brain model of the oviraptorid theropod *Conchoraptor gracilis*. Naturwissenschaften 94: 499–504.

Kundrát, M., and J. Janáček. 2007. Cranial pneumatization and auditory perceptions of the oviraptorid dinosaur *Conchoraptor gracilis* (Theropoda, Maniraptora) from the Late Cretaceous of Mongolia. Naturwissenschaften 94: 769–778.

Kurzanov, S.M. 1981. On the unusual theropods from the Upper Cretaceous of Mongolia. Iskopaemye Pozvonocnye Mongolii. Sovmestnaa Sovetsko-Mongol'skaa Palaeontologisceskaa Ekspedicia Trudy 15: 39–50.

Kurzanov, S.M. 1985. The skull structure of the dinosaur *Avimimus*. Paleontological Journal 1985: 81–89.

Lamanna, M.C., H.D. Sues, E.R. Schachner, and T.R. Lyson. 2014. A new large-bodied oviraptorosaurian theropod dinosaur from the latest Cretaceous of western North America. PloS One 9: 1–16.

Lee, S., et al. 2019. A new baby oviraptorid dinosaur (Dinosauria: Theropoda) from the Upper Cretaceous Nemegt Formation of Mongolia. PLoS One: 1–25.

Lü, J. 2002. A new oviraptorosaurid (Theropoda: Oviraptorosauria) from the Late Cretaceous of southern China. Journal of Vertebrate Paleontology 22: 871–875.

Lü, J. 2005. Oviraptorid dinosaurs from southern China. Ph.D dissertation, Department of Geological Sciences, Southern Methodist University, Texas.

Lü, J.C., Y. Tomida, Y. Azuma, Z.M. Dong, and Y.N. Lee. 2004. New oviraptorid dinosaur (Dinosauria: Oviraptorosauria) from the Nemegt Formation of southwestern Mongolia. Bulletin of the National Science Museum of Tokyo, Series C 30: 95–130.

Lü, J., et al. 2013a. Chicken-sized oviraptorid dinosaurs from central China and their ontogenetic implications. Naturwissenschaften 100: 165–175.

Lü, J., L. Yi, H. Zhong, and X. Wei. 2013b. A new oviraptorosaur (Dinosauria: Oviraptorosauria) from the Late Cretaceous of southern China and its paleoecological implications. PLoS One 8: 1–14.

Lü, J., et al. 2015. A new oviraptorid dinosaur (Dinosauria: Oviraptorosauria) from the Late Cretaceous of Southern China and its paleobiogeographical implications. Scientific Reports 5: 1–15.

Lü, J., R. Chen, S.L. Brusatte, Y. Zhu, and C. Shen. 2016. A Late Cretaceous diversification of Asian oviraptorid dinosaurs: evidence from a new species preserved in an unusual posture. Scientific Reports 6: 1–12.

Lü, J., et al. 2017. High diversity of the Ganzhou Oviraptorid Fauna increased by a new "cassowary-like" crested species. Scientific Reports 7: 1–13.

Makovicky, P.J., and H.D. Sues. 1998. Anatomy and phylogenetic relationships of the theropod dinosaur *Microvenator celer* from the Lower Cretaceous of Montana. American Museum Novitates 3240: 1–27.

Makovicky, P.J., and M.A. Norell. 2004. Troodontidae. *In* D.B. Weishampel, P. Dodson, and H. Osmólska (editors), The Dinosauria, 2nd ed.: 184–195. Berkeley: University of California Press.

Maryanska, T., and H. Osmólska. 1997. The quadrate of oviraptorid dinosaurs. Acta Palaeontologica Polonica 42: 361–371.

Maryanska, T., H. Osmólska, and M. Wolsan. 2002. Avialan status for Oviraptorosauria. Acta Palaeontologica Polonica 47: 97–116.

Nesbitt, S.J., A.H. Turner, M. Spaulding, J.L. Conrad, and MA. Norell. 2009. The theropod furcula. Journal of Morphology 270: 856–879.

Norell, M.A., J.M. Clark, and L.M. Chiappe. 2001. An embryonic oviraptorid (Dinosauria: Theropoda) from the upper Cretaceous of Mongolia. American Museum Novitates 3315: 1–20.

Norell, M., et al. 2002. 'Modern' feathers on a non-avian dinosaur. Nature 416: 36–37.

Norell, M.A., et al. 2006. A new dromaeosaurid theropod from Ukhaa Tolgod (Ömnögov, Mongolia). American Museum Novitates 3545: 1–51.

Norell, M.A., et al. 2009. A review of the Mongolian cretaceous dinosaur *Saurornithoides* (Troodontidae: Theropoda). American Museum Novitates 3654: 1–63.

Norell, M.A., and Makovicky, P.J. 2004. Dromaeosauridae. *In* D.B. Weishampel, P. Dodson, and H. Osmólska (editors), The Dinosauria, 2nd ed.: 196–209. Berkeley: University of California Press.

Norell, M.A., A.M. Balanoff, D.E. Barta, and G.M. Erickson. 2018. A second specimen of *Citipati osmolskae* associated with a nest of eggs from Ukhaa Tolgod, Omnogov Aimag, Mongolia. American Museum Novitates 3899: 1–44.

Osborn, H.F. 1924. Three new theropoda, *Protoceratops* zone, central Mongolia. American Museum Novitates 144: 1–12.

Osmólska, H. 1976. New light on the skull anatomy and systematic position of *Oviraptor*. Nature 262: 683–684.

Osmólska H, P.J. Currie, R. Barsbold. 2004. Oviraptorosauria. *In* D.B. Weishampel, P. Dodson, and H. Osmólska (editors), The Dinosauria, 2nd ed.: 165–184. Berkeley: University of California Press.

Ostrom, J.H. 1969. Osteology of *Deinonychus antirrhopus*, an unusual theropod from the Lower Cretaceous of Montana. Bulletin of the Peabody Museum of Natural History 30: 1–165.

Paul, G.S. 1988. Predatory dinosaurs of the world: a complete illustrated guide. New York: Simon and Schuster Co.

Persons, W.S.P, G.F. Funston, P.J. Currie, and M.A. Norell. 2015. A possible instance of sexual dimorphism in the tails of two oviraptorosaur dinosaurs. Scientific Reports 5: 1–4.

Rauhut, O.W. 2014. New observations on the skull of *Archaeopteryx*. Paläontologische Zeitschrift 88: 211–221.

Shufeldt, R.W. 1909. Osteology of birds. New York State Museum Bulletin 130: 1–381.

Sues, H.D. 1997. On *Chirostenotes*, a Late Cretaceous oviraptorosaur (Dinosauria: Theropoda) from western North America. Journal of Vertebrate Paleontology 17: 698–716.

Tanaka, K., et al. 2018. Incubation behaviours of oviraptorosaur dinosaurs in relation to body size. Biology Letters 14: 1–4.

Turner, A.H., P.J. Makovicky, and M.A. Norell. 2012. A review of dromaeosaurid systematics and paravian phylogeny. Bulletin of the American Museum of Natural History 371: 1–206.

Varricchio, D.J., and F.D. Jackson. 2016. Reproduction in Mesozoic birds and evolution of the modern avian reproductive mode. Auk: Ornithological Advances 133: 654–684.

Varricchio, D.J., et al. 2008. Avian paternal care had dinosaur origin. Science 322: 1826–1828.

Vickers-Rich, P., L.M. Chiappe, and S.M. Kurzanov. 2002. The enigmatic birdlike dinosaur *Avimimus portentosus*. *In* L.M. Chiappe and L.M. Witmer (editors), Mesozoic birds: above the heads of dinosaurs, 65–86. Berkeley: University of California Press.

Wang, S., C. Sun, C. Sullivan, and X. Xu. 2013. A new oviraptorid (Dinosauria: Theropoda) from the Upper Cretaceous of southern China. Zootaxa 3640: 242–257.

Wang, S., S. Zhang, C. Sullivan, and X. Xu. 2016. Elongatoolithid eggs containing oviraptorid (Theropoda, Oviraptorosauria) embryos from the Upper Cretaceous of Southern China. BMC Evolutionary Biology 16: 1–21.

Wei, X., et al. 2022. A new subadult specimen of oviraptorid *Yulong mini* (Theropoda: Oviraptorosauria) from the Upper Cretaceous Qiupa Formation of Luanchuan, central China. Cretaceous Research 138: 1–14.

Wellnhofer, P. 1974. Das fünfte Skelettexemplar von *Archaeopteryx*. Palaeontographica Abteilung A: 168–216.

Wellnhofer, P. 1993. Das siebte Exemplar von *Archaeopteryx* aus den Solnhofener Schichten. Archaeopteryx 11: 1–47.

Witmer, L.M. 1997. The evolution of the antorbital cavity of archosaurs: a study in soft-tissue reconstruction in the fossil record with an analysis of the function of pneumaticity. Journal of Vertebrate Paleontology 17: 1–76.

Xing, L., et al. 2022. An exquisitely preserved in-ovo theropod dinosaur embryo sheds light on avian-like prehatching postures. IScience 25: 1–14.

Xu, X., Y.N. Cheng, X.L. Wang, and C.H. Chang. 2002. An unusual oviraptorosaurian dinosaur from China. Nature 419: 291–293.

Xu, X., et al. 2003. Four-winged dinosaurs from China. Nature 421: 335–340.

Xu, X., Q. Tan, J. Wang, X. Zhao, and L. Tan. 2007. A gigantic bird-like dinosaur from the Late Cretaceous of China. Nature 447: 844–847.

Xu, X., and Han, F.L. 2010. A new oviraptorid dinosaur (Theropoda: Oviraptorosauria) from the Upper Cretaceous of China. Vertebrata PalAsiatica 48: 11–18.

Xu, X., et al. 2013. A new oviraptorid from the Upper Cretaceous of Nei Mongol, China, and its stratigraphic implications. Vertebrata PalAsiatica 51: 85–101.

Yang, T.R., and P.M. Sander. 2022. The reproductive biology of oviraptorosaurs: a synthesis. Geological Society of London Special Publications 521: 19–24.

Yang, T.R, Y.H. Chen, J. Wiemann, B. Spiering, and P.M. Sander. 2018. Fossil eggshell cuticle elucidates dinosaur nesting ecology. PeerJ 6: 1–24.

Yun, C.G. 2019. Heyuanninae clade nov., a replacement name for the oviraptorid subfamily "Ingeniinae" Barsbold, 1981. Zootaxa 4671: 295–296.

Zanno, L.E. 2010. A taxonomic and phylogenetic re-evaluation of Therizinosauria (Dinosauria: Maniraptora). Journal of Systematic Palaeontology 8: 503–543.

APPENDIX

Abbreviations

Institutional Abbreviations

AMNH, American Museum of Natural History, New York, NY; **IGM**, Geological Institute, Mongolian Academy of Sciences, Ulaan Baatar, Mongolia; **ZPAL**, Institute of Paleobiology, Polish Academy of Sciences, Warsaw, Poland; **ROM**, Royal Ontario Museum, Ontario, Canada.

Anatomical Abbreviations

aaf	anterior articular face of sacral vertebrae
acf	axial centrum foramina
an	angular
ar	articular
asi	anterior sockets for axial intercentrum
asp	articular socket on frontal for postorbital
ast	astragalus
atc	atlanatal intercentrum concavity
atr	antitrochanter
bbc	basisphenoid-basioccipital contact
bo	basioccipital
bs	basisphenoid
bsr	basisphenoid recess
bt	basal tubera
btp	basal tubera pneumaticity
cal	calcaneus
cap	caudal pleurocoels
cc	carotid canal
cf	frontal circular foramina
cocs	cochlear space
cp	cervical pleurocoel
csc	caudal semicircular canal
ctib	crista tibiofibularis
ctr	caudal tympanic recess
den	dentary
dia	diapophyses
dnvf	neurovascular foramina on dentary
dpIII	distal phalanx III
dppt	dorsal process of pterygoid
dpt	dorsal pneumaticity on caudal vertebrae
dtIII	distal tarsal III
ebc	exoccipital- basioccipital contact
ec	endocranial space
eocv	exit for occipital vein
ep	epipterygoid
epip	epipophses
eu	eustachian tube
exo	exoccipital
fc	fibula crest
fh	femoral head
flr	floccular recess
fm	foramen magnum
fps	frontal-parietal suture
fpsc	fossae pseudocochlearis
fr	frontal
frs	frontal sinus
fs	femoral shaft
gas	gasserian ganglion
gqj	groove for quadratojugal on quadrate
gt	greater trochanter
hsc	horizontal semicircular canal
il	ilium
isch	ischium
itc	intercondylar groove of femur
itf	intertrochanteric fossa
itg	intertrochanteric groove
ju	jugal
jugc	jugal canal
lat	laterosphenoid
latps	laterosphenoid-parietal articular surface
lc	lateral femoral condyle
let	lesser trochanter
lp	lateral pleurocoel
lpop	laterosphenoid postorbital process
lt	lateral tuberosity on fibula
ltf	lateral temporal fenestra
lvc	laterosphenoid vertical crista
man	mandible
mc	medial femoral condyle
mg	midline groove on ventral surface of sacral vertebrae

mtII	metatarsal 2
mtIII	metatarsal 3
mtIV	metatarsal 4
na	neural arch
nc	neural canal
ns	neural spine
nvf	neurovascular foramina on premaxilla
oc	occipital condyle
od	odontoid process
op	obturator process
orb	orbit
orbt	orbital tectum of laterosphenoid
os	oval scar on ilium
oto	otoccipital
pa	parietal
paf	posterior articular face of sacral vertebrae
para	parapophyses
pb	pubic boot
pbc	parabasisphenoid-basisphenoid contact
pbs	parabasisphenoid
pcf	proximal concavity of fibula
pdpd	posterodorsal process of dentary
phf	proximal head of fibula
plpt	posterolateral process of pterygoid
pmax	premaxilla
pmmp	maxillary process of premaxilla
pmnp	nasal process of premaxilla
pmpt	posteromedial process of pterygoid
po	postorbital
poap	posterior acetabular process
pof	popliteal fossa
pop	paraoccipital process
popn	paraoccipital process pneumaticity
poz	postzygapophyses
ppc	parabasisphenoid-pterygoid contact
pr	prootic
prap	preacetabular process
pre	prearticular
prz	prezygapophyses
psc	parietal sagittal crest
psh	pubic shaft
psr	parasphenoid rostrum
psy	pubic synthesis
pt	pterygoid
pub	pubis
pup	pubic peduncle
qf	quadratic foramen
qj	quadratojugal
qjg	quadratojugal groove
qjp	quadratojugal pneumaticity
qmp	quadrate mandibular process
qpn	quadrate pneumaticity
qu	quadrate
rar	retroarticular process
sac	supraacetabular crest
scb	scapula blade
selt	sella turcica
so	supraoccipital
socr	recess on supraoccipital for cerebellum
sone	supraoccipital nuchal eminence
sopc	supraoccipital-opisthotic contact
sq	squamosal
sqpn	squamosal pneumaticity
su	surangular
tcn	cnemial crest of tibia
tnc	transverse nuchal crest of parietal
tnf	nutrient foramen on tibia
tp	transverse process
upg	groove on ungual phalanx
upII	ungual phalanx 2
upIII	ungual phalanx 3
upIV	ungual phalanx 4
V	trigeminal foramen
vagc	vagal canal
vcr	vagal crista
ves	vesitibular space
VII	facial canal
VIIIc	vestibulocochlear nerve cochlear branch
VIIIv	vestibulocochlear nerve vestibular branch
vlpo	ventrolateral pneumatic opening on cervical vertebrae
vpt	ventral pneumaticity on caudal vertebrae
II	optic canal
X	vagal foramen
XII	hypoglossal foramen

All issues of *Novitates* and *Bulletin* are available on the web (https://digitallibrary.amnh.org/handle/2246/5). Order printed copies on the web from:

https://shop.amnh.org/books/scientific-publications.html

or via standard mail from:

American Museum of Natural History—Scientific Publications
Central Park West at 79th Street
New York, NY 10024

♾ This paper meets the requirements of ANSI/NISO Z39.48-1992 (permanence of paper).